Stony Brook University

Interplay between magnetism and superconductivity in high-temperature superconductors $La_{2-x}Ba_xCuO_4$ and $Fe_{1+y}Te_{1-x}Se_x$: crystal growth and neutron scattering studies

A Dissertation Presented

by

Jinsheng Wen

to

The Graduate School

in Partial Fulfillment of the Requirements

for the Degree of

Doctor of Philosophy

in

Materials Science and Engineering

Stony Brook University

August 2010

Stony Brook University

The Graduate School

Jinsheng Wen

We, the dissertation committee for the above candidate for the Doctor of Philosophy degree, hereby recommend acceptance of this dissertation.

John M. Tranquada—Dissertation Advisor
Senior Physicist/Adjunct Professor, Department of Materials Science and Engineering

Genda Gu—Dissertation Advisor
Physicist/Adjunct Professor, Department of Materials Science and Engineering

Dilip Gersappe—Chairperson of Defense
Associate Professor, Department of Materials Science and Engineering

Guangyong Xu
Physicist, Condensed Matter Physics and Materials Science Department, Brookhaven National Laboratory

This dissertation is accepted by the Graduate School.

Lawrence Martin
Dean of the Graduate School

Abstract of the Dissertation

Interplay between magnetism and superconductivity in high-temperature superconductors $La_{2-x}Ba_xCuO_4$ and $Fe_{1+y}Te_{1-x}Se_x$: crystal growth and neutron scattering studies

by

Jinsheng Wen

Doctor of Philosophy

in

Materials Science and Engineering

Stony Brook University

2010

In this **Dissertation**, I combined neutron scattering with susceptibility, and transport measurements on two types of high-temperature superconductors $La_{2-x}Ba_xCuO_4$, and $Fe_{1+y}Te_{1-x}Se_x$ to study the interplay between magnetism and superconductivity. By studying $La_{2-x}Ba_xCuO_4$ with crystals grown by a floating-zone technique, it is found that static magnetic order competes with superconductivity, with the observation that both magnetic field and Zn impurity reduce the superconductivity and enhance the magnetic order. By studying the doping and magnetic-field dependence on $Fe_{1+y}Te_{1-x}Se_x$ with crystals grown by a horizontal unidirectional solidification method, it is revealed that magnetic fluctuations are essential for superconductivity. The results are consistent with the idea that magnetic excitations act as the "glue" to pair the electrons, and render the superconductivity.

Contents

List of Figures

List of Tables

Acknowledgements

My foremost thank goes to my advisors Dr. John M. Tranquada, and Dr. Genda Gu. Without them, this dissertation would not have been possible. I thank them for their patience and encouragement that carried me on through difficult times, and for their insightful suggestions that greatly helped me shape my research skills. I appreciated more for them to teach me how to think, and telling me what behaviors a good researcher should have. They have set the models for excellent researchers, and I know it is difficult to follow—probably this is a life-time process, but I will try my best. During the course of preparing this dissertation, they provided a lot of feedback that turned out to be critical. Also, their help made my life as a newcomer to the USA much easier.

I would also like to express my sincere thank to the Chairperson of the defense committee, Prof. Dilip Gersappe, who is acting as my sponsor at Stony Brook and dealing with most of the paperwork with Brookhaven National Laboratory (BNL). Without his advice and help, I would not be able to come to this stage.

I am really grateful to our group member Dr. Guangyong Xu, who doubled as teacher and friend. He is effectively my mentor who rendered me knowledge on almost all of the projects I have been involved in the past four years. He taught me to use neutron and x-ray scattering to study superconductors, relaxor ferroelectrics, and multiferroics. As a friend, he made my experience at BNL much more enjoyable.

I also benefit quite a lot from other group members such as Dr. Steve Shapiro, whom I worked with on multiferroics; Dr. Igor Zaliznyak and Dr. Markus Hücker, with whom I collaborated on high-temperature superconductors; Zhijun Xu, my labmate, whom I worked closely with on most of the projects. Thanks also due to research support members in our group, such as Kim Mohanty, Eward Stein, and Eileen Levine. Without any of them, my research and life would be much more difficult.

My collaborations with other researchers and groups have been very fruitful and joyful. These first include those wonderful people from BNL: Dr. Qiang Li's group members, especially Mr. Qing Jie; Dr. Peter Johnson's group

members; Dr. Wei Ku, and Dr. Chicheng Lee; Dr. Liyuan Zhang; Dr. Zhong Zhong. There are more from outside institutions: Dr. Peter M. Gehring at National Institute of Standards and Technology (NIST); Dr. Chris Stock at Rutherford Appleton Laboratory (now moves back to NIST); Dr. M. v. Zimmermann at Deutsches Elektronensynchrotron; Prof. Seung-Hun Lee's group at University of Virginia; Prof. Ali Yazdani's group at Princeton University; Prof. Xingjiang Zhou's group at Institute of Physics, Chinese Academy of Sciences; Prof. Eric Hudson's group at Massachusetts Institute of Technology; Prof. Juan C. Campuzano's group at University of Chicago at Illinois; Prof. Laura Greene's group at University of Illinois at Urbana-Champaign.

Most of my neutron scattering measurements were performed at NIST Center for Neutron Research, and I owe my thanks to the instrument scientists for their helps during my experiments, including Dr. Hye-Jung Kang, Dr. Sung Chang, Dr. Ying Chen, Dr. William Ratcliff, Dr. Yiming Qiu, Dr. Jason Gardner, Dr. Songxue Chi, and Dr. Deepak Singh. I have also used High Flux Isotope Reactor, and Spallation Neutron Source at Oak Ridge National Laboratory. I am also thankful to the instrument scientists there for their kindly help. They are Dr. Andrey Zheludev, Dr. Tao Hong, Dr. Jerel Zarestky, Dr. Wei Tian, Dr. Barry Winn, and Dr. Matthew Stone.

I would also like to use this opportunity to thank all my friends at Stony Brook University and BNL. There are so many names that I cannot make a list here, but I am pretty sure that, without any of them, my life on Long Island will be much less colorful and joyful.

I also want to acknowledge the funding support from the US Department of Energy, Office of Basic Energy Sciences, through Contract No. DE-AC02-98CH10886, and through the Center for Emergent Superconductivity.

Last but not least, I thank all my family members, for always being there when I needed them most. They are the source where I obtain my strength, happiness, and hope. For them, thanks will never be enough, but I will always appreciate their past, on-going and never ending supports. To pay them back, I know the best way is to work harder, and live better. My last and most special thank goes to my dear son, Zhengzheng, who was born on July 5. It is who competed with me to see who is running faster, and it turned out that he won—he was born before I defend this **Dissertation**, but without him, I would not be able to finish my work in a timely manner. More importantly, he brought me tremendous that I have never had before. Of course, all these are tied to his Mom, Xiaobin, who gave up her Ph.D. to join me in 2007, on the same day the baby was born. She has taken good care of me and punched me ever since we met. If there is any chance that I would be able to succeed, 50% of the credit goes to her.

Jinsheng Wen

Curriculum Vitae

Condensed Matter Physics and Materials Science Dept.	Rm. 2-2, Bldg. 510A
Brookhaven National Laboratory (BNL)	Phone: 631-344-3714
Upton, NY, 11973	Email: jwen@bnl.gov

Education

Ph.D. in Materials Science, Stony Brook University, NY, USA, August 2010.

B.S. in Materials Science, Tsinghua University, Beijing, China, July 2005.

Research Performed at the Neutron Scattering Group, BNL

Dissertation —— Advisors: Dr. Genda Gu and Dr. John M. Tranquada
Interplay between magnetism and superconductivity in high-T_c superconductors $La_{2-x}Ba_xCuO_4$ and $Fe_{1+y}Te_{1-x}Se_x$: crystal growth and neutron scattering studies. Grow crystals with floating-zone and horizontal unidirectional solidification method. Use triple-axis and time-of-flight spectrometers. Perform susceptibility and transport measurements.

Other Projects

Sing-crystal growth of cuprates, cobaltates, nickelates, and multiferroics with floating-zone technique. Grow, characterize and prepare samples for measurement purpose.

How inhomogeneities affect the properties of relaxor ferroelectrics? Use neutron spinecho, backscattering, and triple-axis spectrometers, as well as x-ray scattering technique to study the diffuse scattering and phonons with and without electric field.

Magnetic and electrical control of the charge and magnetic structures in a multiferroic $LuFe_2O_4$. Perform elastic neutron scattering measurements on a triple-axis spectrometer, and resistivity measurements to study the electric- and magnetic-field effect on the charge and magnetic order.

Courses Taught as a Teaching Assistant

Fall 2005, 2007, and Spring 2006, ESG-281, Introduction to Solid State Physics.

Fall 2006, ESM-335, Strength of Materials.

Spring 2007, ESM-355, Materials & Processing in Manufacturing Design.

Awards

6/2010	Chinese Government Award for Outstanding Students Abroad, China Scholarship Council, Beijing, China.
4/2010	Sigma Xi Travel Award, Sigma Xi Society, Stony Brook, NY.
7/2009	C. Margrett Student Lecturer Award, American Crystallographic Association, Toronto, Canada.
2007-8	American Association for Crystal Growth Scholarship (twice), American Association for Crystal Growth, Warren, NJ.
8/2006	Dean's Fellowship, Stony Brook University, Stony Brook, NY.
9/2005	Presidential Scholarship, Stony Brook University, Stony Brook, NY.
2001-5	Consecutive Awards for Outstanding Academic Performance, Tsinghua University, Beijing, China.
3/2004	Outstanding Student Leader, Tsinghua University, Beijing, China.

Talks and Presentations

Coupling of spin and orbital excitations in the Iron-based superconductor $FeTe_{0.5}Se_{0.5}$. Lawrence Berkeley National Laboratory, Berkeley, CA, 6/14/2010.

Neutron scattering studies on the interplay between magnetism and superconductivity in high-T_c *superconductors.* Provost Graduate Student Lecture Series, Stony Brook University, Stony Brook, NY, 3/25/2010.

Effect of magnetic field on the spin resonance in $FeTe_{0.5}Se_{0.5}$ *as seen via inelastic neutron scattering.* The 9th International Conference on Spectroscopies in Novel Superconductors, Shanghai, China, 5/27/2010; American Physical Society's Annual March Meeting, Portland, OR, 3/18/2010.

Magnetic- and electric-field effects on the magnetic and charge order in a multiferroic $LuFe_2O_4$. NIST Center for Neutron Research, Gaithersburg, MD, 12/2/2009; American Crystallographic Association's Annual Meeting, Toronto, Canada, 7/30/2009; American Physical Society's Annual March Meeting, Pittsburgh, PA, 3/18/2009; Condensed Matter Physics and Materials Science Department, Brookhaven National Laboratory, Upton, NY, 9/29/2008.

Diffuse scattering and phonons from $K_{0.98}Li_{0.02}TaO_3$. National Synchrotron Light Source, Brookhaven National Laboratory, Upton, NY, 5/29/2009; National Synchrotron Light Source and Center for Functional Materials Users' Meeting, Brookhaven National Laboratory, Upton, NY, 5/21/2007.

Large Bi-2212 single crystal growth by the floating-zone technique. The 15th International Conference on Crystal Growth, Salt Lake City, UT, 8/15/2007.

Publication List (in reverse chronological order)

Published Papers

1. S.-H. Lee, Guangyong Xu, Wei Ku, **J. S. Wen**, C. C. Lee, N. Katayama, Z. J. Xu, S. Ji, Z. W. Lin, G. D. Gu, H.-B Yang, P. D. Johnson, T. Valla, M. Fujita, T. J. Sato, K. Yamada, and J. M. Tranquada, *Coupling of spin and orbital excitations in the iron-based superconductor* $FeSe_{0.5}Te_{0.5}$, Phys. Rev. B **81**, 220502(R) (2010).

2. C. C. Homes, A. Akrap, **J. S. Wen**, Z. J. Xu, Z. W. Lin, Q. Li, and G. D. Gu, *Electronic correlations and unusual superconducting response in the optical properties of the iron-chalcogenide* $FeTe_{0.55}Se_{0.45}$, Phys. Rev. B **81**, 180508(R) (2010).

3. **Jinsheng Wen**, Guangyong Xu, G. Gu, and S. M. Shapiro, *Robust charge and magnetic order under electric field and current in a multiferroic* $LuFe_2O_4$, Phys. Rev. B **81**, 144121 (2010).

4. **Jinsheng Wen**, Guangyong Xu, Zhijun Xu, Z. W. Lin, Q. Li, Y. Chen, S. Chi, G. Gu, and J. M. Tranquada, *Effect of magnetic field on the spin resonance in* $FeTe_{0.5}Se_{0.5}$ *as seen via inelastic neutron scattering,* Phys. Rev. B **81**, 100513(R) (2010).

5. C. V. Parker, A. Pushp, A. N. Pasupathy, K. K. Gomes, **Jinsheng Wen**, Z. Xu, S. Ono, G. Gu, and A. Yazdani, *Nanoscale Proximity effect in the high-temperature superconductor* $Bi_2Sr_2CaCu_2O_{8+\delta}$ *using a scanning tunneling microscope,* Phys. Rev. Lett. **104**, 117001 (2010).

6. A. D. Palczewski, T. Kondo, **J. S. Wen**, Z. J. Xu, G. Gu, and A. Kaminski, *Controlling the carrier concentration of the high temperature superconductor* $Bi_2Sr_2CaCu_2O_{8+x}$ *in Angle Resolved Photoemission Spectroscopy (ARPES) experiments,* Phys. Rev. B **81**, 104521 (2010).

7. U. Chatterjee, M. Shi, D. Ai, J. Zhao, A. Kanigel, S. Rosenkranz, H. Raffy, Z. Z. Li, K. Kadowaki, D. G. Hinks, Z. J. Xu, **J. S. Wen**, G. Gu, C. T. Lin, H. Claus, et al., *Observation of a d-wave nodal liquid in highly underdoped* $Bi_2Sr_2CaCu_2O_{8+\delta}$, Nature Phys. **6**, 99 (2010).

8. R. D. Gann, J. X. Cao, R. Q. Wu, **Jinsheng Wen**, Z. Xu, G. D. Gu, and J. A. Yarmoff, *Adsorption of Iodine and Potassium on* $Bi_2Sr_2CaCu_2O_{8+\delta}$ *investigated by low energy alkali-ion scattering,* Phys. Rev. B **81**, 035418 (2010).

9. S. Blanc, Y. Gallais, A. Sacuto, M. Cazayous, M. A. Measson, G. Gu, **J. S. Wen**, and Z. J. Xu, *Quantitative Raman measurements of the evolution of the Cooper-pairs density with doping in* $Bi_2Sr_2CaCu_2O_{8+\delta}$ *superconductors,* Phys. Rev. B **80**, 140502(R)(2009).

10. **Jinsheng Wen**, Guangyong Xu, Zhijun Xu, Zhi Wei Lin, Qiang Li, W. Ratcliff, G. Gu, and J. M. Tranquada, *Short-range incommensurate magnetic order near the superconducting phase boundary in* $Fe_{1+\delta}Te_{1-x}Se_x$*,* Phys. Rev. B **80**, 104506 (2009).

11. **Jinsheng Wen**, Guangyong Xu, Genda Gu, and S. M. Shapiro, *Magnetic-field control of charge structures in the magnetically disordered phase of multiferroic* $LuFe_2O_4$*,* Phys. Rev. B **80**, 020403(R) (2009).

12. A. Pushp, C. V. Parker, A. N. Pasupathy, K. K. Gomes, S. Ono, **Jinsheng Wen**, Zhijun Xu, Genda Gu, and A. Yazdani, *Extending Universal Nodal Excitations Optimizes Superconductivity in* $Bi_2Sr_2CaCu_2O_{8+\delta}$*,* Science **324**, 1689 (2009).

13. W. D. Wise, K. Chatterjee, M. C. Boyer, T. Kondo, T. Takeuchi, H. Ikuta, Zhijun Xu, **Jinsheng Wen**, G. D. Gu, Y. Wang, and E. W. Hudson, *Imaging nanoscale Fermi surface variations in an inhomogeneous superconductor,* Nature Phys. **5**, 213 (2009).

14. **Jinsheng Wen**, Zhijun Xu, Guangyong Xu, J. M. Tranquada, Genda Gu, S. Chang, and H. J. Kang, *Magnetic field induced enhancement of spin-order peak intensity in* $La_{1.875}Ba_{0.125}CuO_4$*,* Phys. Rev. B **78**, 212506 (2008).

15. J. M. Tranquada, G. D. Gu, M. Hücker, Q. Jie, H.-J. Kang, R. Klingeler, Q. Li, N. Tristan, **J. S. Wen**, G. Y. Xu, Z. J. Xu, J. Zhou, and M. v. Zimmermann, *Evidence for unusual superconducting correlations coexisting with stripe order in* $La_{1.875}Ba_{0.125}CuO_4$, Phys. Rev. B **78**, 174529 (2008).

16. **Jinsheng Wen**, Guangyong Xu, C. Stock, P. M. Gehring, Z. Zhong, L. A. Boatner, E. L. Venturini, and G. A. Samara, *Effect of local dipole moments on the structure and lattice dynamics of* $K_{0.98}Li_{0.02}TaO_3$*,* Phys. Rev. B **78**, 144202 (2008).

17. **Jinsheng Wen**, Guangyong Xu, C. Stock, and P. M. Gehring, *Response of polar nanoregions in* $68\%Pb(Mg_{1/3}Nb_{2/3})O_3$*-*$32\%PbTiO_3$ *to a [001] electric field,* Appl. Phys. Lett. **93**, 082901 (2008).

18. W. Zhang, G. Liu, J. Meng, L. Zhao, H. Liu, X. Dong, W. Lu, **J. S. Wen**, Z. J. Xu, G. D. Gu, T. Sasagawa, G. Wang, Y. Zhu, H. Zhang, Y. Zhou, et al., *High Energy Dispersion Relations for the High Temperature $Bi_2Sr_2CaCu_2O_{8+\delta}$ Superconductor from Laser-Based Angle-Resolved Photoemission Spectroscopy,* Phys. Rev. Lett. **101**, 017002 (2008).

19. Guangyong Xu, **Jinsheng Wen**, C. Stock, and P. M. Gehring, *Phase instability induced by polar nanoregions in a relaxor ferroelectric system*, Nature Mater. **7**, 562 (2008).

20. A. N. Pasupathy, A. Pushp, K. K. Gomes, C. V. Parker, **Jinsheng Wen**, Zhijun Xu, Genda Gu, S. Ono, Y. Ando, and A. Yazdani, *Electronic Origin of the Inhomogeneous Pairing Interaction in the High-T_c Superconductor $Bi_2Sr_2CaCu_2O_{8+\delta}$,* Science **320**, 196 (2008).

21. W. Zhang, G. Liu, L. Zhao, H. Liu, J. Meng, X. Dong, W. Lu, **J. S. Wen**, Z. J. Xu, G. D. Gu, T. Sasagawa, G. Wang, Y. Zhu, H. Zhang, Y. Zhou, et al., *Identification of a New Form of Electron Coupling in the $Bi_2Sr_2CaCu_2O_{8+\delta}$ Superconductor by Laser-Based Angle-Resolved Photoemission Spectroscopy,* Phys. Rev. Lett. **100**, 107002 (2008).

22. **J. S. Wen**, Z. J. Xu, G. Y. Xu, M. Hücker, J. M. Tranquada, and G. D. Gu, *Large Bi-2212 single crystal growth by the floating-zone technique,* J. Crystal Growth **310**, 1401 (2008).

Submitted Papers

1. M. Hücker, M. v. Zimmermann, Z. J. Xu, **J. S. Wen**, G. D. Gu, *Zn doping dependence of stripes in $La_{1.905}Ba_{0.095}CuO_4$,* (submitted to J. Supercond. Nov. Magn.).

2. C. C. Homes, A. Akrap, **J. Wen**, Z. Xu, Z. W. Lin, Q. Li, and G. Gu, *Optical properties of the iron-chalcogenide superconductor $FeTe_{0.55}Se_{0.45}$*, arXiv:1007.1447, (submitted to J. Phys. Chem. Solids).

3. T. J. Reber, N. C. Plumb, Yue Cao, Z. Sun, H. Iwasawa, **J. S. Wen**, Z. J. Xu, G. Gu, H. Eisaki, Y. Yoshida, Y. Aiura, M. Hermele, D. S. Dessau, *The closing of the gap, prepairing, and the role of scattering rates in underdoped $Bi_2Sr_2CaCu_2O_{8+\delta}$,* (submitted to Science).

4. **Jinsheng Wen**, Qing Jie, Qiang Li, M. Hücker, M. v. Zimmermann, Zhijun Xu, D. K. Singh, Liyuan Zhang, Genda Gu, and J. M. Tranquada, *Magnetic-field-induced decoupling of superconducting layers in a copper-oxide compound* (submitted to Nature).

5. M. Hücker, M. v. Zimmermann, G. D. Gu, Z. J. Xu, **J. S. Wen**, Guangyong Xu, H. J. Kang, A. Zheludev, and J. M. Tranquada, *Stripe order in superconducting* $La_{2-x}Ba_xCuO_4$ *for* $0.095 \leq x \leq 0.155$*,* arXiv:1005.5191 (submitted to PRB).

6. Z. Xu, **Jinsheng Wen**, G. Xu, Q. Jie, Z. Lin, Q. Li, S. Chi, D. K. Singh, G. Gu, and J. M. Tranquada, *Disappearance of static magnetic order and evolution of spin fluctuations in* $Fe_{1+\delta}Te_{1-x}Se_x$*,* arXiv:1005.4856 (submitted to PRB).

7. H. Qin, J. Shi, Y. Cao, K. Wu, J. Zhang, E. W. Plummer, **J. Wen**, Z. J. Xu, G. D. Gu, and J. Guo, *Direct Determination of Electron-Phonon Coupling Matrix Element in a Correlated System,* arxiv:1005.1452 (submitted to PRL).

8. W. K. Park, C. R. Hunt, H. Z. Arham, Z. J. Xu, **J. S. Wen**, Z. W. Lin, Q. Li, G. D. Gu, and L. H. Greene, *Strong Coupling Superconductivity in Iron-Chalcogenide* $FeTe_{0.55}Se_{0.45}$*,* arXiv:1005.0190 (submitted to PRL).

9. Z. Xu, **Jinsheng Wen**, G. Xu, C. Stock, J. S. Gardner, and P. M. Gehring, *A two-component model of the neutron diffuse scattering in the relaxor ferroelectric PZN-4.5%PT,* arXiv:1004.5406 (submitted to PRB).

10. T. Kondo, Y. Hamaya, A. D. Palczewski, T. Takeuchi, **J. S. Wen**, Z. J. Xu, G. Gu, J. Schmalian, and A. Kaminski, *Disentangling Cooper-Pair Formation from the Pseudogap in the Cuprate Superconductors,* arXiv:1004.5406 (submitted to Science).

11. S. Blanc, M. C. Y. Gallais, M. A. Measson, A. Sacuto, A. Georges, G. Gu, **J. S. Wen**, Z. Xu, and D. Colson, *Suppressed antinodal coherence with a single d-wave superconducting gap leads to two energy scales in underdoped cuprates,* arXiv:1004.2404 (submitted to Nature Phys.).

12. N. Katayama, S. Ji, D. Louca, S.-H. Lee, M. Fujita, T. J. Sato, **J. S. Wen**, Z. J. Xu, G. D. Gu, G. Xu, Z. W. Lin, M. Enoki, S. Chang, K. Yamada, and J. M. Tranquada, *Investigation of the spinglass regime between the antiferromagnetic and superconducting phases in* $Fe_{1+y}Te_{1-x}Se_x$*,* arXiv:1003.4525 (submitted to PRL).

13. M. Feygenson, X. Teng, S. E. Inderhees, Y. Yiu, W. Du, W. Han, **Jinsheng Wen**, Z. Xu, A. A. Podlesnyak, J. L. Niedziela, M. Hagen, Y. Qiu, C. M. Brown, L. Zhang, and M. C. Aronson, *Spin Waves and Switching: The Dynamics of Exchange - Biased Co Core-CoO Shell Nanoparticles,* arXiv:0909.3833 (submitted to PNAS).

Chapter 1

Introduction

In this Chapter, I will introduce superconductivity, the BCS theory, high-temperature superconductors and the interplay between superconductivity and magnetism in these superconductors. Also, I will introduce one sample system I want to study in this **Dissertation**.

1.1 Superconductors

1.1.1 Conventional superconductivity and the BCS theory

Superconductivity was discovered by Heike Kamerlingh Onnes in 1911 as a result of his investigations on the resistance of Hg. [1, 2] When he cooled Hg, the resistance went down gradually, and suddenly, dropped to zero at a temperature, which is later called critical temperature, T_c. [See Fig. 1.1(a)] The T_c, ~ 4.2 K for Hg is very low, ≈ -269 °C, reached only after Onnes successfully liquified He. Zero resistance is a defining characteristic of superconductors, and another one is the "Meissner Effect", which is describing a superconductor's ability to expel the internal magnetic flux below T_c by creating a large surface current, as illustrated in Fig. 1.1(b). [3] The current generates an opposite field to cancel the external field, and this type of response to the field is called "diamagnetism". These two amazing properties make superconductors extremely useful. First, zero resistance means zero-energy loss to heat when superconductors are used to carry electric current, which is promising for saving the precious energy. They can be also used in making superconducting magnets, with current flowing through them to generate the magnetic field which will persist without power supply, and thus save energy. Because of their diamagnetism, they are also used in magnetic-levitation (maglev) train,

which can "fly" in the air without contacting the track, and thus can avoid the friction from the track and run very fast. This is one of the most promising candidates for future high-speed, and safe transportation.

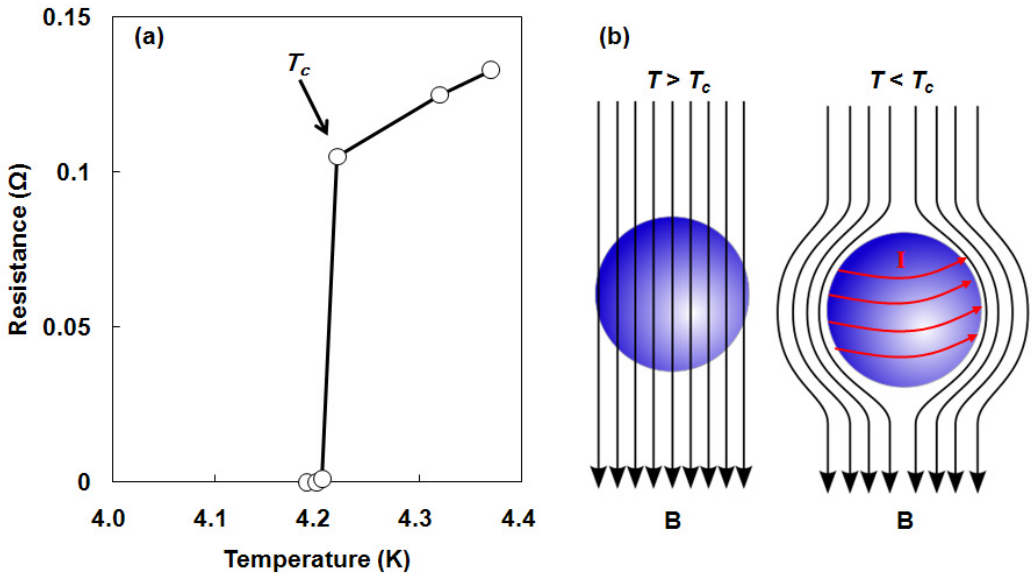

Figure 1.1: Two defining characteristics of superconductors:(a), the resistance is zero below T_c [1, 2]; (b), the magnetic flux B inside the superconductor is expelled when the superconductor establishes superconductivity at $T < T_c$, by creating surface current [3].

Superconductors exhibit many exotic properties, and it is definitely worthwhile to ask why. To answer this question, John Bardeen, Leon Cooper, and Robert Schrieffer came up with a brilliant idea in 1957, for which they were awarded the Nobel Prize. They used the concept that the interactions between electrons and phonons allow two electrons to overcome their charge repulsion, so that they can bind together and form Cooper pairs. [4] These Cooper pairs can travel in the material without crashing into the lattice, and thus avoiding energy loss. The theory is named the BCS theory after their first initials. The BCS theory is a beautiful theory in the sense that it does not only explain the experimental results well, but also has large prediction power. Followings are some important formulae deduced from the BCS theory [4]:

- The BCS theory gives the T_c in terms of the electron-phonon coupling potential N_0V_0, and the Debye cutoff energy E_D:

$$k_B T_c = 1.13 E_D \mathrm{e}^{\frac{-1}{N_0 V_0}}, \tag{1.1}$$

where k_B is the Boltzman constant.

- A formula similar to (1.1) is predicted for the zero-temperature energy gap $\Delta(0)$, with

$$\Delta(0) = 2E_D \mathrm{e}^{\frac{-1}{N_0 V_0}} \tag{1.2}$$

  The ratio of $\Delta(0)$ over $k_B T_c$ is a constant, 1.76, which is material independent.

- The specific heat of the superconductor is decreasing exponentially with temperatures below T_c. At T_c, the specific heat increases abruptly when it is cooled from normal to superconducting state.

- The BCS theory successfully explains the Meissner effect and the variation of the penetration depth (how long a magnetic field can penetrate into the superconductor) with temperature.

- It also describes how the critical magnetic field, H_c, above which a superconductor loses its superconductivity, changes with temperature (T) with respect to the critical field at 0 K, $H_c(0)$, with

$$\frac{H_c(T)}{H_c(0)} \approx 1 - (\frac{T}{T_c})^2 \tag{1.3}$$

BCS works pretty well for the conventional or low-temperature superconductors, such as the element superconductors like Hg. The following section describes a type of superconductors for which the BCS theory does not quite work.

1.1.2 High-T_c superconductivity and theories

In 1986, Georg Bednorz and Alex Müller [5] discovered that barium-doped lanthanum copper oxide (LBCO) became superconducting at $\sim$ 30 K— some 10 K above the previous record temperature. This broke the common belief that T_c cannot higher than 30 K, which triggered researchers' great interests in seeking superconductors with higher T_c, and a flood of new materials were discovered soon afterwards and the record T_c is now around 135 K, in a compound containing Tl, Hg, Ba, Ca, Cu, and O. [6] (See Fig. 1.2) Before the year 2008, all superconductors with high T_c, say larger than 50 K, are materials contain copper oxide layers and are known as cuprates. This monopoly was broken in 2008 by the discovery of superconductivity in Iron-based superconductors

with T_c up to 55 K. [a] [7–10]

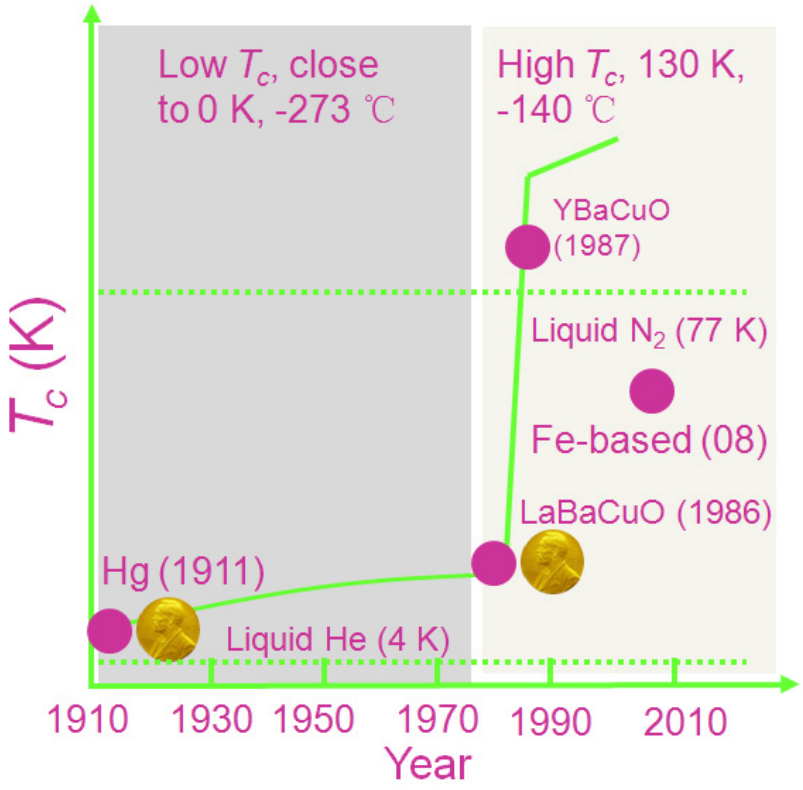

Figure 1.2: Year and T_c for some superconductors. Hg, first superconductor, 1911 [1, 2]; $La_{2-x}Ba_xCuO_4$, first high-T_c superconductor, 1986 [5]; $YBa_2Cu_3O_{7-x}$, $T_c \sim 93$ K, 1987 [11, 12]; Iron-based superconductors, 2008 [8, 10]; the highest $T_c \sim 130$ K [6]. Two horizontal lines indicate liquid He and N_2 temperatures. Two medals represent Nobel Prizes. The darker and lighter shade indicates the years when low- and high-temperature superconductors were discovered.

The discovery of high-temperature superconductors are extremely exciting because it makes the application of superconductors possible. Some of them have T_c higher than the boiling point of liquid N_2, which means that they can be cooled in liquid N_2 to establish their superconductivity. Compared to low-temperature superconductors, for which one has to use liquid He to cool to the superconducting state, the much cheaper liquid N_2 greatly lowers the cost. Now, they are used in many places, such as in maglev train, and

[a] There will be more discussions on the Iron-based superconductors in Chapter 4.

superconducting magnet. Some power cables made of $YBa_2Cu_3O_{7-x}$ are also under test.

While the high-temperature superconductors are encouraging on the application aspect, they frustrate researchers with the fact that many of whose properties *cannot* be explained by the BCS theory, which successfully explains the conventional superconductivity developing from metals. Cuprates are Mott insulators in their stoichiometric form. A Mott insulator is a material whose conductivity vanishes as temperature tends to zero, even though band theory would predict it to be metallic because of electronic interactions. [13, 14] Concerning the high-temperature superconductors, one of the major problems with the BCS theory is that the electron-phonon interaction which induces attractive force between electrons is not large enough to overcome the Coulomb repulsion between electrons, and the electron-phonon coupling strength is too small to have T_c higher than 30 K. Certainly, the "glue" provided by electron-phonon interactions is insufficient for "Cooper pairs" to form! Therefore, it is fundamentally important to look for alternative theories, or at least a modified version of the BCS theory that can account for the high-temperature superconductivity.

From the application point of view, it is also important to understand "what the glue is". Although the T_c has been much raised to ~ 130 K, it is still too cold ($-140\,^\circ$C) for everyday use. Also, there are other properties which limit their use, *e. g.*, low critical current, fragility, etc. If we know why high-temperature superconductors are superconducting, it may then be possible to design superconductors that have higher T_c, and better superconducting properties, which will be more suitable for use.

In whichever aspect, a high-T_c mechanism appears to be emergent, and indeed, there have been tremendous efforts on it, which results a number of theories. [15–36] Some modified BCS theories are also available. [37–39] As can be judged from the number of theories, there have not been consensuses on the high-T_c mechanism. Nevertheless, one of the most promising ways to explaining the high-T_c superconductivity is by studying the interplay between magnetism and superconductivity, because high-T_c superconductivity develops from the vicinity of antiferromagnetism (describing a type of spin arrangement with neighboring spins being anti-parallel to each other).

1.2 Interplay between superconductivity and magnetism in cuprates

High-temperature superconductivity occurs by doping an antiferromagnetic Mott insulator. Since $La_{2-x}Ba_xCuO_4$ is the cuprate system which will be studied in this **Dissertation**, let me use La_2CuO_4, the parent compound for $La_{2-x}Ba_xCuO_4$ and $La_{2-x}Sr_xCuO_4$ as an example. By doping the antiferromagnetic insulating La_2CuO_4, that is, by replacing certain amount of La by Sr or Ba, superconductivity appears. [5] La_2CuO_4 is undoped, and called the parent compound, as it is where superconductivity arises from. In Fig. 1.3, a schematic phase diagram for hole-doped cuprate is plotted. [b] [40–47] As seen from the phase diagram for $La_{2-x}Sr_xCuO_4$, after the antiferromagnetic order is gradually suppressed, superconductivity appears (~ 0.05). The T_c vs. doping x curve has a dome shape (if one ignores the small dip around $x = 1/8$, which will be discussed later), with T_c increasing with x until x reaches 15.5%, where T_c shows a maximum, and the system is optimally doped. For $x < 15.5\%$, it is underdoped. With x further increasing, T_c drops and superconductivity disappears when $x \approx 30\%$, and this region is called overdoped region.

1.2.1 Destruction of antiferromagnetic order in La_2CuO_4

La_2CuO_4 is antiferromagnetic, with Néel temperature $T_N \sim 325$ K, below which it establishes the magnetic order. [49–51] It has a layered structure as shown in Fig. 1.4. [46, 47, 52] The key element shared by cuprate structures is the CuO_2 plane, as shown in Fig. 1.4(b). The CuO_2 planes are stacked in a body-centered fashion, so that the unit cell contains two layers.

Before further discussing the structure, let me first describe the notations. As shown in Fig. 1.4(b), a tetragonal unit cell in plane is indicated by the Cu-O bond, while the orthorhombic cell is shown by the dashed lines, which is the Cu-Cu bond. In a tetragonal unit cell, the lattice constants $a = b \approx 3.81$ Å, while in the orthorhombic notation, the b axis (b_o) is larger than the a axis (a_o). In CuO_2 plane, spins on neighboring Cu atoms are antiparallel to each other [Fig. 1.4(c)], and pointing along b_o. This type of magnetic order with spins arrange in a antiparallel manner is antiferromagnetic order. In this case, spins have a periodicity of 2 unit cells. In reciprocal space, one expects to see the magnetic Bragg peak at $(1/2, 1/2)$ within the $(HK0)$ scattering plane, as illustrated in Fig. 1.5(a) by the star. The scattering plane is defined by two vector $[H00]$ and $[0K0]$. In reciprocal space, a $\mathbf{Q}$-vector (h, k, l) is usually described in reciprocal lattice unit (r.l.u.) of $(a^*, b^*, c^*) = (2\pi/a, 2\pi/b, 2\pi/c)$.

[b] Use 2+ Sr or Ba to replace 3+ La, and thus induces holes.

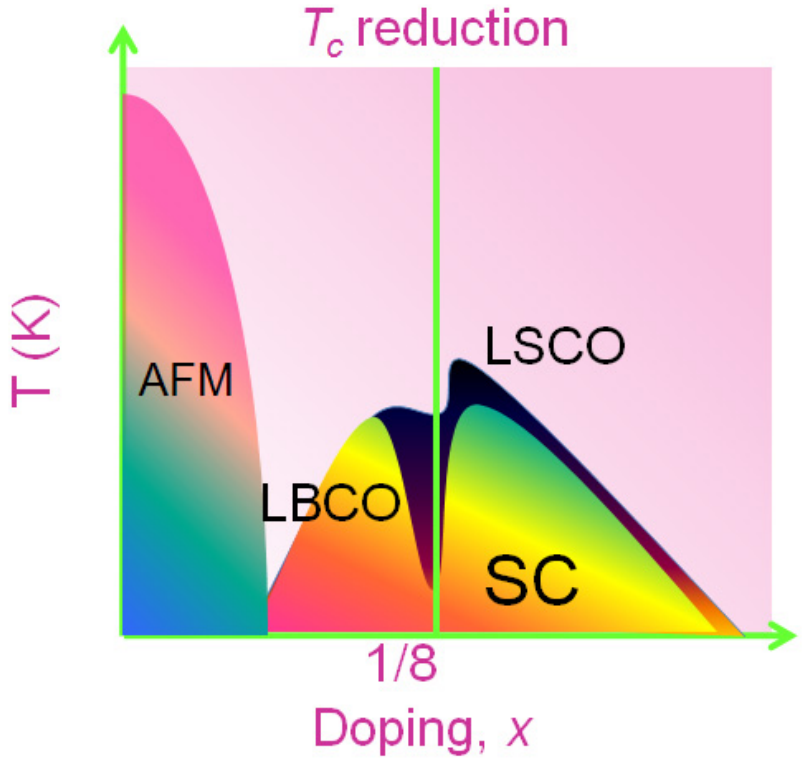

Figure 1.3: A schematic phase diagram of the hole-doped cuprates. AFM, antiferromagnetic; SC, superconducting. Upper curve is for $La_{2-x}Sr_xCuO_4$, and lower one for $La_{2-x}Ba_xCuO_4$. At $x = 1/8$, the T_c vs. x curve shows a dip, known as the "1/8" anomaly. [48]

With doping increasing, the antiferromagnetic order is rapidly suppressed, with ordering temperature T_N decreasing systematically, and magnetic order peak intensity reducing. [53–55, 57–61] In the insulating phase ($x \lesssim 5\%$), below 30 K, the (1/2,1/2) peak intensity shows an anomalous loss, which is related to the onset of incommensurate magnetic diffuse scattering. This scattering is peaked in the diagonal direction along b_o^*, as shown by the two circles in Fig. 1.5(a). [53] This indicates that the magnetic order is modulated unidirectionally along b_o^*. The long-range antiferromagnetic order is completely suppressed at $x \sim 5\%$, [40–44] after which we reach a region of central interest, where several types of order, *e. g.*, superconducting, and spin- and charge-density-wave (SDW and CDW) order, coexist, and possibly compete. [32, 62–65]

Because superconductivity appears after the suppression of the long-range

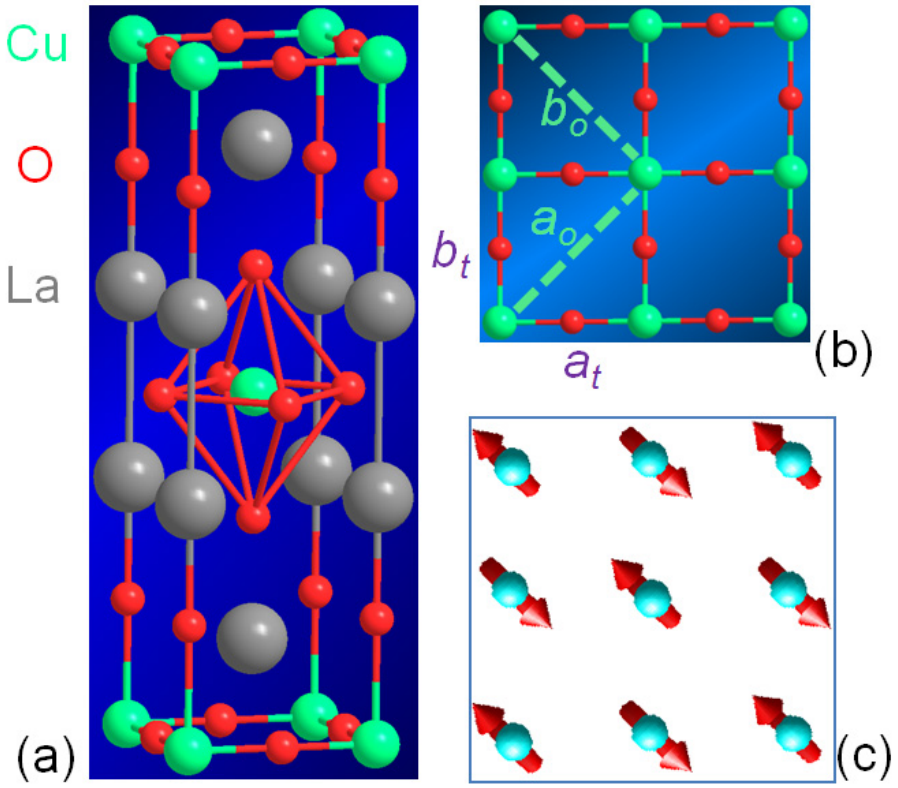

Figure 1.4: (a) Atomic structure for La_2CuO_4; (b) Cu-O_2 plane. a_t, b_t, and a_o, and b_o stand for tetragonal, and orthorhombic a and b axis respectively; (c) Spin arrangements in the Cu-O_2 plane. The arrows indicate the direction of the magnetic moments. [46, 47, 52]

static antiferromagnetic order, it is believed that magnetic fluctuations which survive in the superconducting regime are important for superconductivity. [58, 66–68] When the static magnetic order in the parent compound is suppressed, either through doping or applying pressure, the system is driven to be more dynamic, and then superconductivity appears.

1.2.2 Stripe order and superconductivity in cuprates

In the superconducting regime, there is a phase which has garnered a lot of recent attention and vocal supporters—the "stripe", a phase in which the doped holes self-segregate into one-dimensional charge rivers spaced approximately four unit cells apart. Stripe is a term used to describe unidirectional density-wave states, which can involve unidirectional charge mod-

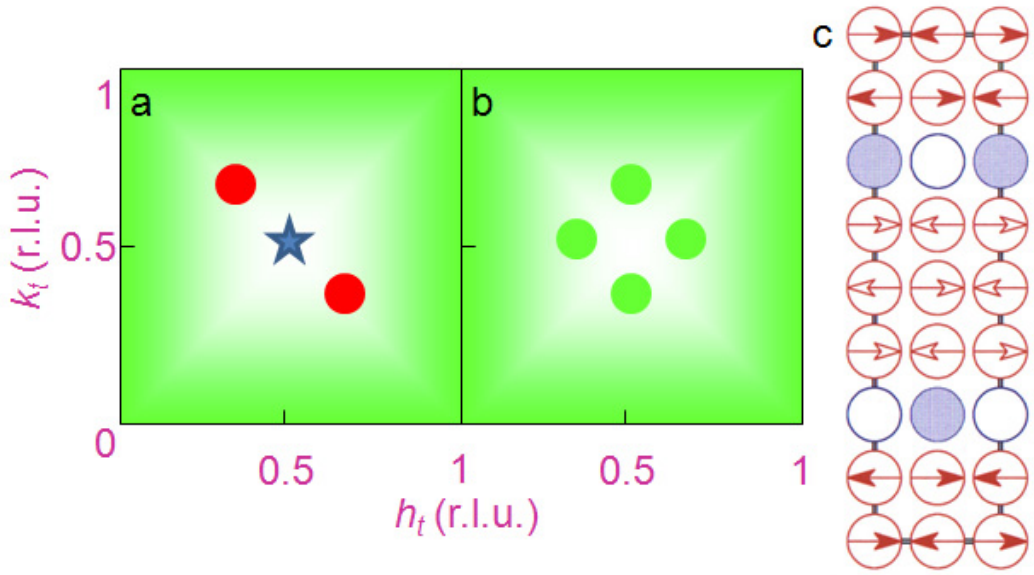

Figure 1.5: Schematic of the magnetic peaks for $La_{2-x}Sr_xCuO_4$ in $(HK0)$ scattering plane, using tetragonal coordinate system for (a), undoped La_2CuO_4 (star), and lightly-doped $La_{2-x}Sr_xCuO_4$ (circles); (b) superlattice peaks for $La_{2-x}Sr_xCuO_4$ with larger doping, arising from spin stripe order. (c) Schematic of the charge and spin stripe. Arrows indicate the moment direction, and the filled arrows indicate the direction rotated by 180° from the antiferromagnetic structure. The sites without arrows represent holes, with filling ratio of 1/2. [53–62]

ulations (charge stripe) and coexisting charge and spin-density order (spin stripe). [69] The existence of a stripe phase in cuprates was first suggested in 1989 in the context of Hartree-Fock studies of the Hubbard model close to half-filling and at zero temperature. [21] In this calculation, stripes are long period CDW arising from Fermi-surface nesting in a weakly incommensurate system. [21, 70–72] Theoretical works on stripes continue to develop. [73–75] However, until 1995, when experimental data from neutron-scattering measurements in cuprates were interpreted consistently within a stripe picture by Tranquada *et al.*, [62] not much attention was paid to the stripe model in connection with high-T_c superconductors. Tranquada *et al.* detected the static stripes in a Nd co-doped compound $La_{2-x-y}Nd_ySr_xCuO_4$ for the first time. [62] For $y = 0.4$ and $x = 0.12$, there are 4 incommensurate peaks displaced from the commensurate peak position (1/2,1/2), as shown in Fig. 1.5(b). In addition, new superlattice peaks appear at the positions $(0, 2 \pm 2\delta)$ and $(\pm 2\delta, 2)$, with

δ being the incommensurability, which are identified as charge-order peaks. The position of the peaks indicates that the stripes are oriented along the vertical and horizontal directions, with a density of one hole per two Cu sites. [See Fig. 1.5(c)] Stripe is now commonly known to exist in La_2CuO_4 doped systems, such as $La_{2-x}Sr_xCuO_4$, and $LaCuO_{4+x}$, [52, 61–63, 76–79] $YBa_2Cu_3O_{7-x}$, [67, 80–87], as well as in $Bi_2Sr_2CaCu_2O_{8+\delta}$ [88, 89]. Besides, the presence of stripe is established in other layered transition-metal oxides. [90–98]

Although the presence of the stripe phase now has little doubt, the role stripe plays in superconductivity remains controversial. They may be crucial, beneficial, or harmful. [60–63, 66, 77, 99–105]. It generally appears that static stripes are antipathetic to bulk superconductivity. The clearest example occurs when $x = 1/8$, where commensurability stabilizes the largest amplitude static stripes in the LNSCO system. [62, 63, 77] This doping corresponds to a local minimum in the curve of T_c-x, as shown in Fig. 1.3. [106] It is an interesting phenomenon in cuprate system known as the "1/8" anomaly, first seen in 1988 by Moodenbaugh *et al.*, who observed a mysterious reduction of T_c around $x = 1/8$ when electrical resistivity measurements in $La_{2-x}Ba_xCuO_4$ were performed. [48] Later on, it is shown that 1/8 anomaly is common to all cuprates. [62, 63, 107–113] Because of 1/8 anomaly, many people believe that the stripe order is a foe to superconductivity. [32, 64, 65]

However, there are indications that stripes may actually be friends to superconductivity. It has been suggested [66] that stripes promote superconductivity if they are not too static. Evidence for a link between fluctuating stripes and superconductivity is provided by Yamada *et al.*, who reported the remarkable linear relationship between T_c and the incommensurability δ. [58] Although first documented in the $La_{2-x}Sr_xCuO_4$ system, there is considerable evidence for the same effect in the YBCO system [67, 68]. It has been suggested that T_c increases if and only if stripes move closer together. A more skeptical view is that T_c and δ increase with x (and saturate near optimal doping) for different reasons. There is a mechanism relating the stripe to the superconductivity in term of spin-gap proximity effect. [66] In this proposal, the superconductivity is sensitive to the magnetic excitations.

Further studies show that the relationship of stripes to superconductivity might be much more complicated than just either a foe or friend. One of the first indications is that a gap appears in the in-plane optical conductivity together with the onset of charge order. [114] Next, photoemission and tunneling measurements provided evidence for a d-wave-like gap at low temperatures, within the stripe ordered phase but above the bulk T_c. [115] These signatures were quite suggestive of superconductivity, and they motivated a careful

examination of transport and susceptibility measurements. [116] The latter study provided evidence that two-dimensional (2D) superconducting correlations coexist with stripe order at a temperature as high as 40 K, even higher than the highest T_c observed in the $La_{2-x}Sr_xCuO_4$ system (32 K), suggesting that stripe order is quite compatible with pairing and superconductivity; however, the three-dimensional (3D) superconductivity does seem to be frustrated by the stripe order. It has been proposed that a sinusoidally modulated superconducting state, minimizing overlap with the spin order, in combination with the 90° rotation of the stripe orientation from one layer to the next, [117] can explain the frustrated Josephson coupling. [118, 119] Independent analyses also indicate that the energy of superconductivity coexisting with charge-stripe order is competitive with that of a uniform d-wave state. [23, 120–123]

With the role of stripe in superconductivity being so controversial, it is definitely worthwhile examining. In § 1.3, I am going to describe the system $La_{2-x}Ba_xCuO_4$ I studied to understand the relationship between stripe and superconductivity.

1.3 Study on $La_{2-x}Ba_xCuO_4$

In above sections, I have briefly introduced what a superconductor is, and a theory, BCS theory, which is quite successful in explaining the low temperature conventional superconductors. As the BCS theory does not work well on the high-T_c superconductors discovered since 1986, a lot of efforts have been put into looking for a high-T_c mechanism, and many theories have been put forward. However, there is still no agreement on the mechanism for the high-T_c superconductors. Nevertheless, more and more people believe that magnetism plays a role in the high-T_c superconductivity, which contradicts the conventional wisdom that these two are incompatible, but what role magnetism plays, and how it plays remain open questions. To study these, $La_{2-x}Ba_xCuO_4$ system is perfect.

Cuprate is an interesting system in one of the senses that an otherwise insulating ceramic can become superconducting when it is doped. Even among such an interesting system as cuprate, it is quite easy to pick up $La_{2-x}Ba_xCuO_4$ for my study for many reasons:

1. Despite the fact that $La_{2-x}Ba_xCuO_4$ is the first high-T_c superconductor system discovered, very limited neutron scattering works have been done on it, unlike its sister system, $La_{2-x}Sr_xCuO_4$, [60–63, 76–79, 124–139] as well as $YBa_2Cu_3O_{7-x}$, [67, 80–87, 140–144] and $Bi_2Sr_2CaCu_2O_{8+\delta}$, [88, 89, 112, 145–152] which are extensively studied with many probes. It

is not because researchers are not interested in studying this system with one of the most powerful tools in characterizing the nature and strength of magnetic correlations, but simply because it is very challenging to grow large single crystals, which are crucial for the success of neutron scattering experiments. To date, there have been only a few measurements on $La_{2-x}Ba_xCuO_4$, [64, 64, 153–156, 156–165] and most of them are on the "1/8" sample because that is one of the few pieces available. Several attempts to grow single crystals of $La_{2-x}Ba_xCuO_4$ by the traveling-solvent floating-zone (TSFZ) method have been reported so far. [166–169] However, the sample availability is still highly limited. And this turns out to be a great opportunity, as well as a challenge.

2. The structure for $La_{2-x}Ba_xCuO_4$ is simpler compared to other cuprate systems. By studying a simple system, one may be able to figure out the more complex systems more easily.

3. The interesting 1/8 anomaly was first seen in $La_{2-x}Ba_xCuO_4$, and the T_c reduction is very strong when $x = 1/8$ ($T_c = 4$ K as shown in Fig. 1.3). This fits very well with the stripe picture, as it is believed that the stripe order in $La_{2-x}Ba_xCuO_4$ is static and strong, and this static order may destroy the bulk superconductivity at this doping level.

4. There have been evidences showing that the stripe order coexists with a special kind of superconducting correlation—2D superconductivity in $La_{2-x}Ba_xCuO_4$ with ($x = 1/8$). [114–116] And this special kind of superconductivity is successfully explained by considering a sinusoidally modulated superconducting state, minimizing overlap with the spin order, in combination with the 90° rotation of the stripe orientation between neighboring layers. [118, 119] The fact that in $La_{2-x}Ba_xCuO_4$ ($x = 1/8$), the superconducting temperature for the 2D superconductivity, T_c^{2D}, is as high as 42 K, higher than that in the optimally-doped $La_{2-x}Sr_xCuO_4$, where no static stripe is present, tends to suggest that the stripe is actually compatible with superconductivity and pairing, or at least compatible with the 2D superconductivity. This contradicts the common belief that stripe is harmful for superconductivity. Therefore, study on this system will be very important and interesting.

1.4 Organization of this Dissertation

The rest of this **Dissertation** is organized as follows:

- In Chapter 2, I will introduce the crystal growth with a floating-zone technique. Neutron scattering techniques, transport and susceptibility measurements, as well as sample preparation will be introduced also in this Chapter.

- In Chapter 3, I will show the results combining neutron scattering and susceptibility and transport measurements on $La_{2-x}Ba_xCuO_4$, demonstrating the interplay between magnetism and superconductivity.

- In Chapter 4, I am going to switch to Iron-based superconductor, an analogue to cuprate. There will be a brief introduction on this new type of superconductor in this Chapter.

- In Chapter 5, neutron scattering and susceptibility measurements on $Fe_{1+y}Te_{1-x}Se_x$ will be presented. The role of magnetism in superconductivity will be examined using $Fe_{1+y}Te_{1-x}Se_x$, and comparisons will be made with $La_{2-x}Ba_xCuO_4$.

- In Chapter 6, I will summarize the results on two superconductor systems, $La_{2-x}Ba_xCuO_4$ and $Fe_{1+y}Te_{1-x}Se_x$. Future studies on these two systems will be also sketched.

Chapter 2

Materials and Methods

In this Chapter, I will introduce the floating-zone technique that I used to grow the $La_{2-x}Ba_xCuO_4$ crystals, and other techniques used to characterize the samples. Also, neutron scattering technique will be discussed.

2.1 Sample preparation

As described in Chapter 1, it is a great challenge to grow large-size, high-quality single crystals for $La_{2-x}Ba_xCuO_4$. Without these crystals in hand, it is not feasible to do neutron scattering experiment. Although neutron scattering is powerful in probing the magnetic correlations, the interaction and the neutron flux are weak, so the magnetic signals from samples are weak, which requires large-size samples to collect reasonable data in a given limited time. In the following section, I will describe the traveling-solvent-floating-zone (TSFZ) technique I used to grow the $La_{2-x}Ba_xCuO_4$ samples, and related methods characterizing the samples.

2.1.1 Crystal growth with floating-zone technique

The technique I am using is the TSFZ method. [151, 169–182] The major advantage of this technique is that crystals can be grown without contact of other materials, such as crucibles, which eliminates a major source for contaminations. Crystals with high melting point as well as a large length can be grown. The latter is particularly important in the case of incongruent melting systems, where large deviations between the nominal composition and that of the grown crystal are observed at the beginning of the growth.

There are two image furnaces in our lab, each of which is equipped with two ellipsoidal mirrors, with surface sprayed with gold, as shown in Fig. 2.1(a).

In Fig. 2.1(b), I plot the vertical cross section of the floating-zone furnace. Inside the mirrors, two Halogen lamps used as heat sources are installed in the mirrors' outer focuses. Their light is reflected into the inner focus, which for both mirrors coincides with the location of the melt. The melt is situated between the polycrystalline feed rod (upper shaft) and the seed rod (lower shaft), and held in place by surface tension, only. Feed rod and growing crystal spin in opposite directions to guarantee a homogenous melt as well as a homogenous temperature distribution in the melt. Feed rod, melt and crystal are located within a sealed quartz tube, which allows performing crystal growth in a controlled atmosphere. Crystal growth is initiated by a slow downward translation of the feed rod and the lower shaft, which effectively corresponds to a melt traveling along the feed rod. The optimum/maximum growth speed depends on the material and varies between a few tenths of a millimeter and several centimeters per hour. The diameter of the crystal is controlled by the diameter of the feed rod, and the ratio of the translation velocity for the feed and seed rod.

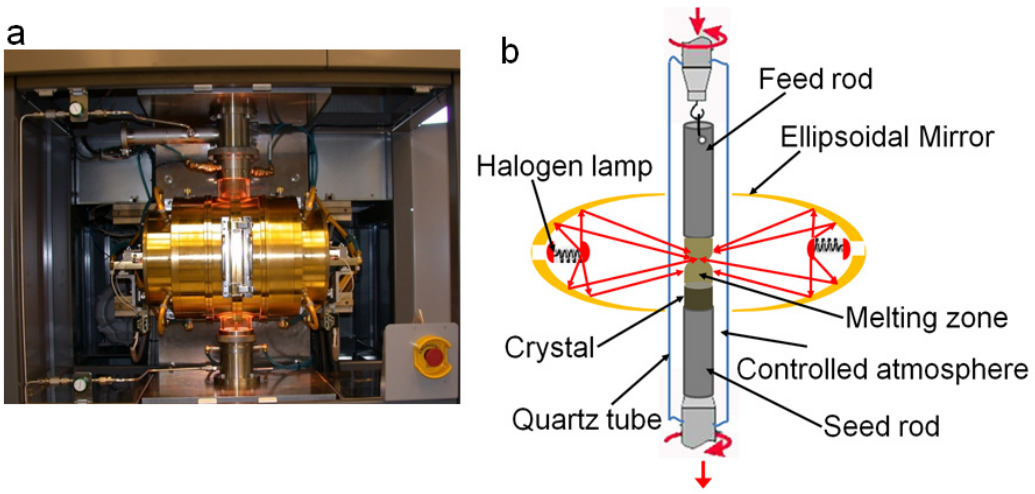

Figure 2.1: (a) The front of an image furnace used in TSFZ technique, and (b) schematic of the vertical cross section of the floating-zone furnace.

For growing $La_{2-x}Ba_xCuO_4$, La_2O_3, $BaCO_3$, and CuO powders were used as raw materials of the feed rod and the solvent. For the feed rod, the powders were mixed in their metal ratios. Extra CuO was added to the powders in order to obtain tightly sintered feed rods in the sintering process and also to compensate for evaporated Cu during the growth. (The amount for extra CuO depends on the growth temperature, which can be seen from Table 2.1.)

The mixed powders were then ground in an agate mortar and calcined in air at 970 °C for 24 hrs. Then the process was repeated twice to obtain homogeneous powders. The fine powders obtained were put into thin-walled rubber tubes and formed into cylindrical rods under a hydrostatic pressure of 4 kbars. The dimensions of the rods were 6-8 mm in diameter and 250 mm in length, typically. One of the most serious problems in the growth process is deep penetration of the molten zone into the feed rod, which makes the molten zone unstable. To avoid this, it is important for the feed rod to be sintered to achieve as higher density as possible. Therefore, we tested the sintering temperature for each composition and the final sintering was performed under the optimized temperature results for 24 hrs in air. For the solvent, the composition of the raw materials was richer in Cu; typically $La_{1.7}Ba_{0.3}Cu_4O_x$ in the molar ratio. The solvent was calcined at 900 °C and then cut into small pieces. About 0.4 g was used for each growth. The seed rods were prepared either in the same way for preparing feed rods or cut from feed rods, and used to hold the solvent and the melted zone.

Then the seed rod, solvent and feed rod were put into the image furnace and grown under certain O_2 pressure. The zone traveling rate was 1.0 mm/hr and the rotation speed of the feed rod and the grown crystal was 30 rpm in the opposite direction. The whole growth process is summarized in Fig. 2.2 and some of the conditions are listed in Table 2.1. Some trends can be seen from Table 2.1: with increasing Ba doping, the melting point for the compound decreases, which requires less extra CuO to compensate the evaporations; the higher the Ba doping, the higher the pressure it needs. At present, the highest pressure we can reach is 11 bars in our system.

Table 2.1: Some conditions for $La_{2-x}Ba_xCuO_4$ growth. x, Ba doping; T, sintering temperature; y, extra CuO, and P, oxygen pressure.

x (%)	T (°C)	y (%)	P (bars)
2	1260	3	2
4	1260	2.5	2
9.5	1260	2	4
11.5	1257.5	1	11
12.5	1255	0.5	11
13.5	1240	0.5	11
15.5	1225	0	11
16.5	1220	0	11

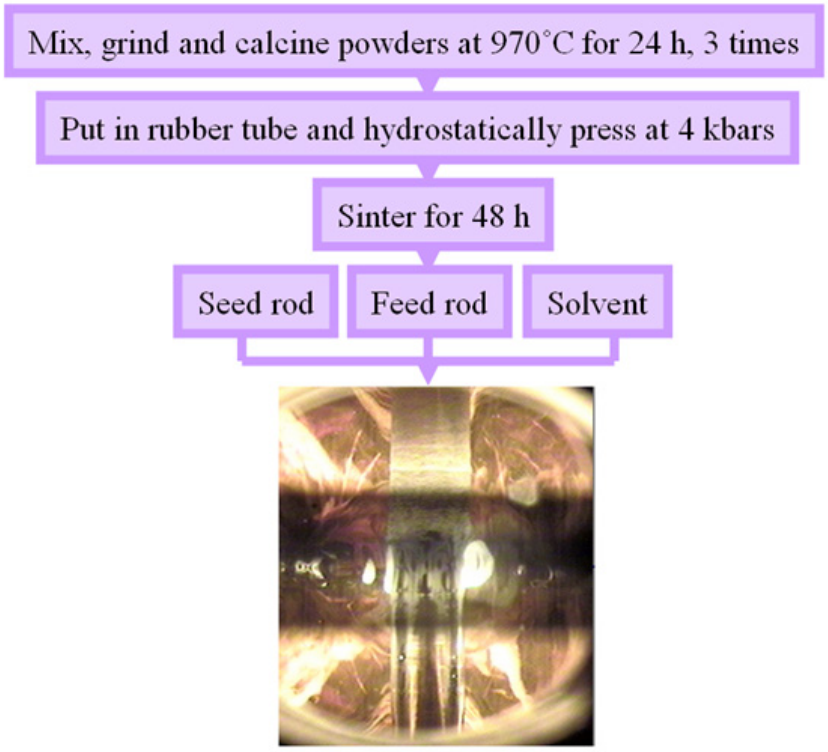

Figure 2.2: A flow chart example of the growth process for $La_{2-x}Ba_xCuO_4$ with TSFZ technique, as described in the text.

2.1.2 Sample characterization

Fig. 2.3(a) shows an entire as-grown crystal rod for $La_{2-x}Ba_xCuO_4$ ($x = 13.5\%$), with c axis roughly perpendicular to the growth direction. The next thing one should do is to check the quality of the crystal. For the crystal shown in Fig. 2.3(a), for the initial part of the rod (0 cm- 6 cm), the growing conditions are not optimized, and the growth is not stable. Therefore, the size of the crystals is not large and the composition may not be right (being affected by the solvent composition). With growth continuing, the crystal composition is approaching the feed rod composition by equilibrium diffusion. The [110] direction is the fastest growth direction for $La_{2-x}Ba_xCuO_4$. [169] Thus the individual crystal growing along [110] direction shall become larger and larger; on the other hand, crystals with other growing directions become smaller and smaller. At a certain point, the growth becomes stable and eventually, one individual crystal will occupy the whole cross section. This can be examined by an optical polarization microscope under which differently oriented crystals

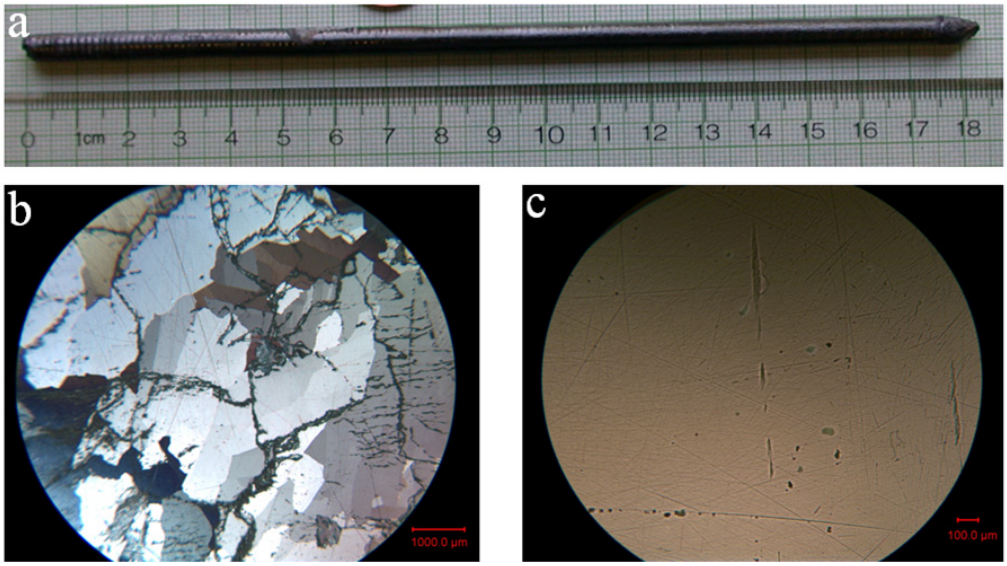

Figure 2.3: $La_{2-x}Ba_xCuO_4$ ($x = 13.5\%$) crystal grown with TSFZ technique. (a), as-grown rod , and its cross section for the starting part (b), and ending part of the growth (c).

appear with different colors. For differently oriented crystals, their optical axes are different and reflect the light in different ways. By using a polarizer and an analyzer, one can observe the contrast (from the difference of light phase and intensity) indicated by different colors (to be more precise, the brightness). Fig. 2.3(b)&(c) are the microscopic images for the bottom and top part's polished cross sections. In Fig. 2.3(b), the cross section consists of many small crystals, indicated by domains of different brightness in the image, while in Fig. 2.3(c), only one large crystal spreads across the whole cross section.

Single crystals were identified and extracted based on the microscopic images. The composition of the crystals and the sample homogeneity are known by measuring the static magnetic susceptibility with a superconducting-quantum-interference-device (SQUID) magnetometer. It is actually counting the flux quantum, which is quite small, and allows one to perform the magnetic measurements accurately. The magnetization was measured under zero-field-cooling (ZFC) and then heat up in the field. For a superconductor, it enters the Meissner state below T_c, and expels the magnetic flux, which can be measured by the SQUID, therefore, one is able to tell the T_c for a particular sample. For $La_{2-x}Ba_xCuO_4$ samples which are not superconducting and have antiferromagnetic transition, the magnetization will peak at the transition temperature called Néel temperature T_N. By comparing the phase diagram obtained from

the the polycrystalline samples for $La_{2-x}Ba_xCuO_4$, [48] we will be able to know the Ba concentrations. By looking at whether the transition is sharp or not, one will be able to know whether the sample is homogeneous or not, roughly. The magnetization data also tells you the Meissner shielding volume fraction, which can be used to estimate the superconducting volume fraction (V). For a good superconductor, it should have V close to 100%.

After checking the crystals' quality, they can be pre-aligned with backscattering Laue x-ray. [a] The quality of the samples can also be confirmed in neutron scattering measurements. (It is important to note that neutrons probe the entire crystal volume.) When we align the samples with neutrons, the rocking curve for a certain Bragg peak usually turns out to have a full-width-at-half-maximum (FWHM) of $< 1^\circ$, showing that the mosaic distribution is approximately Gaussian and reasonably narrow, thus confirming that the crystal is single domain.

2.1.3 Results of crystal growth

Lots of efforts have been put on crystal growth and $La_{2-x}Ba_xCuO_4$ crystals with doping ranging from $x = 0$ to 0.155 are now available for measurements.[b] For $La_{2-x}Ba_xCuO_4$ ($x = 0$), it is antiferromagntic insulator. For $x = 0.02$ and 0.04, they are in the spin-glass regime, where susceptibility shows a cusp and hysteresis. All other crystals ($x \geq 9.5\%$) are superconducting. By performing the magnetization measurements on the superconducting samples, one can obtain the T_c's as shown in Fig. 2.4(b). For these superconducting samples, their T_c's and estimated superconducting volume fraction (V) are listed in Table 2.2. With these high-quality single crystals, neutron scattering experiments can be performed.

2.2 Neutron scattering technique

2.2.1 Principle of neutron scattering

Neutron scattering is powerful tool in studying the magnetic correlations. Neutrons are neutral nuclear particle with both particle- and wave-like properties. Some of the properties are listed in Table 2.3, [183–185] where the nuclear

[a] X-ray hits a crystal, and then backscatters to a camera. For different crystal orientation with respect to the direction of the incident x-ray, they will have different patterns, so that we will be able to know the crystal orientation by analyzing the pattern. We can also rotate the crystal to the orientation we need and check with x-ray again.

[b] We have not managed to get large single crystals for $La_{2-x}Ba_xCuO_4$ ($x = 0.165$).

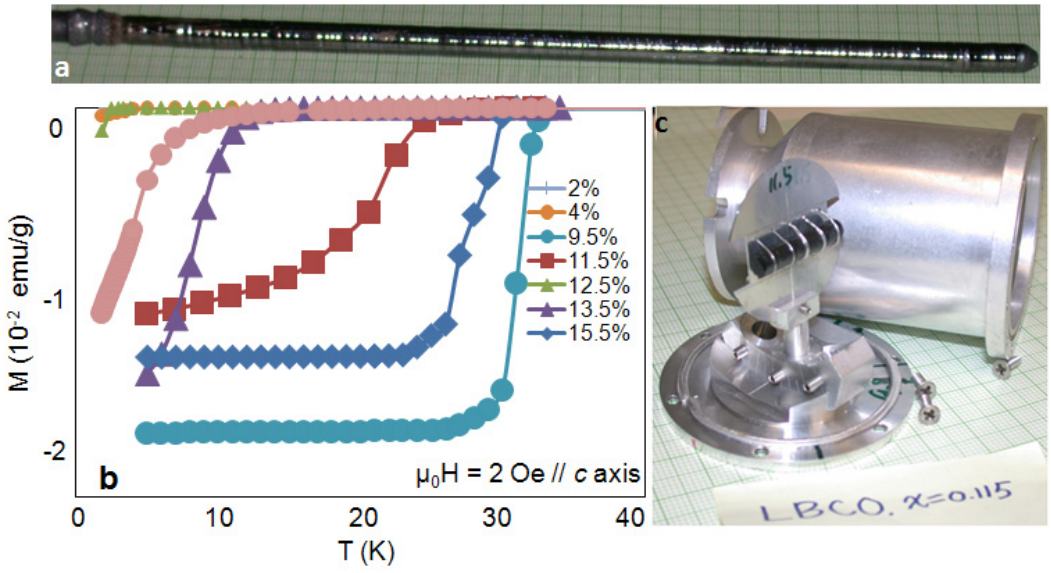

Figure 2.4: $La_{2-x}Ba_xCuO_4$ crystals grown with TSFZ technique. (a), an as-grown rod for $La_{2-x}Ba_xCuO_4$ ($x = 0.115$); (b), magnetic susceptibility measured with 2 Oe magnetic field parallel to the c axis of the $La_{2-x}Ba_xCuO_4$ crystals with x ranging from 2% to 16.5%; (c) one section cut from the as-grown rod of $La_{2-x}Ba_xCuO_4$ ($x = 0.115$), and pre-aligned with Laue x-ray, with c axis pointing vertically. The sample is mounted on the sample holder, which has 4 degrees of freedom (rotation, tilt along and perpendicular to the arc, and height), and by adjusting the way of mounting the sample, one can reach desired orientation. An aluminum can is shown aside the sample, which we used to contain the sample, and mounted the sample onto a displex.

magneton, $\mu_N = e\hbar/2m_p = 5.051 \times 10^{-27}$ J·T^{-1}, with e being the charge of an electron, $\hbar$ is the Planck's constant h divided by 2π, and m_p is the mass a proton. k is the wave vector defined by $2\pi/\lambda$, where λ is the wavelength for neutron with the unit of angstrom (Å).

Neutrons have many advantages for studying material properties, especially the magnetic properties. For instance, their wavelength is comparable with interatomic spacings, and the kinetic energy is comparable with that of atoms in a solid; neutrons interact with atomic nuclei via very short range (fm) forces, thus they can penetrate well into the sample, which allows bulk properties to be measured; their weak interaction with matter aids interpretation of scattering data; the isotopic sensitivity allows contrast variation; most importantly, neutrons have magnetic moment which interacts with magnetic

Table 2.2: Superconducting properties of the $La_{2-x}Ba_xCuO_4$ samples.

x (%)	T_c (K)	V (%)
9.5	32	100
11.5	25	55
12.5	4	<1
13.5	13	28
15.5	30	100
16.5	10	18

Table 2.3: Properties of neutrons.

mass m_n	1.675×10^{-27} kg
spin	1/2
charge	0
magnetic dipole moment μ_n	$-1.913\mu_N$
energy $\hbar\omega$ (meV)	$2.072k^2$

fields caused, *e. g.*, by unpaired electron spins in a material.

There are two types of neutron scattering process as illustrated in Fig. 2.5(a) and (b): elastic, where the final energy of neutrons $E_f = E_i$, the initial energy; when $E_f \neq E_i$, *i. e.*, there is energy transfer into the sample, it is called inelastic neutron scattering. Here, the laws of conservation determine the energy transferred to the sample, E and the wave vector $\mathbf{Q}$,

$$E = E_i - E_f, \mathbf{Q} = k_f - k_i, \tag{2.1}$$

and,

$$E_i = \frac{(\hbar k_i)^2}{2m_n}, E_f = \frac{(\hbar k_f)^2}{2m_n}. \tag{2.2}$$

For us, it is more convenient to express energy in $\hbar\omega$, with ω being the frequency. The wave vector transfer $\mathbf{Q} = 2\pi/d$, where d is the interatomic spacing. For elastic scattering, one obtains the Bragg law from Eq. 2.1, or by studying the scattering triangle in Fig. 2.5(a):

$$\frac{2\pi}{d} = 2 \times \frac{2\pi}{\lambda} \sin\theta, \tag{2.3}$$

thus,

$$2d \sin\theta = \lambda, \tag{2.4}$$

where θ is the scattering angle.

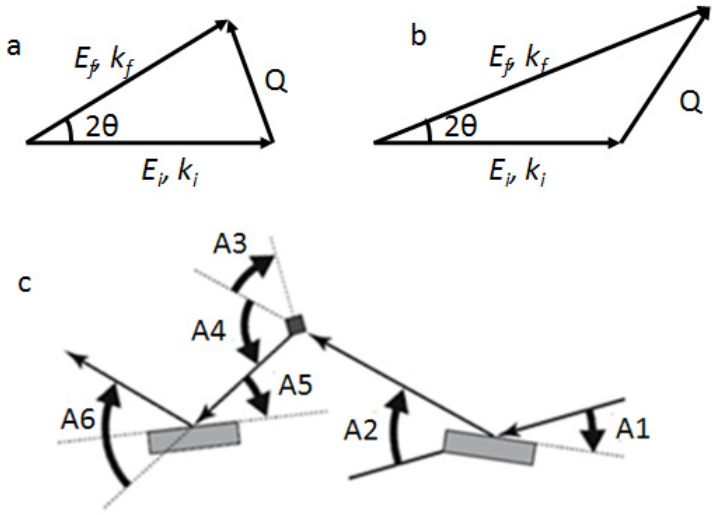

Figure 2.5: Schematic of (a) elastic , and (b) inelastic neutron scattering; (c), a triple-axis spectrometer. E_i, k_i, and E_f, k_f, energy and wave vector for incident and scattered neutrons. $\mathbf{Q}$, wave vector transfer. θ, scattering angle. A1-6 are angle pairs for three axes, monochromator, sample, and analyzer axis, as explained in the text.

Before further proceeding, it is necessary to introduce some formulae for neutron scattering, which are available in Refs. [183–191]. For nuclear Bragg scattering, the intensity I satisfies:

$$I(\mathbf{Q}) \propto N|F(\mathbf{Q})|^2, \tag{2.5}$$

where N is the number of unit cells, and $F(\mathbf{Q})$ is the structure factor,

$$F(\mathbf{Q}) = \sum_j \bar{b}_j \mathrm{e}^{-i\mathbf{Q}\cdot R_j}, \tag{2.6}$$

where $\bar{b}_j$ and R_j are the coherent scattering length and the position of a particular nucleus respectively. Neutron has a magnetic dipole moment equals to $-\gamma\mu_N$, where γ is the gyromagnetic ratio and equal to 1.913, so that neutron can scatter from the magnetic moment of an atom via the dipole-dipole interaction and can be used to probe magnetic structure. For magnetic elastic scattering, the intensity of magnetic Bragg peaks $I_M(\mathbf{Q})$ can be expressed as

follows using the ordered magnetic moment μ,

$$I_M(\mathbf{Q}) = p^2 n^2 \mu^2 \sin^2\beta |F(\mathbf{Q})|^2. \tag{2.7}$$

In this formula,

$$p = \frac{\gamma r_0}{2} g f(\mathbf{Q}), \tag{2.8}$$

where r_0 is the classical electron radius, g is the Landé splitting factor (g=2 for spin-only moment), and $f(\mathbf{Q})$ is the the $\mathbf{Q}$-dependent magnetic form factor. The parameters n, and β, represent the number of spins in a magnetic unit cell, and the angle of the spins with respect to the scattering vector respectively. For inelastic scattering, the differential scattering cross-section with respect to the corresponding phase variables, defined by the phase space density of the scattered current, normalized to the incident flux is used. The one most commonly measured and calculated is the double differential scattering cross-section, which can be obtained by Fermi's Golden Rule,

$$\left.\frac{d^2\sigma}{d\Omega dE_f}\right|_{s_i \to s_f} = (\frac{m_n}{2\pi\hbar^2})^2 \frac{k_f}{k_i} \left| V(\mathbf{Q}) \left\langle s_f \left| \sum_l \mathrm{e}^{i\mathbf{Q}\cdot\mathbf{r}_l} \right| s_i \right\rangle \right|^2 \delta(\hbar\omega + E_i - E_f). \tag{2.9}$$

Here, V is the interaction operator for the neutron with the sample, and s_i and s_f are the quantum numbers for the initial and final states of the sample. By averaging over initial states and summing over final states, and letting $P(s_i)$ being the statistical weight factor for initial state $|s_i\rangle$, then,

$$\frac{d^2\sigma}{d\Omega dE_f} = \frac{k_f}{k_i} \sum_{s_i, s_f} P(s_i) \left| \left\langle s_f \left| b \sum_l \mathrm{e}^{i\mathbf{Q}\cdot\mathbf{r}_l} \right| s_i \right\rangle \right|^2 \delta(\hbar\omega + E_i - E_f). \tag{2.10}$$

For magnetic scattering,

$$\frac{d^2\sigma}{d\Omega dE_f} = \frac{N}{\hbar} \frac{k_f}{k_i} p^2 \mathrm{e}^{-2W_{\mathbf{Q}}} S(\mathbf{Q}, \omega). \tag{2.11}$$

where $\mathrm{e}^{-2W_{\mathbf{Q}}}$ is the Debye-Waller factor, and $S(\mathbf{Q}, \omega)$ is the dynamical scattering function, and,

$$S(\mathbf{Q}, \omega) = \sum_{\alpha,\beta} (\delta_{\alpha,\beta} - \mathbf{Q}_\alpha \mathbf{Q}_\beta / \mathbf{Q^2}) \mathbf{S}^{\alpha\beta}(\mathbf{Q}, \omega). \tag{2.12}$$

Here,

$$S^{\alpha\beta}(\mathbf{Q},\omega) = \frac{1}{2\pi}\int_{-\infty}^{\infty} dt\, \mathrm{e}^{-i\omega t} \sum_r \mathrm{e}^{iQ\dot{r}} \langle S_o^\alpha(0) S_r^\beta(t)\rangle. \tag{2.13}$$

Here $S_r^\beta(t)$ is the $\beta(= x, y, z)$ component of the component of the atomic spin at lattice site r and time t, and the angle brackets, $\langle\cdots\rangle$ denote an average over configurations. $S(\mathbf{Q},\omega)$ is related to the imaginary part of the dynamical spin susceptibility, $\chi''(\mathbf{Q},\omega)$ via the fluctuation-dissipation theorem,

$$S(\mathbf{Q},\omega) = \frac{1}{1-\mathrm{e}^{-\hbar\omega/k_BT}}\chi''(\mathbf{Q},\omega)\,, \tag{2.14}$$

where $(1-\mathrm{e}^{-\hbar\omega/k_BT})^{-1}$ is referred to as Bose factor, or detail-balance factor.

From Eqs. 2.6, 2.7, 2.10, and 2.11, it can be seen that by doing neutron scattering experiment, one can obtain information on the static lattice and magnetic structure (elastic neutron scattering) as well as motion of lattice and spins (inelastic neutron scattering), *i. e.*, phonons, and magnetic excitations in a material.

2.2.2 Triple-axis spectrometer

There are several neutron scattering instruments such as triple-axis, time-of-flight, backscattering, and neutron-spin-echo spectrometers. Triple-axis spectrometer is the instrument I used most, and here I will focus on this type of instrument. It is the most versatile and convenient instrument for use in a scattering experiment because it allows one to probe nearly any coordinates in energy and momentum space in a precisely controlled manner. The three axes correspond to the axes of rotation of the monochromator, the sample, and the analyzer, as illustrated in Fig. 2.5(c). The incident neutron wave vector k_i is selected by Bragg reflection on a crystal monochromator (determined by A1 and A2 in the figure). The orientation of the vector k_i in the sample's reciprocal space is controlled by orienting the sample with respect to it [rotation around a vertical axis (A3) plus double-goniometer or eulerian cradle]. The analyzer performs a similar function for the scattered or final beam as the monochromator—select the scattered wave vector k_f by Bragg reflection on a crystal analyzer (A5, A6). The orientation of the vector k_f in the the reciprocal space is determined by the value of the scattering angle at the sample position (A4).

2.3 Summary

In this chapter, I discussed the floating-zone technique, which I used to grow the $La_{2-x}Ba_xCuO_4$ single crystals, as well as neutron scattering technique, which is powerful in studying the magnetic correlations. I have also shown that I have successfully grown high-quality, large-size $La_{2-x}Ba_xCuO_4$ single crystals by the TSFZ method, with Ba concentration ranging from $x = 0$ to 0.155. With these crystals on hand, and knowledge on neutron scattering, study on the interplay between stripe order and superconductivity can be performed.

Chapter 3

Stripe and Superconductivity in $La_{2-x}Ba_xCuO_4$

In this Chapter, I will present some of our neutron scattering results on $La_{2-x}Ba_xCuO_4$, demonstrating the correlations between stripes and superconductivity in this system. Some of the results here have been published in Refs. [151, 192, 193], and some of them are to appear. [194–198]

The neutron experiments were done on SPINS (at NCNR, National Institute of Standards Technology), HB1, and HB1A (at HFIR, Oak Ridge National Laboratory). All three are triple-axis spectrometers. For elastic scattering measurements, Be [pyrolytic graphite (PG)] filters were put before and after the sample to eliminate higher-order neutrons (neutrons with shorter wavelength, λ/n, and $n > 1$). For inelastic measurements, only one filter was put after the sample. Elastic scans were performed with $E_i = E_f$ (= 5 meV on SPINS, 13.5 meV on HB1, and 14.7 meV on HB1A) mode and inelastic scans were done with fixed E_f, and varying E_i. The samples are mounted with $(HK0)$ zone parallel to the scattering plane. $(HK0)$ is defined with vectors [100] and [001] in tetragonal notation. Data are described in terms of reciprocal lattice unit (r.l.u.), where 1 r.l.u. $= a^* = b^* = 2\pi/a = 1.661$ Å^{-1} ($a = 3.78$ Å).

3.1 Doping dependence

The fact that superconductivity appears after the suppression of antiferromagnetic order makes many people believe that magnetic fluctuations are promoting the superconductivity, and the static magnetic order is competing with the superconductivity. [32, 62–65] These arguments seem to hold for the the magnetic correlations in "stripe" form—the static stripe order is harmful

for bulk superconductivity, while the dynamic stripes are believed essential for superconductivity. [62, 154] To examine this, we picked four samples with Ba concentrations at and around "1/8", where the strongest suppression of superconductivity [48] and the presence of strong static stripe order have been observed [156]—0.095, 0.115, 0.125, and 0.135.

In fact, static stripe order has been mostly observed in compounds with low-temperature-tetragonal (LTT) symmetry. [62, 156, 159, 199–201] We have measured the transition temperatures from low-temperature-orthorhombic (LTO) to LTT phase in the four samples, and the results are shown in Fig 3.1(a). Except for the 0.095 sample, we obtained the results by sitting on (100) Bragg peak and counted the intensity at different temperatures. For the 0.095 Ba doped sample, we got the results by plotting the (100) peak intensity (obtained from scans along the peak) as a function of temperature. (100) Bragg peak is forbidden in LTO but not in LTT phase, therefore, when the sample is cooled through the phase transition temperature, T_S, the (100) Bragg peak intensity increases abruptly, as can be clearly seen in Fig 3.1(a). For these four samples, T_S's are 32, 52, 54 and 55 K respectively.

In all four samples, we observed static spin-stripe order, and scans through one of the four superlattice peaks at 5 K are plotted in Fig. 3.2. We can get incommensurability δ for the four samples, which are 0.105, 0.115, 0.118, and 0.120 r.l.u. respectively. The correlation between δ and the doping x has been predicted from the similarities to other cuprates such as $La_{2-x}Sr_xCuO_4$ and $YBa_2Cu_3O_{7-x}$: when hole doping is less than 1/8, $\delta \approx x$ and saturates at 1/8 at that point. [52, 54, 55, 58, 59, 62, 63, 67, 76, 80, 82] Since δ is proportional to the inverse of the charge modulation period, the $\delta \sim x$ behavior suggests that the amplitude of the charge modulation remains constant while the period decreases with increasing x. This is consistent with an effective segregation of the doped holes, such that an initially antiferromagnetic CuO_2 plane is broken up into antiferromagnetic stripes, with the stripes becoming narrower as the hole density increases. In the saturated region, where the charge stripes are separated by about 4 lattice spacings, it seems unlikely that added holes would be forced into the existing stripes, increasing the hole density per stripe. It seems more likely that the added holes will form uniformly-doped regions, so that, with increasing x, the fractional area occupied by stripes at any point in time will decrease.

As for the strength of the spin stripe, it is quite clear that the order is strongest in the "1/8" sample, and weakest in the 0.095 Ba doped sample. For 0.115, 0.125, and 0.135 samples, there are very well-defined peaks, while for the 0.095 sample, the peak is broad, and not well defined. It is clear that the intensity for the "1/8" doped sample is strongest, which has lowest T_c, while

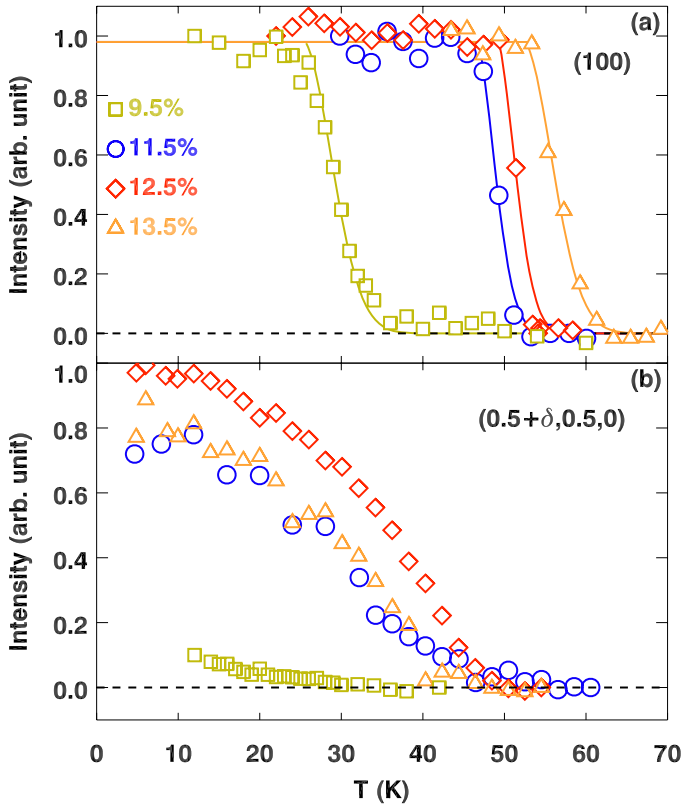

Figure 3.1: Temperature dependence of the intensity for (a) (100) Bragg peak, and, (b) super lattice peak (0.5+δ,0.5,0) corresponding to the spin-stripe order for $La_{2-x}Ba_xCuO_4$ with $x = 0.095$, 0.115, 0.125 and 0.135. The stripe-order peak intensity has been normalized to the results of the 0.125 sample. Lines through data are guides to the eyes.

the 0.095 doped sample has lowest intensity but highest T_c. The intensity for the 0.095 sample is only $\sim 1/10$ of that for the 1/8 sample. It clearly suggests that the more ordered the static spin stripe is, the stronger the T_c reduction will be. This conclusion is completely consistent with previous results showing that the static stripe order is "bad" for bulk superconductivity. [32, 62–65]

The spin-spin correlation lengths ξ can also be estimated from the peak width fitted with a Lorentzian function convoluted with the resolution function. For 0.095 sample, the peak is very broad, and the correlation length is the shortest, $\sim$ 100 Å; for 0.115 and 0.135 samples, $\sim$ 160 Å, and $\sim$ 200 Å for the 0.125 sample. Again, the trend is clear that, ξ for the 0.125 sample is the largest, while it is the smallest for the 0.095 sample, which serves as another evidence that the static spin-stripe order is competing with the bulk

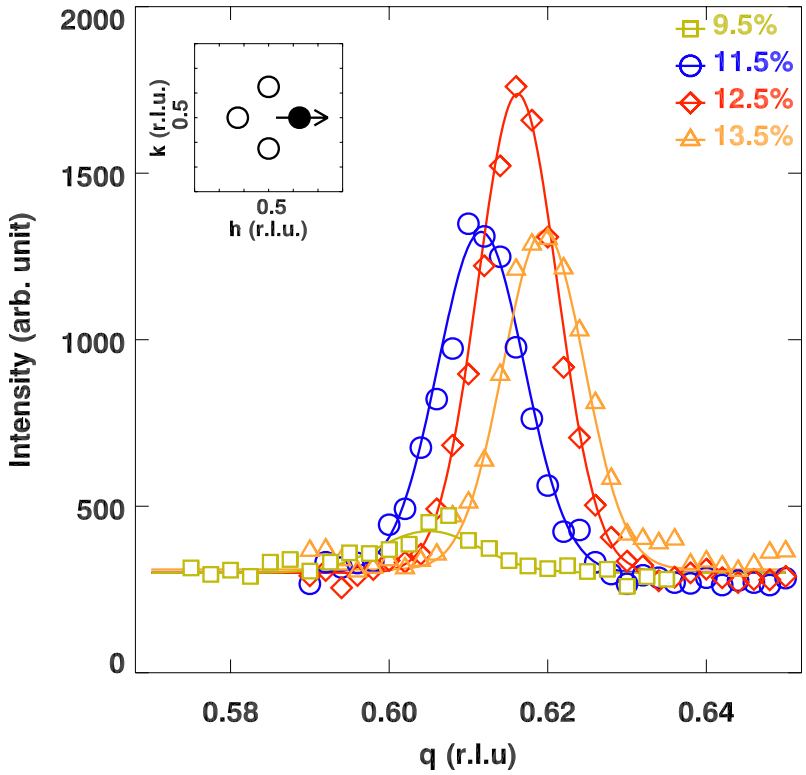

Figure 3.2: Scans through one of the magnetic peak $(0.5 + \delta,0.5,0)$ (see the inset) for four Ba concentrations, 0.095, 0.115, 0.125, and 0.135, with scan direction indicated by the arrow in the inset. Errors represent square root of the counts. Lines are fits to the data with Lorentzian function convoluted with the resolution function. The peak intensity has been normalized to the results of the 0.125 sample.

superconductivity.

The spin-order peak intensities for these four samples are plotted as a function of temperature in Fig. 3.1(b). The peak intensity is extracted from the scans at various temperature and is normalized to the results of the 1/8 sample. The onset of the stripe-order peak intensity are $\sim$ 30 K, for 0.095, and $\sim$ 50 K for other three samples. It appears that these temperatures are higher than the actual stripe ordering temperature T_{so}, which can be obtained from examining the temperature dependence of the peak width. It is because that it picks up some low-energy spin fluctuations at higher temperatures, which will be discussed in later section. Except for the 1/8 sample, others do not have well-defined width vs. temperature curve, *i. e.*, the development of the stripe order in other compositions is not as good as in the 1/8. Nevertheless,

we can estimate the T_{so}'s to be $\sim$ 30, 36, 42, and 35 K for the four samples, with the highest T_{so} at 1/8, and the lowest T_{so} at 0.095. The development of the stripe order in the 1/8 will be further discussed in § 3.2.

The doping x, T_c, charge and spin ordering temperature T_{co}, and T_{so}, incommensurability δ, normalized spin-order peak intensity I_{so} at 5 K, and correlation length ξ at 5 K are summarized in Table 3.1. From the table, it is quite clear that the static spin-stripe order coexists with the superconductivity, and in the meantime, competes with it. It appears that the 0.095 and 1/8 samples are the most interesting ones—one has the highest T_c and the weakest stripe order, while the other is the opposite, so we did further measurements on these two samples, as shown in the following sections.

Table 3.1: Doping dependence of the T_c and the stripe order in $La_{2-x}Ba_xCuO_4$.

x (%)	T_c (K)	T_S (K)	T_{so} (K)	δ (r.l.u.)	I_{so}	ξ (Å)
9.5	32	33	30	0.105	0.1	100
11.5	15.5	50	36	0.115	0.8	160
12.5	4.15	53	42	0.118	1	200
13.5	10.5	55	35	0.120	0.8	160

3.2 Spin dynamics in $La_{1.875}Ba_{0.125}CuO_4$

For optimally-doped cuprates, the most dramatic change in the magnetic scattering with temperature is the opening of a spin gap, with redistribution of spectral weight from below to above the gap. A clear example of this has been presented by Christensen *et al.* [139] for $La_{2-x}Sr_xCuO_4$ with $x = 0.16$. This is a nearly optimally doped sample without static order, so it is fair to ask whether there is a spin gap for $La_{2-x}Ba_xCuO_4$, where static stripe order is present. In order to answer this question, we performed inelastic neutron scattering measurements on the 1/8 sample, where the stripe is most ordered.

We performed inelastic scans at one superlattice peak (0.618,0.5,0) along tetragonal [100] direction with several energies under different temperatures. It has been shown that the spin dispersion in 1/8 sample has an "hour-glass" shape and the incommensurability becomes commensurability only at an excitation energy called resonance energy $E_r \approx$50 meV [62, 155]. The spectral weight is greatly enhanced at "E_r", but the origin of the enhancement is not clear yet. Within the energy range 0.5-3 meV we used, the magnetic

peaks are incommensurate in **Q**. We integrated the intensity for the constant-energy scans, and converted the integrated intensity to the susceptibility, χ'' by Eqn. 2.14, and the results are shown in Fig. 3.3.

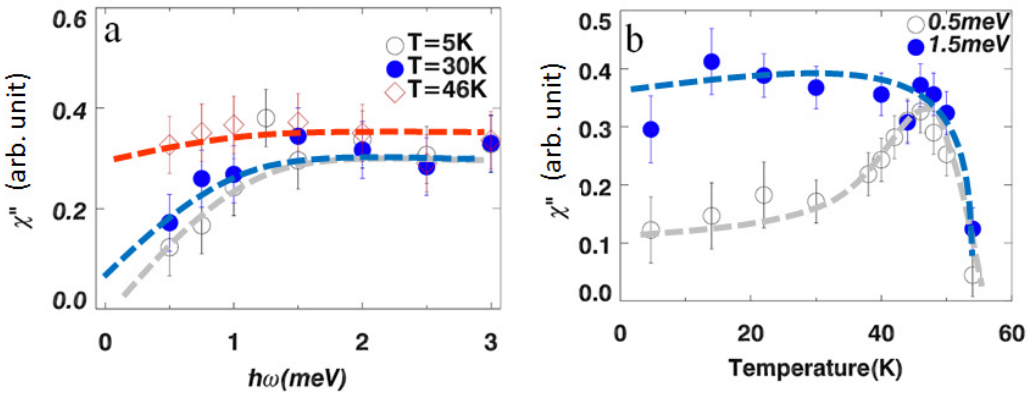

Figure 3.3: The susceptibility χ'' converted from the constant-energy **Q** scan around (0.618,0.5,0) along [100] for different energies and temperatures. Lines are guide to the eyes, as described in the text.

Figure 3.3(a) shows the susceptibility χ'' as a function of excitation energy and in Fig. 3.3(b) I plotted χ'' vs. temperature. In Fig. 3.3(a), at T = 46 K, where the nominally elastic scattering is very weak, we find that χ'' remains almost constant during the whole energy range within the error bar, which is consistent with a previous study which shows that this is the case in the 3-12 meV energy range. [156] There appears to be a slight hump around 1.25 meV and indications of a falloff below 0.5 meV. For reference, the dashed line through the data corresponds to

$$\chi''(\omega) = 0.32\tanh(\hbar\omega/\Gamma) + 0.16\frac{\hbar\omega/\Gamma'}{(\hbar\omega)^2 + \Gamma'^2}, \tag{3.1}$$

with Γ = 0.4 meV and Γ' = 0.5 meV; the energy resolution of the measurement is 0.4 meV (FWHM). If we overlook the small variations with energy, the general behavior is quite similar to what one would expect for spin waves in a 2D antiferromagnet even though muon spin relaxation (μSR) and magnetization studies indicate the absence of order. Thus, it appears that we have an effective spin-liquid state (spatially modulated by the charge-stripe order) at 46 K. Note that our spin-liquid state is distinct from the much-discussed quantum spin liquid. [202] For 30 and 5 K, χ'' drops at $\sim$ 1.25 meV after a plateau from 3-1.5 meV, which suggests the presence of a gap. Below 46 K,

the spectrum weight is shifted to $E = 0$, to the elastic magnetic peak. At low temperature with a gap, the curves through the data in Fig. 3.3(a) correspond to

$$\chi''(\omega) = 0.16 \left[1 + \tanh \left(\frac{E - E_g}{\Gamma} \right) \right], \tag{3.2}$$

with $E_g = 0.5$ meV at 30 K and 0.7 meV at 5 K. For more detailed characterization of the temperature dependence of the gap, we compare χ'' at 0.5 and 1.5 meV vs. temperature in Fig. 3.3(b). The values are comparable between T_{co} and T_{so}, indicating a modulated spin-liquid state throughout this regime. Near T_{so}, $\chi''(0.5$ meV) starts to decrease, while $\chi''(1.5$ meV) stays roughly constant, indicating the opening of the gap. Furthermore, the observation of almost-gapless spin excitations for $T_{so} < T < T_{co}$ is consistent with the appearance of anisotropy in the bulk susceptibility for $T < T_{co}$. [158]

The gap observed here is intriguing since a spin gap frequently appears in the superconducting state at least for optimal doping and above. [81, 83, 136, 141, 143, 203–205] By focusing on the spin-gap energy E_g, it is possible to identify a correlation between magnetic excitations and T_c that applies to a variety of cuprates. [46] It has been argued that the magnetic excitation spectrum observed in the cuprates is associated with stripe correlations, and dynamic stripes may not only underlie the superconductivity in the hole-doped cuprates, but also be an essential component of the superconductivity. [206] The spin-gap proximity effect is based on this sort of picture. [66] The correlation between T_c and E_g is predicted by this approach. [138, 148, 204, 207] If the gap observed in $La_{1.875}Ba_{0.125}CuO_4$ is similar to those in Refs. [81, 83, 136, 141, 143, 203–205], which are associated with d-wave superconductivity, then we expect that the gap, especially such a small one, should be impacted by an applied magnetic field. [137, 208] We applied a 7-T magnetic field to test this possibility, and the results are shown in the following section.

3.3 Magnetic-field effect

3.3.1 $La_{1.875}Ba_{0.125}CuO_4$

The role that charge- and spin-stripe orders play in the superconductivity of cuprates has been quite controversial. It is commonly believed that the stripe order is harmful for pairing, given the fact that the superconducting temperature T_c vs. hole content x curve shows an anomaly at $x = 1/8$ for $La_{2-x}Ba_xCuO_4$, $La_{2-x}Sr_xCuO_4$, and $La_{1.6-x}Nd_{0.4}Sr_xCuO_4$, where static spin-stripe order is observed. [48, 62, 107, 156] However, there has been recent evidence from transport and susceptibility measurements showing that the

stripe order is compatible with pairing and 2D superconductivity, although it can inhibit 3D superconducting phase order. [116, 209]

One possible way to explore the correlation between superconductivity and spin-stripe order is to apply a magnetic field and study the spin order. One of such initial studies was done by Dai *et al.* [210] on $YBa_2Cu_3O_{6.6}$ (T_c = 63 K). They showed that applying a 6.8-T field along the c axis caused a 30% reduction in the low-temperature intensity of the resonance peak (at 34 meV). The lost weight presumably is shifted to other parts of phase space, but it was not directly detected. (Applying the field parallel to the CuO_2 planes has negligible effect.) In an earlier study on $YBa_2Cu_3O_7$, Bourges *et al.* [211] applied an 11.5-T field and found that the resonance peak broadened in energy but did not seem to change its peak intensity. The difference in response from $YBa_2Cu_3O_{6.6}$ is likely due to the difference in the upper critical field, H_{c2}, which is about 5 times larger in $YBa_2Cu_3O_7$ [212].

A series of studies on $La_{2-x}Sr_xCuO_4$ [137, 208, 213–215] and $La_2CuO_{4+\delta}$ [216, 217] samples with various dopings have now been performed. For samples with lower doping, there is a small elastic, incommensurate, magnetic peak intensity in zero field that is substantially enhanced by application of a c-axis magnetic field. The intensity growth follows the prediction of Demler *et al.*, [32] who analyzed a model of coexisting but competing phases of superconductivity and spin-density-wave (SDW) order:

$$I \sim (H/H_{c2}) \ln(H_{c2}/H). \tag{3.3}$$

For $La_{2-x}Sr_xCuO_4$ crystals with $x = 0.163$ [208] and 0.18 [137] there is no field-induced static order. For an intermediate doping concentration of x = 0.144, Khaykovich *et al.* [125] have shown that, although no elastic magnetic peaks are seen at zero field, a static SDW does appear for $\mu_0 H \gtrsim 3$ T, which is consistent with Demler's proposal.

In contrast, it has been reported that the magnetic field has no impact on the pre-existing stripe order in $La_{2-x}Ba_xCuO_4$ (x = 0.095), [162] and $La_{1.6-x}Nd_{0.4}Sr_xCuO_4$ (x = 0.15), although the ordering of the Nd "spectator" moments is affected by the field in the latter case. [218] In all of these cases, the applied field causes T_c to decrease, but the onset temperature of the magnetic order remains constant or increases slightly. Rather surprisingly, a transverse-field muon spectroscopy study [219] found a substantial field induced enhancement of the μSR rate for $La_{2-x}Ba_xCuO_4$ with $x = 1/8$, suggesting increases in both the onset temperature for quasistatic magnetic order and the low-temperature hyperfine field.

An applied magnetic field can also affect magnetic excitations. For example, the spin gap [136] observed in optimally- and over-doped $La_{2-x}Sr_xCuO_4$

is readily modified by an applied field. [137, 208, 215] In § 3.2, we report on the observation of a rather small spin gap of ~ 0.7 meV at low temperature in $La_{1.875}Ba_{0.125}CuO_4$. It would be exciting if this gap were associated with superconductivity (although the bulk superconductivity appears at a very low temperature, ~ 4 K, the 2D superconductivity has a pretty high onset temperature ~ 42 K [116]); however, it could also be due to spin-orbit or exchange-anisotropy effects, as for antiferromagnetic spin waves. [220] The two possibilities are potentially distinguishable by testing the impact of a magnetic field.

To gain insight into the issues discussed above, we carried out elastic and inelastic neutron-scattering measurements on $La_{1.875}Ba_{0.125}CuO_4$ to look at the magnetic field effect on the spin-stripe order and low-energy magnetic fluctuations. In this section, we will show that the main effect of a magnetic field along the c axis is to slightly enhance the spin-order peak intensity, while the peak width and the low-energy magnetic excitations, as well as the gap feature, remain unchanged (within experimental uncertainty). By analyzing the spin-order peak width, we find that the correlation length parallel to the stripes is larger than that perpendicular to them.

In Fig. 3.4 we plot the background subtracted spin-order peak intensity (obtained by sitting at the peak position and counting) and width (obtained by fitting scans through the peak) as functions of temperatures in zero field and in a field of 7 T. In zero field, the peak intensity starts to grow at ~ 54 K, higher than the temperature, ~ 42 K, where the peak width reaches its minimum value. The situation here is similar to that in $La_{1.6-x}Nd_{0.4}Sr_xCuO_4$, where the nominally elastic signal detected at higher temperature was attributed to integrated intensity of low-energy spin fluctuations. [200]

After cooling in a 7-T magnetic field, there is small but clear peak intensity enhancement, as shown in Fig. 3.4(a). However, the peak width, either along H or K, is not noticeably affected. When we plot the difference between $H = 7$ T and $H = 0$ T measurements [Fig. 3.4(b)], it can be seen that the difference grows as the spin order develops, with the same onset temperature as the zero-field peak intensity, and reaches a maximum when the peak width saturates. When taking into account the relative intensity difference S, defined as $(I_{7T}-I_{0T})/I_{0T}$, one can see that it reaches a maximum near 46 K, just before the zero-field onset of static spin ordering. This behavior suggests a slight increase in the spin-ordering temperature, a result qualitatively consistent with the μSR results. [219]

When looking at the peak width [see Fig. 3.4(c)], we found that the width for the scan along $\mathbf{Q} = (0.618 + h, 0.5, 0)$ is larger than that for the scan along $(0.618, 0.5 + k, 0)$. Those widths are obtained by fitting the data with a Lorentzian function convolved with Gaussian function representing the instru-

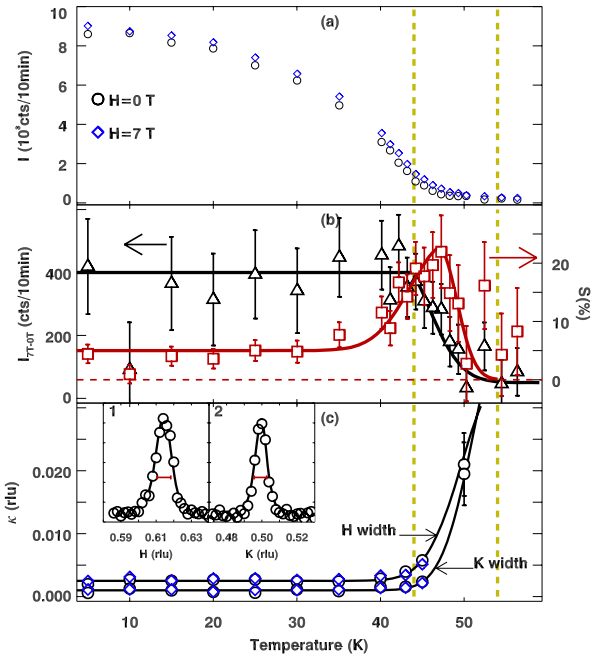

Figure 3.4: (a) Background subtracted spin-order peak (0.618,0.5,0) intensity in zero and 7-T field. (b) Peak intensity difference between 7- and 0-T measurements, and relative intensity difference S. (c) Resolution corrected peak width along H and K directions in zero and 7-T field obtained by the scans shown in the insets in (c). Lines through the data are guides to the eyes. Vertical lines denote the onset temperatures, as discussed in the text. Two horizontal lines in the insets show the instrumental resolutions.

mental resolution. The resolutions (FWHM) at (0.618,0.5,0) along H and K directions are 0.0078 and 0.0072 r.l.u., respectively. Insets 1 and 2 in Fig. 3.4(c) show scan profiles along H and K directions at 5 K, from which one can see that the H scan FWHM is slightly above resolution FWHM, while the K scan is almost resolution limited. From these scans, it appears that the correlation length parallel to the antiferromagnetic stripes is greater than that perpendicular to them.

Next we examine the field effect in finer detail by looking at selected $(0.618 + h, 0.5, 0)$ scans at 5 and 45 K (see Fig. 3.5). At both 5 and 45 K, there are well defined peaks at (0.618,0.5,0), well above the background, as represented by the 55 K data, although the peak at 45 K is much broader and the intensity is weaker. At 5 K, where we have already seen that the enhancement is relatively weak compared to that near 45 K, zero-field and 7-T

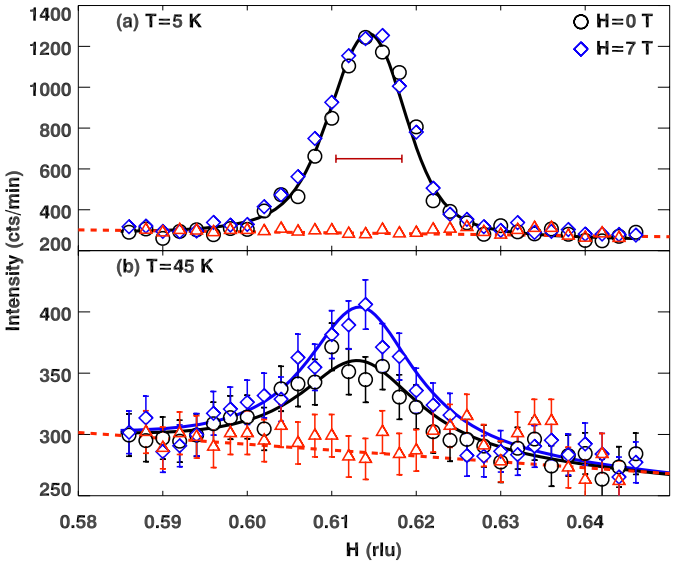

Figure 3.5: Selected elastic scans along $\mathbf{Q} = (H, 0.5, 0)$ in zero and 7-T field at 5 and 45 K. Solid lines are guides to the eyes. The triangles show 55 K data as the background, as indicated by the dashed lines. The horizontal line in (a) shows the instrumental resolution.

data are almost identical when measured with a counting time of 1 min per point. At 45 K, the difference in intensity is quite apparent—the enhancement is $\sim 20\%$—while the peak width shows little change.

We have applied different fields from 0 to 7 T at various temperatures to check the field and temperature dependences of the peak intensity; the results are shown in Fig. 3.6. It is clear that with increasing magnetic field, the peak intensity increases but only by a small amount.

We performed inelastic neutron-scattering measurements to study the low-energy spin excitations. We scanned energy from 0.5 to 2.5 meV at $\mathbf{Q}_0 = (0.618, 0.5, 0)$ to look at the peak intensity's energy dependence in fields of 0 and 7-T at various temperatures, and then the intensity has been converted to the imaginary part of the dynamical susceptibility χ'', which is plotted in Fig. 3.7. At 60 K, χ'' is negligible (at the level of sensitivity in this experiment), and at 45 K, the inelastic signal remains almost constant in the energy range from 0.5 to 2.5 meV. At 30 K, there seems to be a small gap at low energy, which are consistent with the results discussed in § 3.2. After applying a 7-T magnetic field, the inelastic signals do not seem to be affected, as evidenced from $\chi''(\mathbf{Q}_0, \omega)$.

The field effect is also absent in the $\mathbf{Q}$ scans. Constant-energy scans with

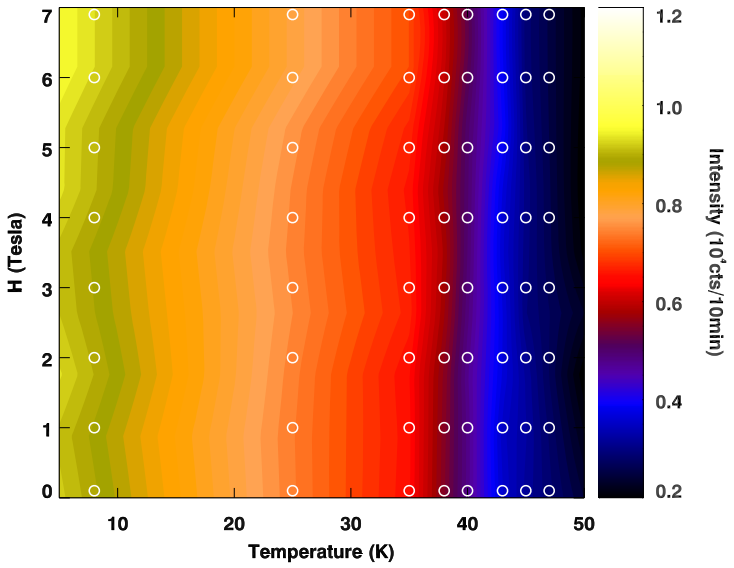

Figure 3.6: Contour map of the spin-order peak (0.618,0.5,0) intensity as a function of temperature and magnetic field. Circles indicate the fields and temperatures at which the measurements were performed.

$\hbar\omega = 0.5$ and 1.5 meV along $(0.618{+}h, 0.5, 0)$ in zero field and 7-T field for 30 K are plotted in Fig. 3.8. These $\mathbf{Q}$ scans are not distinguishable, and no magnetic field impact on the gap is observable here. Since the spin gap associated with superconductivity is rather sensitive to magnetic field, the lack of field dependence seems to rule out a connection between the spin gap and superconductivity. Most likely, the gap is due to spin-orbit or exchange-anisotropy effects; however, even a conventional spin-wave gap should be reduced by an applied field due to Zeeman splitting of the spin-wave energies. Clearly, much better counting statistics and higher magnetic field would be needed in order to detect a finite change due to the field.

There is a sum rule for scattering from spin-spin correlations, and hence one might ask whether the field induced enhancement of the elastic peak should result in an observable decrease in the inelastic magnetic scattering. Applying a 7-T field at low temperature causes an increase in the elastic magnetic signal of approximately 200 counts per 5 min of counting. The measured energy half-width of the elastic peak is 0.06 meV; thus, if this were compensated by a decrease in inelastic scattering spread over an energy range of 1 meV, we would expect to see a signal decrease of about 12 counts per 5 min. Looking at Fig. 3.8, such a change would be big enough to be detectable. One possible reason that such an effect is not seen could be that the decrease in scatter-

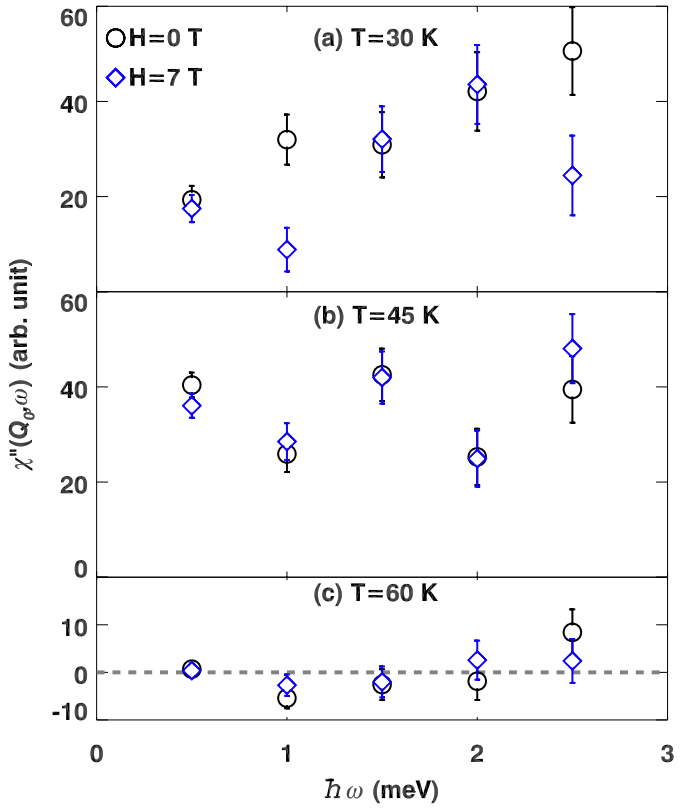

Figure 3.7: $\chi''(\mathbf{Q}_0, \omega)$ with $\mathbf{Q}_0 = (0.618, 0.5, 0)$ in zero and 7-T field at 30, 45, and 60 K converted from the integrated intensity.

ing is spread over a significantly larger energy range, in which case the effect would be in the noise. Another possibility is that the elastic enhancements come at the expense of spin degrees of freedom associated with 2D superconducting correlations, as the superconductivity is significantly depressed by the magnetic field. [116]

To summarize, we have demonstrated that a c-axis magnetic field shows its impact on the spin-stripe order by causing a slight enhancement of the spin-order peak intensity, with no influence on the peak width. The biggest field effect on the intensity is near the onset of spin order. Analysis of the peak width in zero field reveals that the correlation length of the spin order along the stripes is greater than that perpendicular to them. Finally, we have seen a small spin gap with no significant magnetic field dependence.

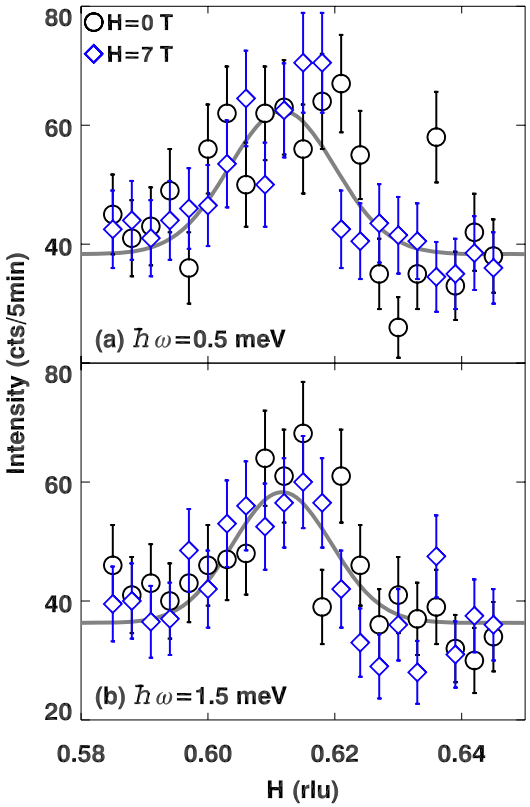

Figure 3.8: Scan profiles along $\mathbf{Q} = (H, 0.5, 0)$ at 30 K, with $\hbar\omega = 0.5$ and 1.5 meV, in zero and 7-T field. Lines through data are guides to the eyes.

3.3.2 $La_{1.905}Ba_{0.095}CuO_4$

In this section, I am going to show that the the magnetic-field effect on $La_{1.905}Ba_{0.095}CuO_4$ is to enhance the stripe order and induce a superconducting layers decoupling.

In $La_{2-x}Ba_xCuO_4$, which are layered materials, the coupling between superconducting layers can be extremely weak, resulting only from quantum mechanical tunneling. [133, 221] An early proposal [222] that such layers might be decoupled by parallel magnetic fields was later shown to be theoretically impossible. [223] Here we show that in $La_{1.905}Ba_{0.095}CuO_4$, a layered superconductor with a T_c of 32 K in zero field, there is a novel state in which electrical resistivity remains zero parallel to the layers but is finite, and quite large, perpendicular to the layers, when a perpendicular magnetic field is applied. It appears likely that the layer decoupling is a consequence of the enhanced stripe order by the field, as our diffraction measurements show that the field

enhances the charge- and spin-stripe order.

The resistivity measurements were performed by the standard four-probe technique, in a Physical Properties Measurement System from Quantum Design. Different crystals, cut from the same parent, were used for resistivity measurements with currents running parallel ($\rho_{||}$) and perpendicular ($\rho_{\perp}$) to the planes, and the $\rho_{||}$ results were confirmed on a third crystal. For $\rho_{\perp}$, the crystal is 1.1 mm high $\times$ 2.7 mm thick, with 1.7 mm between voltage contacts; for $\rho_{||}$, 1.3 mm high $\times$ 0.8 mm thick, with 2.9 mm between contacts. The dc measuring current is 1 mA, and repeated measurements at each temperature were averaged. In the voltage vs. current measurements to determine the critical current density J_c, the threshold voltage for finite resistivity is 1.6 μV. The x-ray diffraction measurements were performed at beam line BW5 at DESY using 100 keV photons. The sample is a disk with 5 mm in diameter and 1 mm in thickness, oriented such that the charge-order reflection was measured in transmission geometry.

As discussed in Chapter 1, the crystal structure of $La_{2-x}Ba_xCuO_4$ consists of CuO_2 planes, in this case alternating with $(La,Ba)_2O_2$ layers. In the normal state, the electronic charge carriers are concentrated in the CuO_2 planes, where they provide metallic conductivity. For carrier concentrations below that required for the maximum superconducting T_c ("underdoped" regime), as in our case, normal-state carrier motion perpendicular to the planes is incoherent. On cooling towards T_c, superconducting correlations initially develop within the planes. [224] Below T_c, the superconducting phase coherence between planes is maintained through the Josephson effect, [133, 221, 225] whereby quantum mechanical tunneling provides coherence even when the intervening layer is insulating. [226]

We have measured the temperature dependence of $\rho_{||}$ and $\rho_{\perp}$ in $La_{2-x}Ba_xCuO_4$ $x = 0.095$, and investigated the impact of a magnetic field of strength H applied either parallel ($H_{||}$) or perpendicular ($H_{\perp}$) to the planes. The results are shown in Fig. 3.9. For the case of $H_{\perp}$, the field has a drastic effect on $\rho_{\perp}$, significantly depressing the temperature at which $\rho_{\perp} \to 0$. In contrast, the impact of $H_{||}$ is rather weak. Turning to the case of $\rho_{||}$, we see that the effect is modest for both $H_{||}$ and $H_{\perp}$.

For a better view of the resistivity as it approaches zero, we have replotted the data in Fig. 3.9 in logarithmic form in Fig. 3.10a-d. The remaining data sets for $\rho_{\perp}$ are shown in Fig. 3.11. The resulting phase diagrams defined by the transition to zero resistivity are presented in Fig. 3.10e and f. For the case of $H_{\perp}$, we find that there is a broad regime where $\rho_{||}$ is zero but $\rho_{\perp}$ is not. A similar but narrower regime is also found for $H_{||}$. (The sharp peak in $\rho_{\perp}$ observed at 27 K for smaller magnetic fields is correlated with

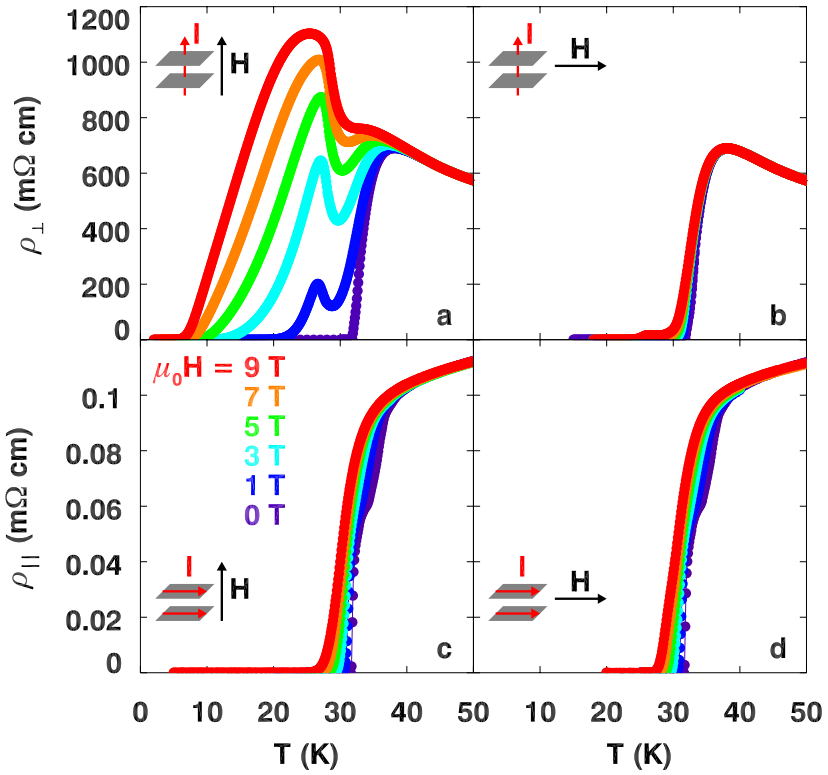

Figure 3.9: Magnetoresistance in $La_{2-x}Ba_xCuO_4$ with $x = 0.095$. Resistivities vs. temperature for a range of magnetic fields, corresponding to the configurations: a, $\rho_\perp$ in $H_\perp$; b, $\rho_{||}$ in $H_\perp$; c, $\rho_\perp$ in $H_{||}$; d, $\rho_{||}$ in $H_{||}$. The values of $\mu_0 H$, ranging from 0 T (violet) to 9 T (red), are indicated in c. The orientations of the measuring current, I, and the magnetic field are indicated in the insets.

a structural transition, discussed below, and is likely associated with critical fluctuations. [227])

We have learned, through trial and error, that attempts to measure $\rho_{||}$ for $T < T_c$ are extremely sensitive to the measurement configuration. For example, in Fig. 3.12a we compare measurements of $\rho_{||}$ in $\mu_0 H_{||} = 9$ T for two different choices of the current direction. With the current parallel to the field, we see $\rho_{||}$ drop to zero at a high temperature, but with the current perpendicular to the field, the transition is reduced by ~ 20 K and looks qualitatively like $\rho_\perp$. This difference is easily understood. We are applying the current in the presence of a high field, so that vortices are present for $T < T_c$. When the current is perpendicular to the field, the vortices feel a Lorentz force that pushes them perpendicular to the planes; however, as long as $\rho_\perp$ is finite, the vortices cannot move coherently between the planes and the

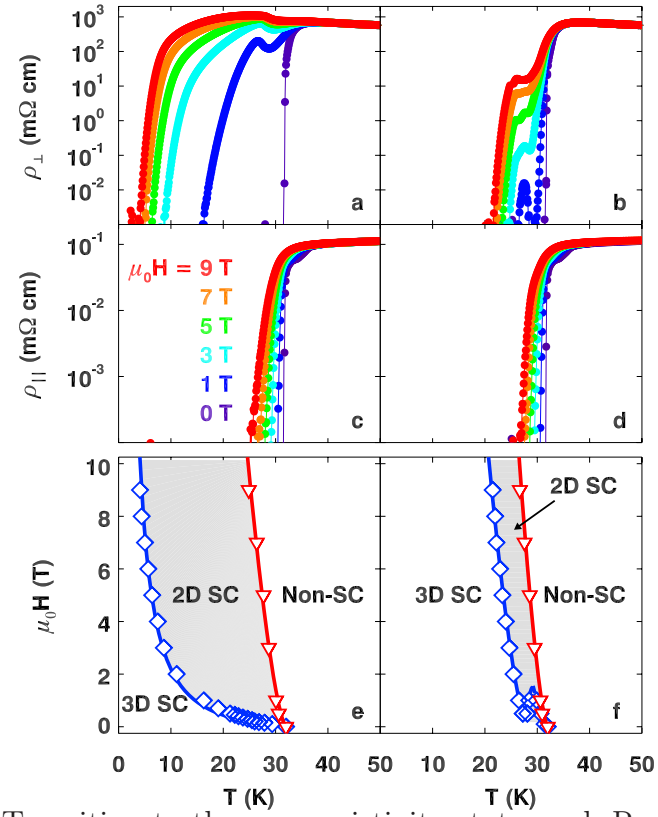

Figure 3.10: Transition to the zero-resistivity state. a-d, Resistivities for the configurations of Fig. 3.9, plotted on a logarithmic scale. e, Zero-resistivity transitions for $\rho_\perp$ (blue diamonds) and $\rho_{||}$ (red triangles) with $H_\perp$; SC = superconductor. f, Same as e, but for $H_{||}$.

measured resistivity remains large. If, instead, we apply the current parallel to the field, then there is no Lorentz force, and we obtain the true $\rho_{||}$.

A different effect is illustrated in Fig. 3.12b. Here we show measurements on a crystal prepared with two sets of voltage contacts. The current contacts are at the ends of the crystal, on faces that are perpendicular to the CuO_2 planes. The pairs of voltage contacts are on: A) a face perpendicular to c, and B) a face perpendicular to the planes. Case B corresponds to our standard configuration, as it directly probes the response of the CuO_2 planes; the results for $\rho_{||}$ in $H_\perp$ are indicated by the filled symbols in Fig. 3.12b. The results for case A, indicated by the open symbols, are quite different. Even in the normal state, the resistivity is apparently larger than for case B, and for $T < T_c$ and $\mu_0 H_\perp = 9$ T, the measured resistivity remains large until $\rho_\perp$ heads to zero. This behavior is clearly a consequence of the extreme transport anisotropy in the 2D superconductor phase. To properly measure $\rho_{||}$, the voltage contacts

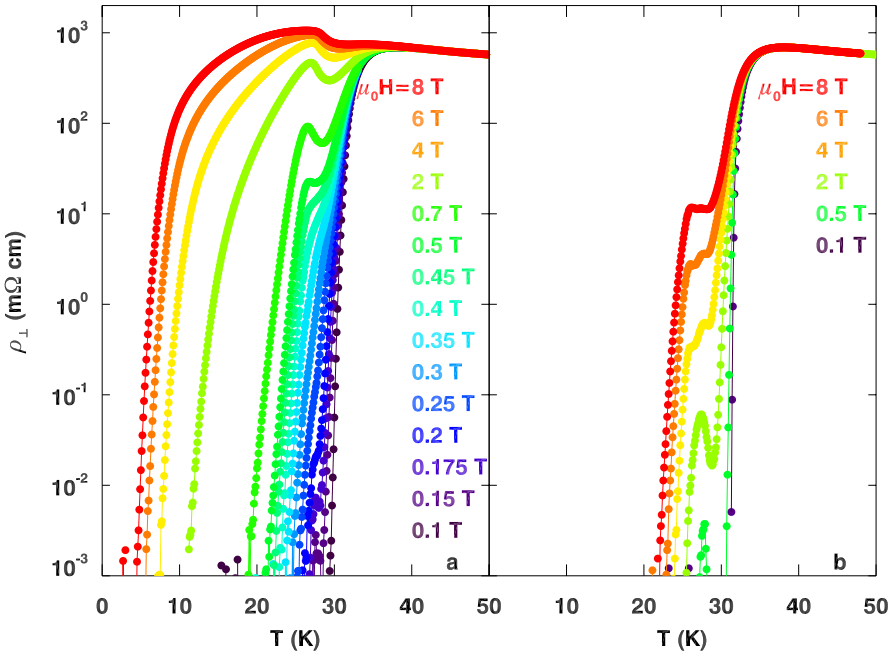

Figure 3.11: Further data sets for $\rho_\perp$ with: a, $H_\perp$; b, $H_\perp$.

must be connected to the same planes to which the current is applied.

Is this anisotropic behavior representative of the bulk of the sample? Could there be a tiny amount of a second superconducting phase that short circuits the measurement for $\rho_{||}$ but not for $\rho_\perp$. To test this possibility, we have performed measurements of voltage vs. current in $\mu_0 H = 0$ and 9 T, and the results are shown in Fig. 3.13. In both cases, the highest temperature data (red) are in the normal state; there, the slope is 1 for $I \gtrsim 1$ mA, indicating ohmic behavior. In Fig. 3.13a, we can see that a finite current threshold (critical current) develops for finite voltage as T is reduced through T_c. (The voltage minimum, indicated by the dashed line, is determined by the resistance in the contacts.) In Fig. 3.13b, where a large field is present, the V vs. I curves at lower temperatures show rounded transitions to resistive behavior. We have estimated the critical current by choosing a small voltage threshold (1.6 μV) where the resistance definitely becomes finite; however, it is not possible to rule out finite dissipation at lower currents.

The critical current density J_c determined from Fig. 3.13, at which $\rho_{||}$ becomes finite are shown in Fig. 3.14. We find that J_c grows exponentially below the temperature where $\rho_{||} \to 0$, and rapidly exceeds our ability to directly measure it. For reference, the critical current density of a good superconductor at $T \ll T_c$ and $H = 0$ is 1×10^6 A/cm^2. We conclude that we have observed a

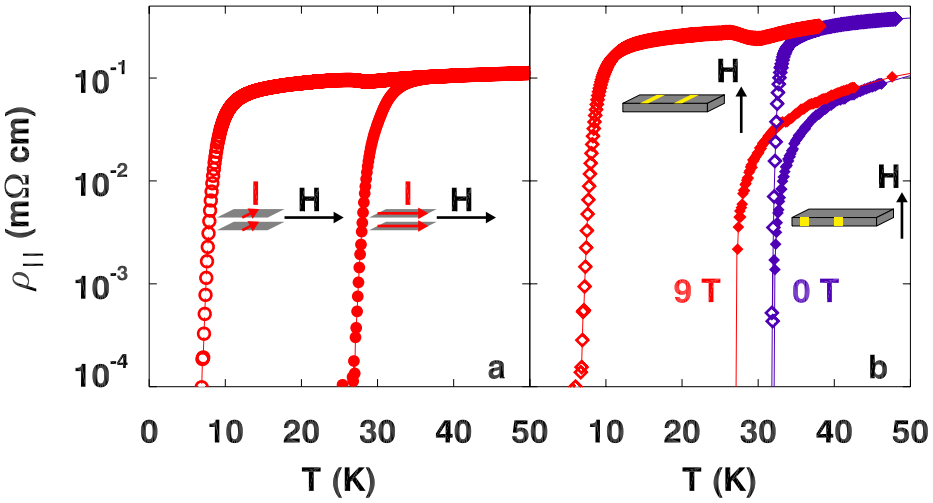

Figure 3.12: Comparison of measurements with alternate configurations. a, Results for $\rho_{||}$ in $\mu_0 H_{||} = 9$ T with current perpendicular (open circles) and parallel to the field (filled circles). b, Results for $\rho_{||}$ measured in $H_\perp$ with voltage contacts on a crystal face perpendicular (open diamonds) and parallel to the crystallographic c axis (filled symbols), as indicated by the insets. In both cases, violet symbols correspond to zero field, red to $\mu_0 H_\perp = 9$ T.

bulk effect. Could we have most layers superconducting and a small fraction insulating? Such a scenario could not explain the observations for $\mu_0 H_\perp \gtrsim 7$ T and 15 K $\lesssim T \lesssim$ 25 K, where $\rho_\perp$ is greater than in the normal state. In fact, between 30 K and 28 K, $\rho_\perp$ increases faster than any extrapolation of normal state behavior, while $\rho_{||}$ is rapidly dropping. We conclude that $H_\perp$ induces a decoupling transition, resulting in a quasi-2D superconducting phase; we also find a 2D superconducting phase for $\rho_{||}$, but for a narrower temperature range. In principle, 3D correlations can survive through electromagnetic coupling of the supercurrents that screen the magnetic field [228]; such interactions may be essential to the stability of the 2D superconducting phase in the presence of a substantial magnetic field. There is supporting evidence for decoupling from a recent optical reflectivity study on closely related $La_{2-x}Sr_xCuO_4$ with $x = 0.10$, where it was observed that the Josephson plasma resonance, a measure of the interlayer Josephson coupling, is completely suppressed by modest magnetic fields perpendicular to the planes. [133] (The $H_\perp$ transition field vs. temperature is slightly above our line for $La_{2-x}Ba_xCuO_4$ $x = 0.095$). This leads to the question: what suppresses the Josephson coupling?

The applied magnetic field penetrates the superconductor as quantized flux lines screened by vortices of supercurrent. Meandering of the vortices from layer to layer can greatly weaken the average Josephson coupling, [229] but

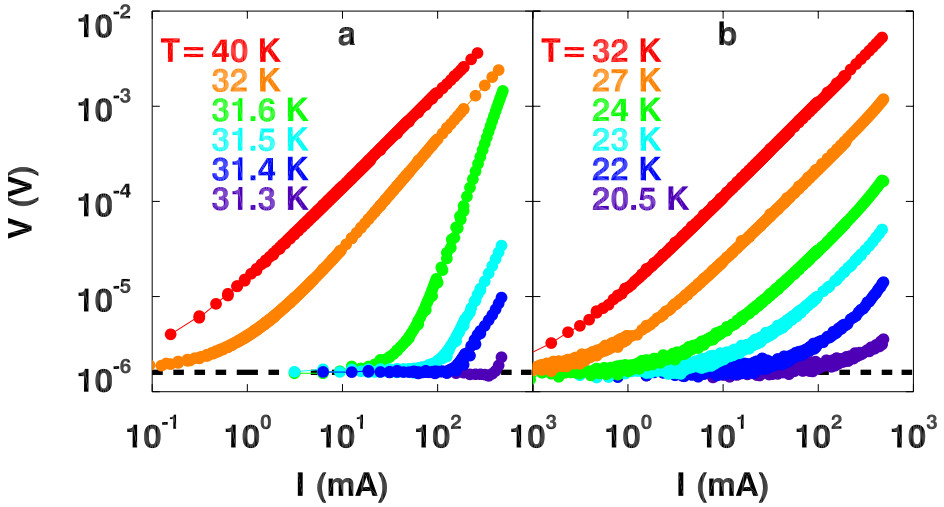

Figure 3.13: Voltage vs. current measurements. $\mu_0 H_\perp = 0$ T, a; 9 T, b. Each curve corresponds to a different temperature, as indicated in the legends.

is not expected to cause 2D superconductivity. Instead, spin-stripe order has been associated with vortices in $La_{2-x}Sr_xCuO_4$. [214, 215] For $La_{2-x}Ba_xCuO_4$ $x = 0.095$, we have shown that weak spin stripe order develops in zero field below a structural phase transition at $T_d \approx 27$ K in § 3.1. In our previous work [194], we also showed that there is charge-stripe order in $La_{2-x}Ba_xCuO_4$ $x = 0.095$. Fig. 3.15 shows that both the spin and charge orders are enhanced by $H_\perp$, while the structural transition is unaffected. In the case of $La_{2-x}Ba_xCuO_4$ $x = 0.125$, where the spin and charge order parameters are much larger, [156, 194] evidence for dynamical decoupling of the superconducting layers in zero field has been reported. [116] The most likely explanation for the frustration of the Josephson coupling involves a sinusoidally-modulated, striped-superconductor phase that competes with the spatially uniform superconducting state common to the cuprates. [26, 118, 119] For $La_{2-x}Ba_xCuO_4$ $x = 0.095$, the Josephson coupling is finite in zero field and comparable to that in $La_{2-x}Sr_xCuO_4$ $x = 0.10$. [230] The field-induced reduction of the Josephson coupling in $La_{2-x}Sr_xCuO_4$ has been attributed to the field-induced enhancement of stripe order. [133] Consistent with such an interpretation, the impact of $H_\perp$ and $H_{||}$ in $La_{2-x}Ba_xCuO_4$ is greater for $T \lesssim T_d$ than for $T > T_d$. An earlier indication of this connection appeared in a study of Nd-doped $La_{2-x}Sr_xCuO_4$ with $x = 0.15$. [225]

For completeness, we note that another model of quasi-2D superconductivity is the "sliding" phase, [231] which is a consequence of special derivative couplings between the layers. As there is no obvious reason for such couplings to be important in the cuprates, we believe that the sliding phase is not

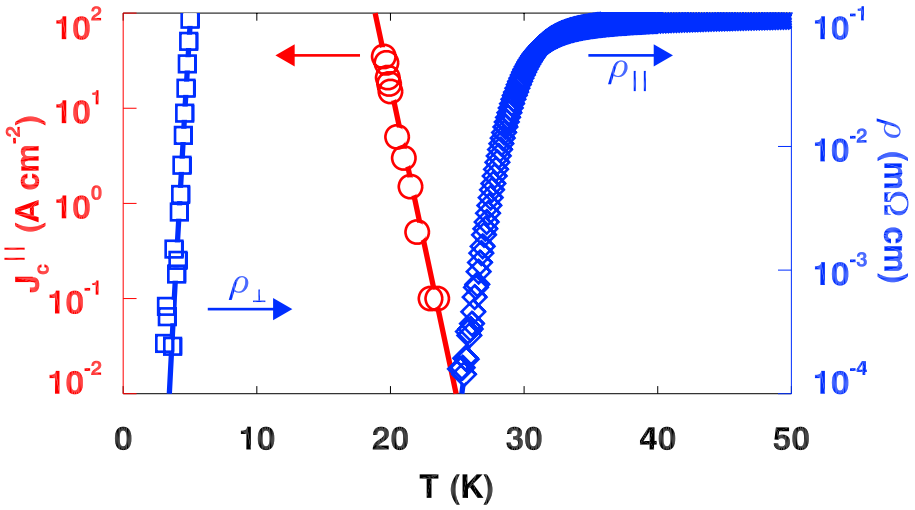

Figure 3.14: Critical current density J_c in the 2D superconducting phase. J_c (red circles) measured for current parallel to the planes in $\mu_0 H = 9$ T. For reference, $\rho_\perp$ (blue squares) and $\rho_{||}$ (blue diamonds) are also shown.

relevant to the field-induced transition we observe.

There have been studies of magnetoresistance in underdoped $La_{2-x}Sr_xCuO_4$ [232] and $La_{2-x}Ba_xCuO_4$ [233] crystals, and the divergent anisotropy between T_c in the normal state was clearly identified by Komiya *et al.* [234]. The extreme anisotropy in the superconducting state makes the resistivity measurements quite sensitive to sample geometry and alignment, as discussed above. We suspect that discrepancies between our results and those of earlier work [233] involve crystal alignment issues. In particular, in preliminary measurements to 18 T, we continue to find no evidence for upturns in $\rho_{||}$ before it drops to zero at $T \gtrsim 17$ K.

We believe that the observed decoupling transition is likely to be of broad relevance to underdoped cuprates. For example, optical reflectivity studies of underdoped $YBa_2Cu_3O_{7-x}$ indicate that a modest $H_\perp$ readily suppresses the superfluid response perpendicular to the planes, but there is no signature of the depaired quasiparticles one would normally expect to see due to magnetic-field suppression of superconductivity. [235] The observed response becomes understandable if $H_\perp$ drives the $YBa_2Cu_3O_{7-x}$ sample into a 2D superconducting phase. Another example involves magnetization studies of underdoped $La_{2-x}Sr_xCuO_4$. [236] The transition from irreversible to reversible behavior with increasing field has been interpreted as a transition to a state (vortex liquid) in which one would expect to observe finite $\rho||$. The decoupled phase presents a new perspective on such results.

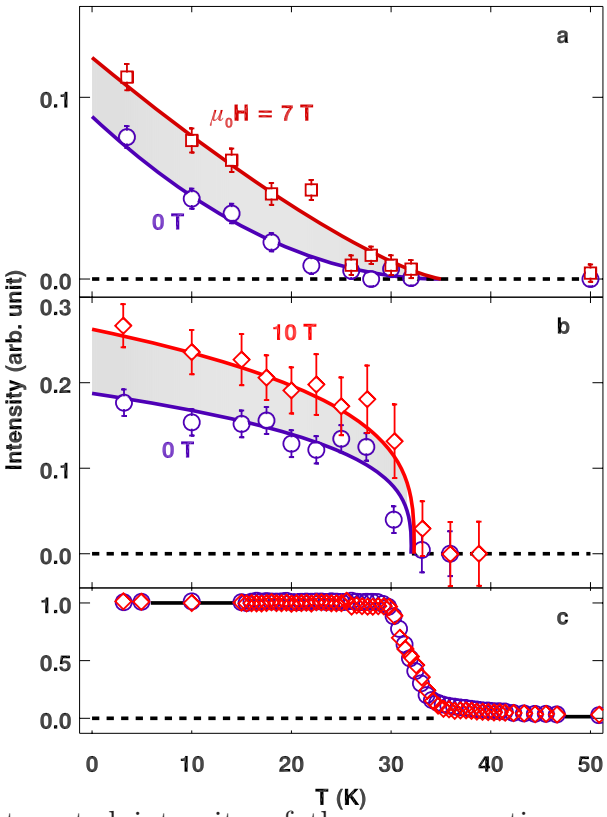

Figure 3.15: Integrated intensity of the, a, magnetic superlattice peak in $\mu_0 H = 0$ T (violet circles) and 7 T (red squares); b, charge-order superlattice peak in 0 T (violet circles) and 10 T (red diamonds); c, (300) superlattice peak, in 0 T and 10 T as in b.

3.4 Zn doping effect in $La_{1.905}Ba_{0.095}CuO_4$

We have previously shown that, in $La_{2-x}Ba_xCu_{1-y}Zn_yO_4$, at $x = 1/8$, $y = 0$, the bulk superconductivity is strongly suppressed by the occurrence of spin stripe order at 42 K. The stripe order is pinned by the LTT phase, which replaces the LTO phase below 54 K. We have also performed some measurements on sample with $x = 0.095$, $y = 0$, as discussed in § 3.1, where the bulk susceptibility shows an initial onset of superconducting diamagnetism at a rather high temperature of 32 K. We have seen that there is an LTO to LTT transition that starts at ~ 35 K and ends at ~ 27 K, and relatively weak magnetic superlattice peaks compared to that in $x = 1/8$, $y = 0$ sample.

Now we begin to investigate the relationship between superconductivity, spin correlations, and stripe order with Zn doped $La_{2-x}Ba_xCuO_4$. Zn impurity effect has been extensively studied in $La_{2-x}Sr_xCuO_4$, and $YBa_2Cu_3O_{7-x}$. [86, 112, 113, 128–130, 132, 237–252] For $La_{2-x}Sr_xCuO_4$ with $x = 0.15$, substitut-

ing about 1% or less Zn causes the appearance of excitations within the spin gap of the Zn-free compound. [128, 132] Substitution of 1.7% Zn is sufficient to induce weak elastic magnetic peaks. For $x = 0.12$, where weak elastic magnetic peaks are present without Zn, substitution of Zn does not only increase the peak intensity, but also the **Q**-widths of the peaks [61, 253]. Wakimoto *et al.* [130] have found that Zn substitution into overdoped samples ($x > 0.2$) significantly enhances the low-energy (< 10 meV) inelastic magnetic scattering.

In $YBa_2Cu_3O_{7-x}$, Zn substitution causes weight to shift from E_r into the spin gap. [86, 254] While it causes some increase in the Q-width of the scattering at E_r, [255] it does not make a significant change in the **Q** dependence of the (unresolved) incommensurate scattering at lower energies. [86] Muon-spin-rotation studies indicate that Zn-doping reduces the superfluid density proportional to the Zn concentration, [246] and this provides another parallel with the properties of the magnetic vortex state.

3.4.1 Magnetization and neutron scattering results

The work discussed above show that the effects of Zn substitution for Cu are quite similar to those caused by an applied magnetic field—Zn impurity induces local magnetic moments and greatly reduces the superfluid density. Recently, there have been a few reports on $La_{2-x}Ba_xCu_{1-y}Zn_yO_4$, which shows both charge and magnetic peak intensity enhancements. [164, 256] Compared to $La_{2-x}Sr_xCuO_4$, and $YBa_2Cu_3O_{7-x}$, the Zn effects on $La_{2-x}Ba_xCuO_4$ are much less studied mainly because of the limited sample availability, and therefore no detailed information on Zn impurity effects on this system is available at the moment. We successfully replaced 1% Cu by Zn in $La_{1.905}Ba_{0.095}CuO_4$, and got large-size, high-quality single crystal, which enables this study.

Our magnetization measurements show that the T_c of the $La_{1.905}Ba_{0.095}CuO_4$ sample is reduced form 32 to 17 K by 1% Zn doping, as shown in Fig. 3.16(a). Obviously, the superconductivity in $La_{1.905}Ba_{0.095}CuO_4$ is greatly suppressed by the Zn doping. It is interesting to examine the magnetization of the Zn-free sample. At 27 K, the curve shows a kink, which is likely to be a result of the structural transition from LTO to LTT phase upon cooling. With this transition, the superconductivity seems to be affected. It is interesting in the sense that an order as robust as superconducting order can be affected by this structural change. In principle, this is consistent with the idea proposed for the $La_{1.875}Ba_{0.125}CuO_4$ sample that when the system changes from LTO to LTT phase, with latter being able to pin the stripe, and thus frustrate the interplane Josephson coupling, and effectively, induce a layer decoupling, with superconductivity only appearing in the plane. [116, 209]

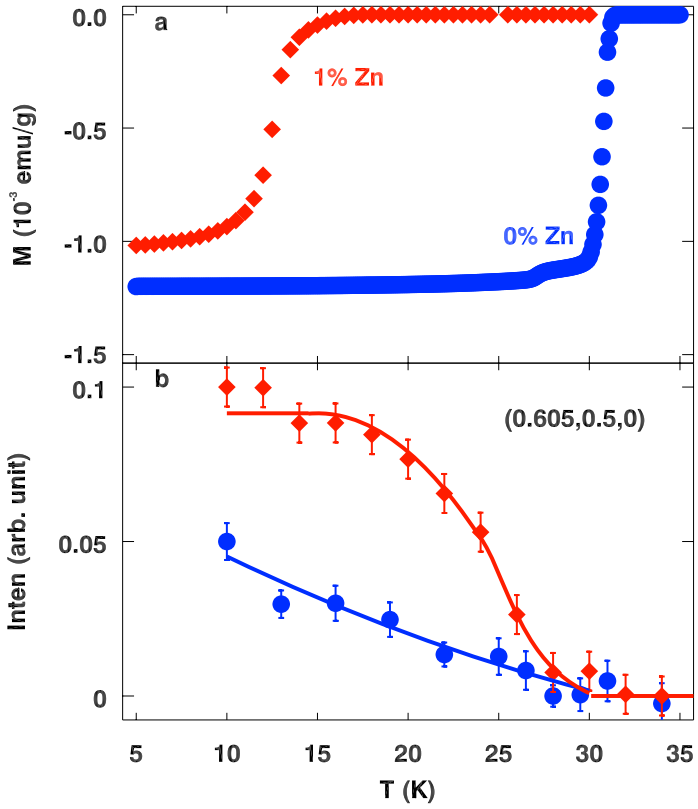

Figure 3.16: (a) Temperature dependence of the magnetization measured with 2-Oe field parallel to the c axis under ZFC condition for $La_{1.905}Ba_{0.095}CuO_4$ with and without 1% Zn. (b) Normalized (to the results of the $La_{1.875}Ba_{0.125}CuO_4$ sample) spin-order peak (0.605,0.5,0) intensity as a function of temperature for the two samples. Lines through data are guides to the eyes.

As expected, with the superconductivity being suppressed, the magnetic order should be enhanced, which is the case in Fig. 3.16(b), where we plot the normalized (to the results of $La_{1.875}Ba_{0.125}CuO_4$ sample) spin-order peak (0.605,0.5,0) intensity as a function of temperature for both Zn-doped and Zn-free sample. The spin order in the Zn-free sample is weak, as we discussed in § 3.1. When we doped 1% Zn and measured the spin-order peak, the peak intensity is greatly enhanced, and the peak becomes much more well-defined. As can be seen from Fig. 3.16(b), at low temperatures, the peak intensity is enhanced by $\sim 100\%$. Also, how the order develops changes. For the Zn-free sample, it shows a glassy nature, with spins ordering slowly with cooling. For the 1% Zn doped sample, it certainly becomes ordered more rapidly. Zn is

a non-magnetic element, and such a small doping level should not affect the magnetic order too much itself, but by creating non-superconducting "island", it can reduce the superconducting volume effectively. [128, 240] As a result, the magnetic order is enhanced at the expense of the superconductivity.

Besides, we have done magnetic-field measurements on both samples, which show that magnetic field induces enhancement of the stripe-order-peak intensity, similar as the results in $La_{1.875}Ba_{0.125}CuO_4$. All these are evidences that the magnetic order is competing with the bulk superconductivity.

3.4.2 Thermoelectric power and thermal conductivity

I have also measured thermoelectric power and thermal conductivity on $La_{1.905}Ba_{0.095}CuO_4$ with and without Zn doping. The thermoelectric power (thermopower), or Seebeck coefficient of a material measures the magnitude of an induced thermoelectric voltage in response to a temperature difference across that material. The thermopower has units of (V/K), though in practice it is more common to use microvolts per kelvin (μV/K). An applied temperature difference causes charged carriers in the material, whether they are electrons or holes, to diffuse from the hot side to the cold side, similar to a classical gas that expands when heated. Mobile charged carriers migrating to the cold side leave behind their oppositely charged and immobile nuclei at the hot side thus giving rise to a thermoelectric voltage (thermoelectric refers to the fact that the voltage is created by a temperature difference). Since a separation of charges also creates an electric potential, the buildup of charged carriers onto the cold side eventually ceases at some maximum value since there exists an equal amount of charged carriers drifting back to the hot side as a result of the electric field at equilibrium. Only an increase in the temperature difference can resume a buildup of more charge carriers on the cold side and thus lead to an increase in the thermoelectric voltage. The thermopower of a material, represented by S, is defined (approximately) as [257, 258]:

$$S = \frac{\Delta V}{\Delta T}, \tag{3.4}$$

and a thermoelectric voltage ΔV is seen at the terminals.

Thermal conductivity, κ, is the property of a material that indicates its ability to conduct heat. Thermal conductivity is measured in watts per kelvin per meter ($W{\cdot}K^{-1}{\cdot}m^{-1}$. Multiplied by a temperature difference (in K) and an area (in m^2), and divided by a thickness (in m) the thermal conductivity predicts the power loss (in W) through a piece of material. It is defined

as [257, 258]:

$$\kappa = \frac{Q}{At}\frac{x}{\Delta T}, \tag{3.5}$$

where Q, is the heat transmitted during time t through a distance x, in a direction normal to a surface of an area A, due to a temperature difference ΔT. It works under steady state conditions and when the heat transfer is dependent only on the temperature gradient.

The thermopower and thermal conductivity were measured at the same time with a four-probes method in a Physical-Properties-Measurement-System (PPMS). The setup of the measurement is shown in the inset of Fig. 3.17(a). The sample used has a dimension of 8 mm (L)×0.8 mm (W)×1.3 mm (H, the length along the c axis). The distance between the two contacts for measuring the voltage and temperature difference is 2.9 mm. To make such a sample, we first painted both ends with silver paint for applying temperature gradient. We also painted two places in the middle of the sample where we want to measure the voltage and heat with silver paint. After this, the sample was put into a furnace to anneal at 400 °C for 1 hr, to let the silver paint diffuse into the sample, which is an important process for making good contacts. Then, four copper leads were put on top of the silver paint with silver epoxy, and then mounted on the sample holder for the measurements. During the measurement, magnetic fields with strength up to 9 T were applied along the c axis. A steady temperature gradient was applied on the two ends with cross section $A = 1.0$ mm^2, with heat flowing on the a-b plane, and the temperature gradient and voltage were measured on the two leads with a distance of $x =$ 2.9 mm. By using Eqs. 3.4 and 3.5, we got the in-plane thermopower S_{ab} and κ_{ab}, which are plotted in Fig. 3.17.

Since $S = \Delta V/\Delta T$, when the sample enters superconducting state, $\Delta V \approx 0$. This provides another measure of the T_c, as shown in the bottom panels of Fig. 3.17. The T_c's obtained by measuring thermal power are almost the same as those measured with susceptibility, which are 32 and 17 K for the Zn-free and 1% Zn doped sample respectively. Before the sample becomes superconducting, and for low temperature, S_{ab} can be approximately described as [259],

$$S_{ab} = \frac{\pi^2 k_B^2 T}{3\mathrm{e}}\frac{d\ln(\sigma)}{dE}\bigg|_{E=E_F}, \tag{3.6}$$

where σ is the conductivity, and E_F is the Fermi energy. When the Fermi surface changes, *e. g.*, due to a structural change, S_{ab} will be affected, which is the case in Fig. 3.17(b) in high field. In low field (<3 T), the T_c is higher than 27 K, and the kink which we saw for the higher field is absent because $S_{ab} = 0$. In higher field, the superconductivity is suppressed, and the T_c is lower (than

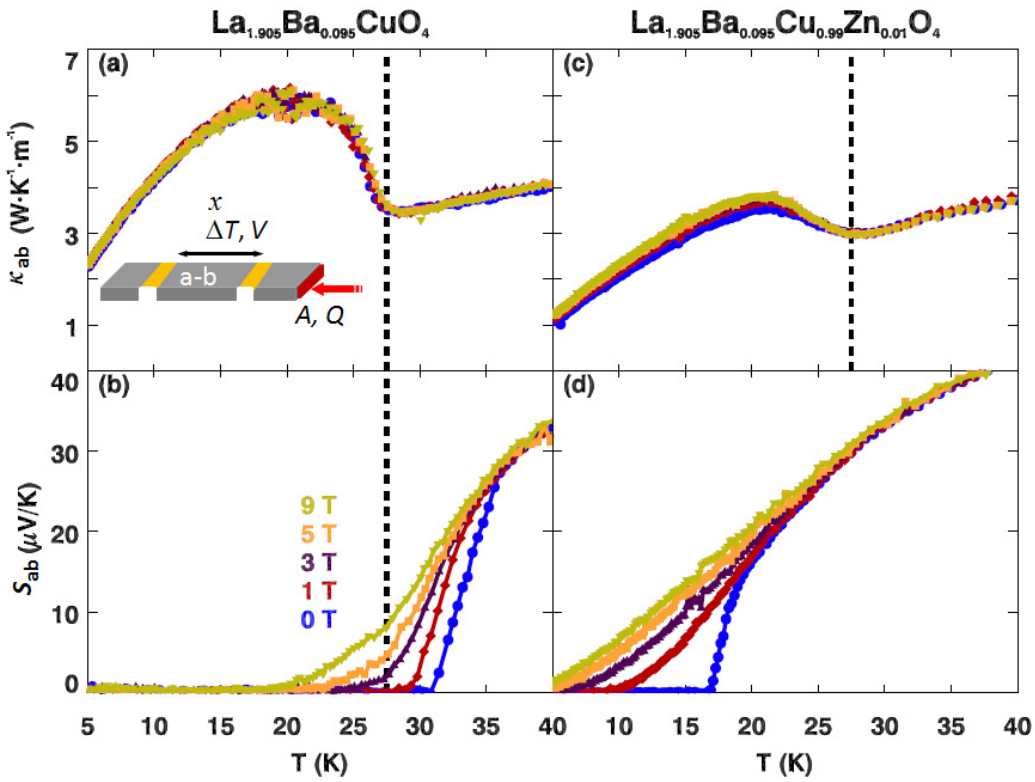

Figure 3.17: Thermal conductivity (top panels), and thermopower (bottom panels) measured in the a-b plane for $La_{1.905}Ba_{0.095}CuO_4$ without and with 1% Zn, under different magnetic field strengths, with $H \perp a$-b plane. Dashed lines represent the structural transition temperature. Inset in (a) shows a schematic for the measurement setup.

27 K), then we saw a kink around 27 K, as indicated by the dashed line. This is consistent with our previous observation that the structure changes from LTO to LTT phase at this temperature. However, this kink is also absent in the 1% Zn doped sample, which is probably because the value of the S_{ab} is too large for the small kink to be pronounced. In other words, there should be such a kink since there is still a structural transition at a similar temperature from our neutron scattering measurement, but it is too small to be seen.

For both samples, κ_{ab} increases from 27 K, indicated by the dashed lines in both Figs. 3.17(a) and (c). Since the temperature is low, thermal conductivity

has contributions from both phonons (κ_{ab}^{ph}) and electrons (κ_{ab}^{el}), [260–262]

$$\kappa_{ab} = \kappa_{ab}^{ph} + \kappa_{ab}^{el} = AT + BT^{\alpha}, \tag{3.7}$$

with A, and B being constants, and $\alpha \sim 3$. In the 1% Zn doped sample, the electrons seem to have more contributions—with magnetic field increasing, κ_{ab} increases, which indicates that the density of states (DOS) increases by the magnetic field. κ_{ab}^{el} can be roughly taken as [260, 261]

$$\kappa_{ab}^{el} = \frac{N\langle v\rangle \lambda C_V}{3N_A}, \tag{3.8}$$

where N is the DOS, $\langle v\rangle$ is the mean particle velocity, λ is the mean free path, C_V is the Molar heat capacity, and N_A is the Avogadro's number. The overall magnitude of the 1% Zn doped sample is smaller than that of the Zn-free one, which is likely due to the shortening of λ by the scattering by the impurities.

3.5 Summary

In summary, in this Chapter, I have shown results on doping dependence of stripe order and superconductivity with four samples, $La_{2-x}Ba_xCuO_4$ $x =$ 0.095, 0.115, 0.125, and 0.135; magnetic-field effects in $x = 0.095$, and 0.125 samples; and Zn impurity effects in $La_{1.905}Ba_{0.095}CuO_4$. From these results, I conclude that the static spin-stripe order is competing with the bulk superconductivity, consistent with what one expects typically. The consequence of the stripe order is to decouple the superconducting layers effectively, and induce a 2D superconducting state, with superconductivity only appearing in the a-b planes.

Chapter 4

Iron-based Superconductors

From this Chapter, I will switch gear and discuss the other type of high-T_c superconductors, the Iron-based superconductors.

4.1 Discovery

In the year 2008, researchers witnessed a big breakthrough in condensed matter physics—a new type of superconductors with high T_c were discovered, which broke the monopoly of cuprates as the only high-T_c superconductors. In fact, the first Iron-based superconductor, LaFePO (1111) was discovered in the year 2006 by Hosono's group. [7] However, the T_c is $\sim$5 K, which is pretty low, so not much attention was paid into this new superconductor. In February 2008, the same group reported that by substituting O by F in LaFeAsO, the T_c was raised to 26 K. [8] Soon after that, the T_c was raised to 43 K, either by replacing La with Sm ($SmFeAsO_{1-x}F_x$), [9] or by applying high pressure (4 GPa) in $LaFeAsO_{1-x}F_x$, [263] and now the highest T_c is reported to be 55 K [10]. The discovery of the Iron-based superconductor is probably the biggest news since the discovery of the Copper-based superconductors in 1986 in condensed matter physics. [5] It ignites tremendous interests in searching for new superconductors with higher T_c, and studying these new superconductors. Almost every day, there will be progress reported on the preprint server. A couple of reviews are now available on these superconductors. [264–269]

Until now, besides the 1111 system, there are other three classes of Iron-based superconductors typified by $BaFe_2As_2$ (122), [270–273] LiFeAs (111), [274–280] and $Fe_{1+y}Te_{1-x}Se_x$ (11) [281–286] which have been discovered. The crystal structures for all the Iron-based superconductors discovered are all tetragonal at room temperature. [7, 8, 278, 287–295] Schematics for these four types of structures are shown in Fig. 4.1. The important common aspect for the crys-

tal structure is that the Fe^{2+} ions form square-planar sheets, where the direct iron-iron interactions render the d-electrons metallic in nature. This resembles the case in cuprates, which has CuO_2 acting as a very important element. It appears that the layered structure is required for high-T_c superconductors.

Among the four systems, the LiFeAs related systems are superconducting and does not order magnetically nor does the structure distort at low temperatures, [276, 278] which is also the case for the LaFePO related systems [296]. All the other undoped systems undergo a subtle structural distortion below room temperature that breaks the tetragonal symmetry. This transition is thought to be magnetically driven [297]. Doping reduces and eventually completely suppresses the structural as well as the magnetic transition as superconductivity develops. [298–303]

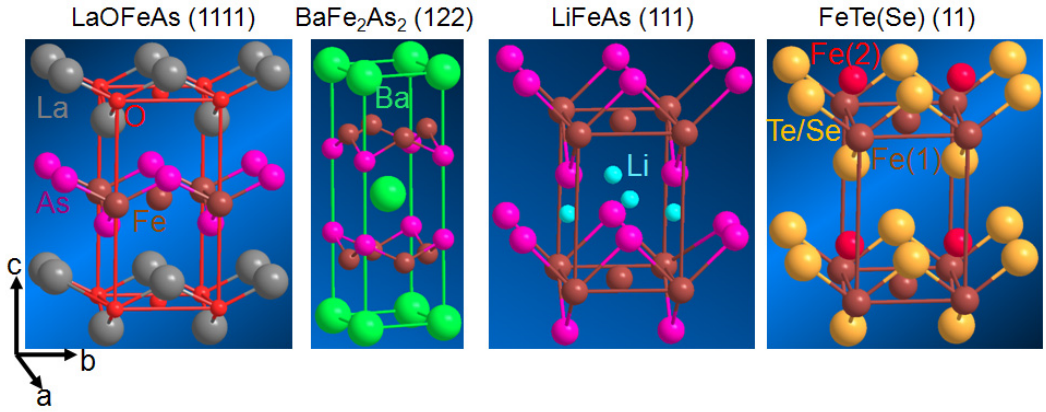

Figure 4.1: Schematic crystal structures for four types of Iron-based superconductors discovered so far.

4.2 Interplay between magnetic correlations and superconductivity

Extensive research has been carried out to study the structural and magnetic structures in these materials, [294, 304–309] and it is now well established that in (1111) (except LaFePO related systems) [298, 299, 310] and (122) [300–303]) type compounds, the long-range magnetic order is suppressed with doping, while the superconductivity appears above a certain doping value. While there are some rare cases where superconductivity appears sharply after magnetic order disappears, [310] in most systems short-range magnetic order

coexists with superconductivity over some range of doping. [298–303] Two representatives [298, 301] of these phase diagrams are shown in Fig. 4.1, from which one can see that it is what happens in cuprates—superconducting and magnetic order are competing with each other, as discussed in Chapter 3.

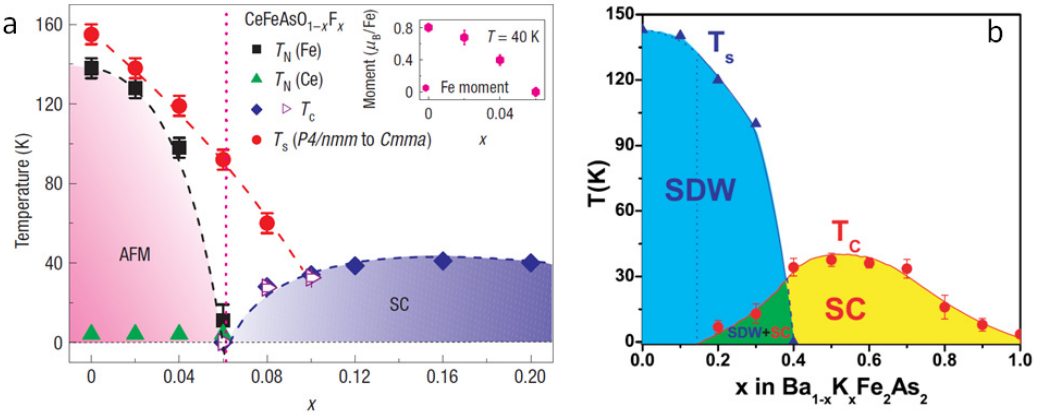

Figure 4.2: Phase diagrams for $CeFeAsO_{1-x}F_x$ [298] and $Ba_{1-x}K_xFe_2As_2$ [301].

The fact that the superconductivity develops after the suppression of the long-range antiferromagnetic order, [304, 311, 312] similar as that in the cuprates suggests that the superconductivity in the Iron-based superconductors is similar as that in cuprates—unconventional high-T_c superconductivity, with magnetic excitations acting as possible glue to pair the electrons. [313–318] In other words, Iron-based superconductors provide another source to study the high-T_c mechanism, and it is a more promising system, as it offers much more compositional choices. An essential step in elucidating the role of magnetism in the superconductivity of these materials is the observation of the "resonance" in magnetic excitations, where the spectral weight at the resonance energy shows a significant increase when the system enters the superconducting phase, in a number of these Iron-based superconductors [319–323]. More recently, a resonance has been reported in the 1111 compound. [324]. The resonance is always observed at the energy $\hbar\Omega_0 \sim 5k_BT_c$. These results suggest that the resonance in the magnetic excitations should be similar across different Iron-based superconductor systems, and are closely related to the onset of superconductivity, and once again, similar as in high-T_c cuprates. [81, 83, 137, 255, 325–333]

In these superconductors, angle resolved photoemission (ARPES) studies [334–336] have provided evidence for electron and hole pockets that are nearly nested by the stripe antiferromagnetic wave-vector. [313, 337, 338] A spin resonance detectable by neutron scattering is predicted to occur at a par-

ticular wave-vector only if that wave-vector connects portions of the Fermi surface that have opposite signs of the superconducting gap, so that observations of the resonance may provide important information relevant to the symmetry of the superconducting gap. [339, 340]

In any case, to understand the high-T_c superconductivity, it will be extremely promising to study the magnetic correlations in the Iron-based superconductors.

4.3 $\mathbf{Fe_{1+y}Te_{1-x}Se_x}$

As one can see from the chemical formulae of the four types of Iron-based superconductors, except the 11 system, all others are un-friendly to human being and environment. Thanks to the discovery of the 11 compound, we are able to perform research on the Iron-based superconductors. Since it is the system I want to study, I will put some more words here.

The superconductivity in 11 compound is discovered in $Fe_{1+y}Se$, with $T_c \approx 8$ K. [281]. Later, it was found that by substituting part of Se by Te, the T_c can be increased to ~ 14 K, with Te:Se ratio ~ 11. [282, 283, 286, 341–349] $Fe_{1+y}Se$ does not exhibit static magnetic order for pressures up to ~ 30 GPa, [284] although short-range spin fluctuations, which are strongly enhanced towards T_c, were observed. [350] However, a Tetragonal-to-Orthorhombic structural phase transition was reported to be at 90 K in $Fe_{1.01}Se$. [351] The superconducting transition temperature of $Fe_{1+y}Se$ was found to increase continuously to 36.7 K at 9 GPa. [284] The pure $Fe_{1+y}Te$ is not superconducting, and exhibits magnetic and structural transition around 65 K. [341, 352–355] As the $Fe_{1+y}Te$ is more like the undoped compound for 1111 and 122 and cuprates, it is more often referred to the parent compound for the 11 system. [355]

For the 11 system, the tetragonal phase with PbO structure has an Iron-based planar sublattice equivalent to the layered Iron-based quaternary oxypnictides, which have a layered crystal structure belonging to the P4/nmm space group. The crystal of the 11 compound is composed of a stack of edge-sharing $Fe(TeSe)_4$-tetrahedra layer by layer, as shown schematically in Fig. 4.1(11). The crystal structure of the 11 system is relatively simple, which will make the study easier. Also, it is relatively easy to grow large-size single crystals, which will be discussed in § 5.1.

Despite that the 11 system shares many similarities with other Iron pnictides and cuprates, it is quite distinct from others.

"Doping" Unlike other systems, where holes or electrons are introduced into the systems by substituting with inequivalent elements, in the 11 system,

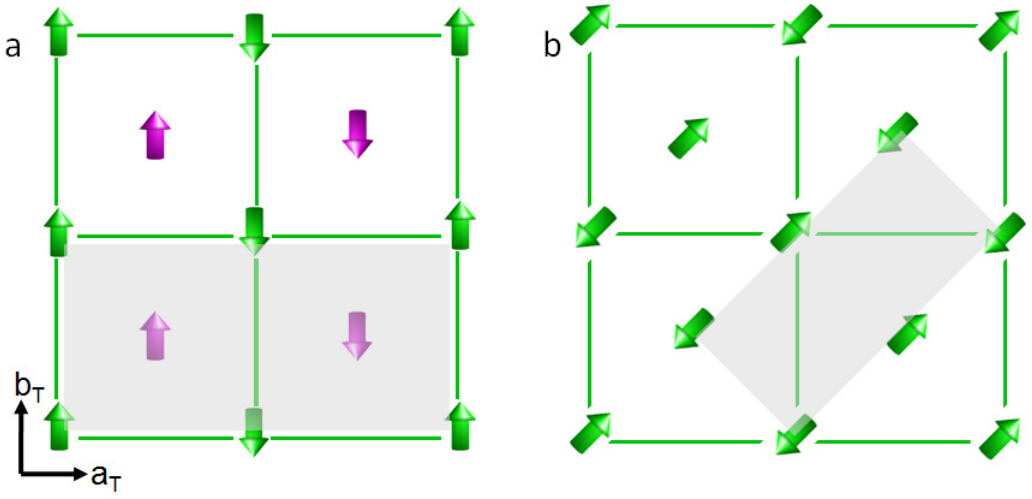

Figure 4.3: Schematic in-plane spin structure of the 11 compound (a), and other Iron-pnictides (b). Arrows in different color in (a) indicates spins on different sublattice. Shadow indicates the magnetic unit cell. From Refs. [298, 305, 353, 356].

superconductivity appears after replacing some Te with the same valance Se (2+). In this case, the "doping" probably does not bring in extra electrons or holes, but to make the description easier, I will continue using the word "doping" to describe the process that Te is replaced by Se.

Doping dependence In cuprates, and other Iron-based superconductors, (except LiFeAs and LaFePO related systems), superconductivity appears after suppressing the long-range antiferromagnetic order, and then T_c increases as doping increases, until it reaches a maximum at the optimal doping, and then T_c decreases with doping, and finally superconductivity disappears around doping $\approx 30\%$. [298–303, 310] For the 11 system, superconductivity survives even at $x = 100\%$, in the pure $Fe_{1+y}Se$ case. [281, 357] Furthermore, one may notice that 11 system's chemical formula has two variables: Fe can also be non-stoichiometric. These will be further discussed in the crystal growth part § 5.1.

Magnetic structure Bao *et al.* [352] found that in the parent compound $Fe_{1+y}Te$, the magnetic structure is quite different from that in other Iron pnictides: i) The ordering wavevector is different. In tetragonal notation where there are two iron atoms per unit cell, the magnetic or-

dering vector is (0.5,0) in plane, rotated 45° from that in other Iron-based superconductors. [294, 304, 311, 352, 353] In other Iron-based superconductors, the antiferromagnetic order has been predicted by the Fermi surface nesting mechanism, [315, 316] and spin excitations from the only known mode at (1/2,1/2) have been proposed as the "glue" mediating high T_c superconductivity in these ferrous materials. [313–318, 358, 359] Although the same (1/2,1/2) SDW order has been predicted for the 11 compound by first-principle calculation, [360] the magnetic order is observed to be around (1/2,0) [352]. This raises questions on the mechanism of the magnetism and the role magnetism plays in the superconductivity. [352] Besides, the SDW order can be either commensurate, or incommensurate, depending on the Fe content. [352, 353] Calculations using the local spin density approximation for hypothetical stoichiometric FeTe yield a commensurate magnetic ground state consistent with that seen experimentally[307, 361]; however, the (0.5,0.5,0.5) SDW order is calculated to have the lowest energy for FeSe. [361]

Nevertheless, the resonance is still observed to be near the antiferromagnetic (1/2,1/2) point below T_c in $FeTe_{0.6}Se_{0.4}$, [362] and $FeTe_{0.5}Se_{0.5}$, [363] which suggests that the resonance in the magnetic excitations should be similar across different Iron-based superconductor systems, and are connecting to the superconductivity intimately.

4.4 Summary

In this Chapter, I have introduced a new high-T_c superconductor system, the Iron-based superconductors, which provides more opportunities to study the interplay between superconductivity and magnetism. The system I will study is the 11 system, since it is much more human and environmentally friendly, compared to other systems. Although the pace of the research has been extremely rapid, it is still a new field, and there are many things left to be done. First, I will study the doping evolution of the magnetic order (§ 5.2.2). Second, I will study the magnetic excitations close to where resonance is observed [(0.5,.5)] in an optimally doped system (§ 5.2.3). Then, I will check the magnetic correlations around two in-plane wavevectors (0.5,0) and (0.5,0.5) (§ 5.2.4). Of course, before all these can be done, crystals have to be available, and the method for growing the crystals and the results on the crystal growth will be presented in § 5.1.

Chapter 5

Crystal Growth and Neutron Scattering on $Fe_{1+y}Te_{1-x}Se_x$

In this Chapter, I will first discuss the crystal growth of the $Fe_{1+y}Te_{1-x}Se_x$ superconductors, and present the crystals grown with the horizontal unidirectional solidification method. Then I will show our neutron scattering results on the interplay between magnetism and superconductivity in this system. This Chapter includes some of the works published in Refs. [364–367], and in some which are to appear. [368–370]

5.1 Crystal growth

We have tried floating-zone, Bridgman, and horizontal unidirectional solidification methods to grow single crystals for $Fe_{1+y}Te_{1-x}Se_x$, and it turns out that the latter gives the best results, and the crystal growth using this method is described below.

The raw materials used for the crystal growth are 99.9999% Te, 99.999% Se and 99.98% Fe pieces. They were weighed and mixed with the desired molar ratio, and then double-sealed in high-purity (99.995%) quartz tubes in vacuum, which were then put in the furnace horizontally. In the furnace, a certain temperature gradient was applied from one end to the other (*e. g.*, at 850 °C, ΔT/distance $\approx$ 5 °C/cm). The quartz tubes were heated to 660 °C, and the temperature was maintained for 12 hrs; then heated to 900 °C and stayed there for 12 hrs, and then at 1050 °C for another 12 hrs. At 1050 °C, the quartz tubes were rocked for 2 hrs before they were cooled to 930 °C in 0.5 hrs, and then cooled with a cooling rate of 2 °C/hr to 300 °C, after which they were cooled to room temperature. The schematic of the method is shown in Fig. 5.1. With this method, large-size high quality single crystals can be relatively easily

grown, and some of the crystals grown with this method is also shown in this figure. These crystals have nice cleavage surface which is the a-b plane. It saves a lot of time for aligning the crystals, and provides convenience for surface studies, such as optical conductivity, Andreev reflection, ARPES, scanning tunneling microscopy (STM), etc. Now we have large-size single crystals for Se doping ranging from 0 to 70%, with sample mass up to 25 g for one single piece. For a certain Se doping, we have different extra Fe concentrations. For Se doping larger than 70%, it is very difficult to get single crystals. Other than this, the crystal quality is very good, and many measurements can be performed on them. [364–369, 371]

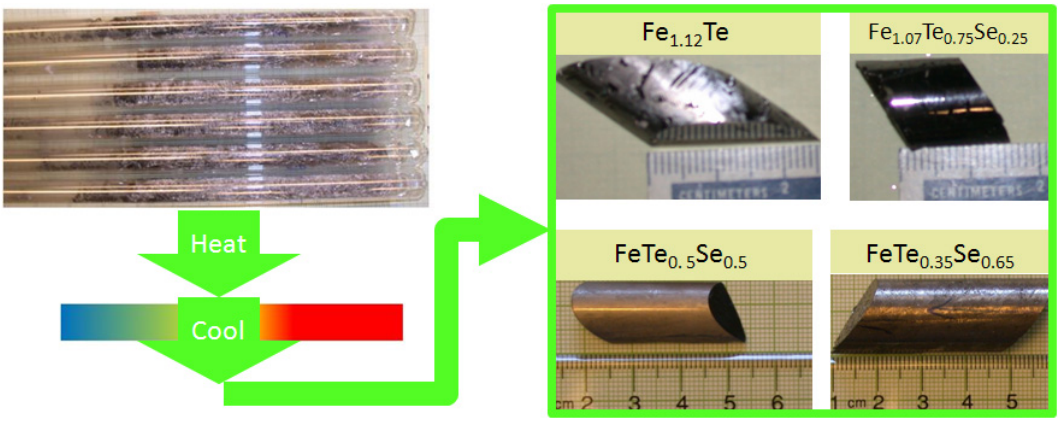

Figure 5.1: Schematic of the horizontal unidirectional solidification method for crystal growth and some of the $Fe_{1+y}Te_{1-x}Se_x$ crystals grown using this method.

We have measured the bulk magnetization using a SQUID magnetometer for the crystals and some of the results are shown in Fig. 5.2. For Se doping $< 10\%$, the system changes from a paramagnetic to antiferromagnetic state, and the transition temperature T_{SDW} (T_N) can be obtained from the magnetization vs. temperature curve. In the lightly underdoped regime ($15\% \lesssim x \lesssim 30\%$), the magnetization shows a cusp at certain temperature, and there is a hysteresis under ZFC and FC conditions, and the characteristic temperature is referred to as a spin-glass temperature T_{SG}. The T_c can be obtained by the diamagnetic response. With these measurements, the phase diagram for $Fe_{1+y}Te_{1-x}Se_x$ is now available, as shown in Fig. 5.3. The left part of the phase diagram ($x < 70\%$) is remarkably similar as those of other Iron-based [40, 41, 298–303, 310] and cuprate superconductors [42–47]—in the parent compound, there is antiferromagnetic order, which is suppressed with doping, and then there is a spin-glass regime, with superconductivity possibly

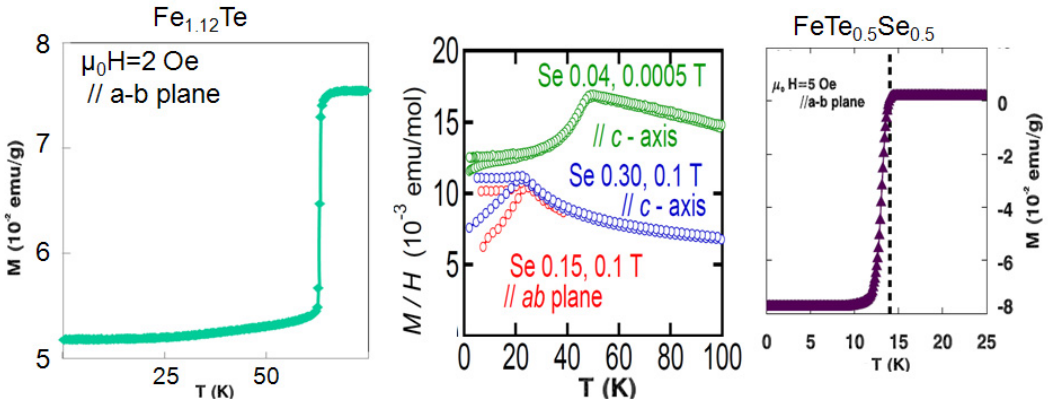

Figure 5.2: Magnetization vs. temperature for $Fe_{1+y}Te_{1-x}Se_x$ crystals.

coexisting; T_c increases with x up to 14 K, and then decreases with further doping. However, the superconductivity extends all the way to 100% Se doping, which is distinct from other systems. Another interesting thing about this phase diagram is the excess Iron, which seems to be an important parameter deciding the crystal's properties. [285] It turns out that when there is more extra Fe, the superconductivity is suppressed, and can even be destroyed, which is consistent with the theoretical prediction that the excess Fe acts as a magnetic electron donor, [372] suppresses the superconductivity, and induces a weakly localized electronic state. [373]

5.2 Neutron scattering study

5.2.1 Experiment

Neutron scattering experiments have been carried out on the triple-axis spectrometers BT-9, BT-7, and SPINS located at NIST Center for Neutron Research. On BT-9, we used horizontal beam collimations of 40′-40′-S-40′-80′ (S represents "sample") with $E_i = E_f = 14.7$ meV and two PG filters were put before and after the sample to reduce higher-order neutrons. On BT-7, we used collimations of open-50′-S-50′-240′ with fixed $E_f = 14.7$ meV. On SPINS, the collimations are Guide-80′-S-80′-240′ with fixed $E_f = 5$ meV and a cooled Be filter was put after the sample for inelastic measurements; for elastic measurements, an additional Be filter was put before the sample. The data are described in reciprocal lattice unit (r.l.u.) of $(a^*, b^*, c^*) = (2\pi/a, 2\pi/b, 2\pi/c)$ in tetragonal notation with two Irons per unit cell. In this case, $a = b \approx 3.81$ Å,

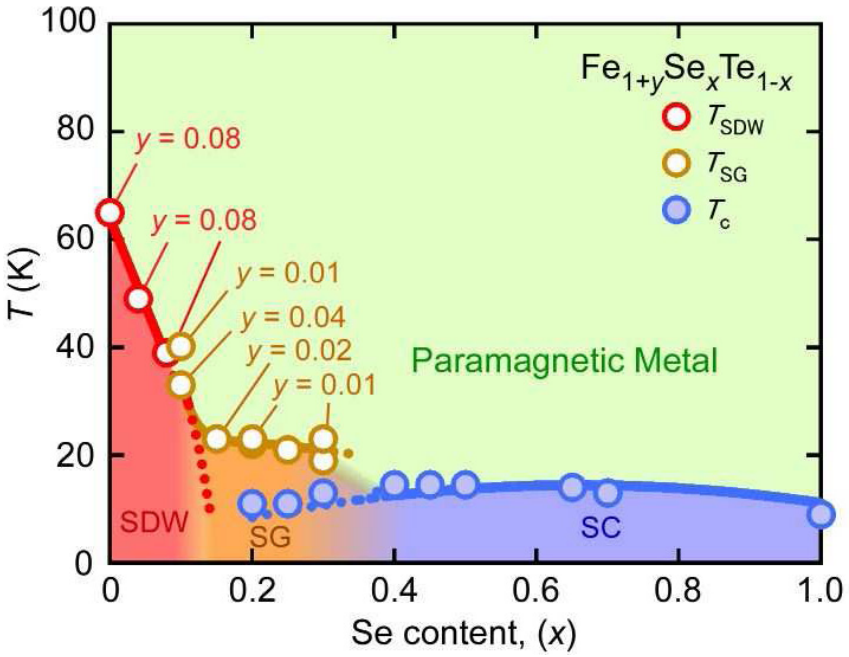

Figure 5.3: Phase diagram of $Fe_{1+y}Te_{1-x}Se_x$ with $y = 0$ as a function of x and T, constructed from single crystal bulk magnetization data. For $x = 100\%$, the data point is from Refs. [281, 344, 347]. The nominal Fe content, $y = 0$ unless it is specified. Temperature labels are described in the text.

and $c \approx 6.15$ Å.

5.2.2 Short-range incommensurate magnetic order near the superconducting phase boundary

To address the evolution of the magnetic correlations with Se concentration, we have performed elastic neutron scattering and magnetization measurements on high quality single crystals with different Fe and Se contents. We show that there is short-range incommensurate magnetic order in both $Fe_{1.07}Te_{0.75}Se_{0.25}$ and $FeTe_{0.7}Se_{0.3}$ at low temperature. Broad magnetic peaks appear at positions slightly displaced from the antiferromagnetic wave-vector $(0.5, 0, 0.5)$ in both samples when cooled below $\sim$ 40 K. The peak intensity increases with further cooling and persists into the superconducting phase. The magnetic peak intensity drops with more Se and less Fe content, and with strengthening superconductivity.

In the magnetization measurements, each sample was oriented so that the

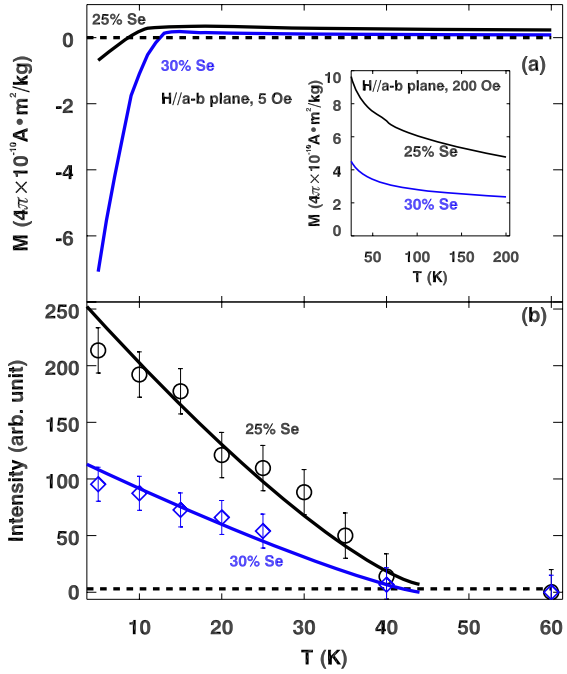

Figure 5.4: (a) ZFC magnetization, and (b) background subtracted magnetic peak intensity measured along [100] (normalized to the sample mass) as a function of temperature for $Fe_{1.07}Te_{0.75}Se_{0.25}$, and $FeTe_{0.7}Se_{0.3}$. Error bars represent square root of the counts. Lines through data are guides for the eyes.

(001) plane was parallel to the magnetic field. The ZFC magnetization vs. temperature for each sample is shown in Fig. 5.4(a), where one can see that the 25% Se sample only shows a trace of superconductivity, while the 30% Se sample clearly has a $T_c \sim 13$ K. We estimate that the superconducting volume fraction for the latter sample is $\sim 1\%$. The inset of Fig. 5.4(a) shows that the paramagnetic magnetization grows on cooling, and is greater in the sample with less Se (and more Fe). The paramagnetic response does not follow simple Curie-Weiss behavior, so it is not possible to make a meaningful estimate of effective magnetic moments. For the 25% Se sample, there is a shoulder at ~ 60 K which could be due to 2–3% of $Fe_{1+y}Te$ as a second phase, which has a magnetic phase transition temperature of ∼65 K. [353]

In our elastic neutron scattering measurements, each sample was aligned on the (200) and (001) nuclear Bragg peaks with an accuracy and reproducibility in longitudinal wave vector of better than 0.005 r.l.u.. For the magnetic peaks, linear scans were performed along [100] and [001] directions at various temper-

atures. The temperature dependence of the peak intensity is summarized in Fig. 5.4(b), and representative scans are shown in Fig. 5.5. No net peak intensity is observed at 60 K, but a weak magnetic peak appears at slightly lower temperature, growing in intensity with further cooling. For $Fe_{1.07}Te_{0.75}Se_{0.25}$, the magnetic structure is clearly incommensurate, and the peak position is determined to be $(0.5-\delta, 0, 0.5)$, with $\delta = 0.04$ r.l.u. From Fig. 5.5(a), we did not observe a peak at $(0.5+\delta, 0, 0.5)$. For $FeTe_{0.7}Se_{0.3}$, the magnetic peak center is at (0.48,0,0.5), although this differs from the commensurate position by less than the peak width. Our observations are qualitatively consistent with the previous result [352] for $Fe_{1.08}Te_{0.67}Se_{0.33}$, where the magnetic peak is at (0.438,0,0.5); it appears that both the Fe and Se concentrations impact the ordering wavevector. We have also searched for SDW order around (0.5,0.5,0.5) in the (HHL) zone, but no evidence of magnetic peaks was found.

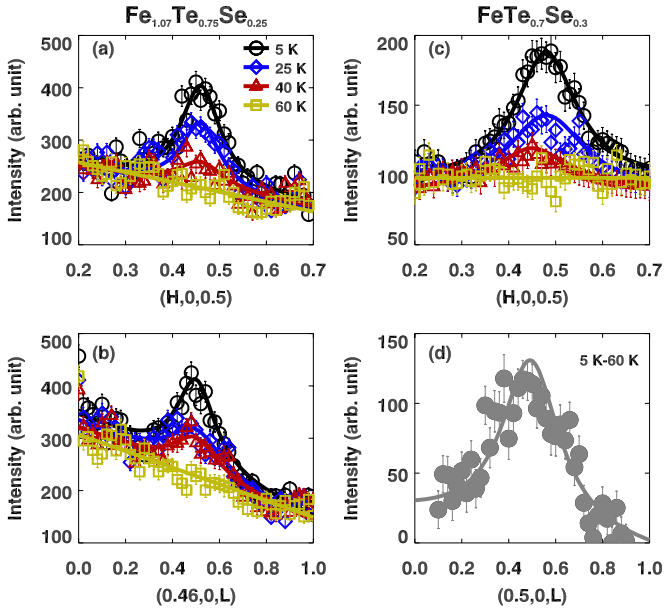

Figure 5.5: Short-range magnetic order in $Fe_{1+y}Te_{1-x}Se_x$. The left and right columns show the magnetic peak profiles for $Fe_{1.07}Te_{0.75}Se_{0.25}$ and $FeTe_{0.7}Se_{0.3}$, respectively. Top and bottom rows are scans along [100] and [001] respectively. (a), (b), and (c) are data taken at various temperatures. For the 30% Se sample, there is a temperature-independent spurious peak in the [001] scans, so in (d) we only plot 5 K data with the 60-K scan subtracted. All data are taken with 1 minute counting time and then normalized to the sample mass. The lines are fits to the data using Lorentzian functions.

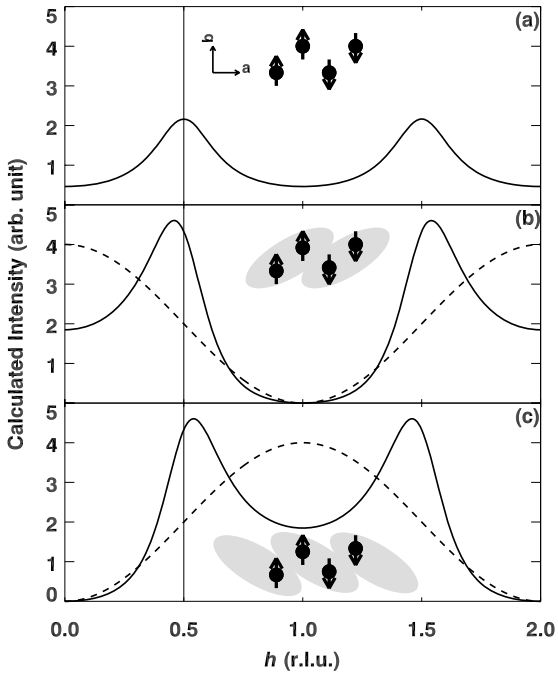

Figure 5.6: (a) Inset shows the commensurate magnetic unit cell within a single layer of $Fe_{1+y}Te$, with spin arrangements in a-b plane; solid line shows the calculated scattering intensity assuming uniform exponential decay of spin correlations. (b) Dashed line shows the magnetic structure factor $|F|^2$ and solid line shows calculated intensity for exponential decay of correlations between ferromagnetic spin pairs (inset). (c) Same as (b) but for exponential decay of correlations between antiferromagnetic spin pairs.

At 5 K, the peak width for $Fe_{1.07}Te_{0.75}Se_{0.25}$ [100] scan is 0.10 r.l.u., which corresponds to a correlation length of 6.1(1) Å. The width along [001] is 0.20 r.l.u., giving a correlation length of 4.9(1) Å. As can be seen from Fig. 5.5, the peaks for $FeTe_{0.7}Se_{0.3}$ along [100] and [001] are broader than their counterparts for $Fe_{1.07}Te_{0.75}Se_{0.25}$, and the correlation lengths are determined to be 3.8(1) Å along [100] and 3.3(1) Å along [001]. Also, from Fig. 5.4(b), one can see that the magnetic peak intensity for $Fe_{1.07}Te_{0.75}Se_{0.25}$ is always higher than the other one. Although the SDW order is short-ranged in both compounds, and starts at around the same temperature, $\sim$ 40 K, the order is apparently stronger in the 25% Se sample.

The magnetic structure of the parent compound $Fe_{1+y}Te$ can be described by the schematic diagram in the inset of Fig. 5.6(a), which is adopted from Refs. [352, 353]. Here the magnetic structure consists of two spin sublattices.

The spins in both sublattices are found to be aligned along the b axis. Within each sublattice, the spins have an antiferromagnetic alignment along a and c axes, and ferromagnetic along the b-axis. The spins have a small out-of-plane component, but here, for simplicity, we are only considering the components in the a-b plane. With low excess Fe, [353] this configuration gives rise to magnetic Bragg peaks at the commensurate antiferromagnetic wave-vector (0.5,0,0.5). The extra Fe is considered to reside in the interstitial sites of the Te/Se atoms. [352] With more excess Fe, the ordering wavevector becomes incommensurate, which can be explained by a modulation of the ordered moment size and orientation, propagating along the a axis. [352] The connection between excess Fe and the transition from commensurate to incommensurate order has been modeled theoretically. [374]

With Se doping, the magnetic order is depressed and becomes short ranged. It is intriguing that magnetic order can survive without a lowering of the lattice symmetry from tetragonal, although perhaps there are local symmetry reductions on the scale of the magnetic correlation length. The incommensurability is also interesting. A uniform sinusoidal modulation of the spin directions or magnitudes will give incommensurate peaks at $(0.5 \pm \delta, 0, 0.5)$, whereas we see a peak only on the $-\delta$ side. One can model this with phase shifted modulations on the two sublattices, but the modulation length required to describe the incommensurability is much greater than the correlation length.

We have found that a simple description of the incommensurability can be obtained when the decay of correlations between ferromagnetic nearest-neighbor spins is different from that of antiferromagnetic spin neighbors. We will consider correlations only along the modulation direction within an a-b plane, and assume that they are independent of correlations in the orthogonal directions. Let us break the spin system into perfectly correlated nearest-neighbor pairs, with exponential decay of the spin correlations from one pair to the next along the a axis. The neutron scattering intensity can then be expressed as [375]

$$I \propto |F|^2 \frac{1 - p^2}{1 + p^2 - 2p\cos(2\pi h)}, \tag{5.1}$$

where F is the structure factor for the selected pair of spins, h is the wave-vector component along the a axis, and

$$p = -e^{-a/\xi}; \tag{5.2}$$

p is the correlation function between neighboring pairs, where the negative sign suggests that the inter-pair correlation is antiferromagnetic; and ξ is the correlation length. (In all cases discussed below, we set $\xi = a$.)

Let us first consider the case of ferromagnetic spin pairs with exponentially decaying correlations between pairs, as illustrated in Fig. 5.6(b). The structure factor for this case corresponds to

$$|F|^2 = 4\cos^2(\tfrac{1}{2}\pi h), \tag{5.3}$$

as indicated by the dashed line in Fig. 5.6(b). Plugging this into Eq. 5.1 gives the solid line shown in Fig. 5.6(b). Note that the calculated peaks are incommensurate, with the peak near $h = 0.5$ shifted to lower h. Alternatively, we can start with an antiferromagnetic spin pair, in which case

$$|F|^2 = 4\sin^2(\tfrac{1}{2}\pi h). \tag{5.4}$$

This yields the result shown in Fig. 5.6(c), with the peaks shifted in the opposite direction. If the decay of correlations is identical for ferromagnetic and antiferromagnetic nearest neighbors, then we can average over these two cases, obtaining $|F|^2 = 2$; the resulting commensurate peaks are shown in Fig. 5.6(a).

Our experimental results look similar to Fig. 5.6(b). This suggests that the ferromagnetic correlations are stronger than the antiferromagnetic ones. For the model illustrated in Fig. 5.6(b), the incommensurability grows as the correlation length gets shorter. The trend in our two samples does not follow this relationship; however, one could describe a more general relationship between the ferromagnetic and antiferromagnetic correlations by taking a weighted average of Eqs. 5.3 and 5.4.

In summary, we have observed short-range magnetic order in $Fe_{1.07}Te_{0.75}Se_{0.25}$ and $FeTe_{0.7}Se_{0.3}$. In both samples, the magnetic order is incommensurate and only observed on one side of the commensurate wave-vector (0.5,0,0.5), which is likely a result of the imbalance of ferromagnetic/antiferromagnetic correlations between neighboring spins. The parent compound $Fe_{1+y}Te$ is not superconducting, [352, 353] and the optimally doped sample with 50% Se has no static magnetic order [362]. Our samples have Se content lying in the middle, where we see that with larger Se doping, the SDW order becomes weaker, while the superconductivity is enhanced. This could imply the coexistence and competition between SDW order and superconductivity in this system, similar to other Iron-based [298–301, 316] and cuprate superconductors [32, 48, 376]. This is consistent with recent theoretical works which predict the competition in the Iron-based superconductors. [377] Interestingly, in the $Fe_{1+y}Te_{1-x}Se_x$ system, the SDW order and superconductivity can be tuned not only by doping Se, but also by adjusting the Fe content. [285, 341, 372] Our results are completely consistent with these results—with less Fe and more Se, the SDW order is weaker; with more excess Fe and less Se, superconductivity is weaker.

5.2.3 Effect of magnetic field on the spin resonance in $FeTe_{0.5}Se_{0.5}$

Incommensurate resonance

As discussed in the previous Chapter, a spin resonance has been observed to develop below T_c in $Fe_{1+y}Te_{1-x}Se_x$ with $x = 0.4$ and 0.5 at the in-plane wave vector (0.5,05) and an energy of 6.5, and 7 meV respectively. [362, 363] We have confirmed the presence of a resonance in our $x = 0.5$ sample, as shown in Fig. 5.7(a). The wave vector is the same as the magnetic ordering wavevector found in other Iron-based systems, which is different from the ordering vector in the 11 compound by 45°. [266, 352, 353, 362] In the normal state, 20 K, an energy scan at the constant $\mathbf{Q} = (0.5, 0.5)$ results in an almost flat intensity vs. energy $\hbar\omega$ profile. [Fig. 5.7(a)] Below T_c, the spectral weight is greatly redistributed—at $\hbar\omega = 6.5$ meV, the intensity is greatly enhanced, while that below 5 meV is reduced, showing a gap-like feature. The intensity enhancement at 6.5 meV is referred to as "resonance". In Fig. 5.7(b), I plot the resonance peak intensity as a function of temperature, from which one can see that the resonance develops like the superconducting order parameter, with onset temperature around T_c, obtained from the magnetization results, as shown in Fig. 5.7(c). The intensity $I(T)$ was fit with the mean-field theory [260] using T_c determined by the onset of the diamagnetism in Fig. 5.7(c), with $I(T) = I(0)(1 - T/T_c)^{1/2} + A$, where $I(0)$, and A are constants. This formula results in the solid lines, which fit the data reasonably well. This is a strong evidence that the resonance is closely tied to the onset of superconductivity.

More interestingly, we found that the resonance is in fact incommensurate in $\mathbf{Q}$, peaking at $(0.5 \pm \delta, 0.5 \mp \delta)$, in a direction transverse to (0.5,0.5). The results on the $\mathbf{Q}$ dependence of the magnetic response at the resonance energy of 6.5 meV are plotted in Fig. 5.8. Transverse scans along $[1\bar{1}0]$ exhibit pair of peaks as shown in Fig. 5.8(a), while longitudinal scans only show a broad peak centering at (0.5,0.5), as shown in Fig. 5.8(b). In both cases, the intensity is enhanced when the sample is cooled below T_c, which is evident from both Figs. 5.8(a), and (b). In the upper inset of Fig. 5.8(a), the data at 1.5 K was subtracted from the 20 K data, which still gives a double-peak shape. The color-coded plot of intensity vs. $\mathbf{Q}$ at 6.5 meV and at 1.5 K, Fig. 5.8(c), demonstrates an intriguing anisotropy: the transverse peaks are not reproduced along the longitudinal direction. Our collaborators have performed ARPES measurement on the sample and found the Fermi surface near (1/2,1/2) appears to consist of four incommensurate pockets. [366] In a Fermi-surface nesting picture, one would expect to see one pair along the longitudinal direction from the nesting between a hole pocket and the four electron pockets.

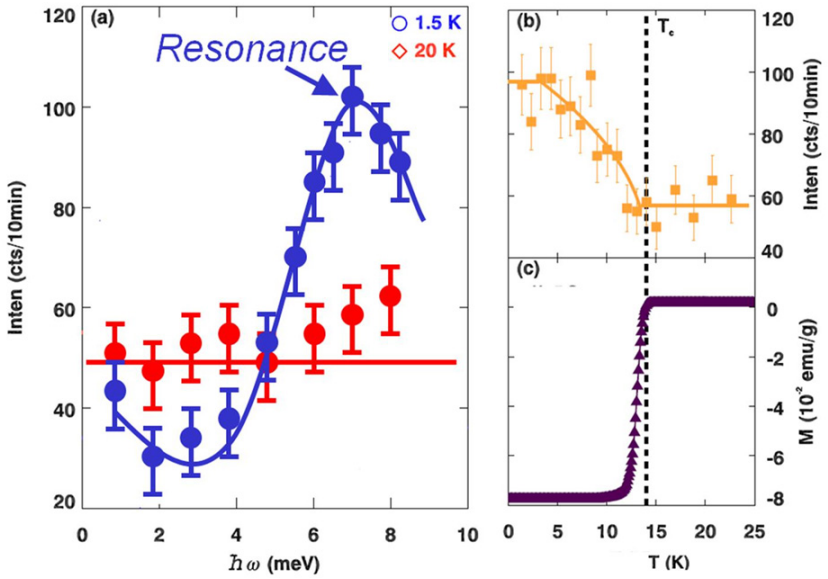

Figure 5.7: (a) Energy scans at (0.5,0.5) below (5 K) and above (20 K) T_c, 14 K. (b) Resonance peak intensity, obtained by sitting at $\mathbf{Q} = (0.5, 0.5)$, and $\hbar\omega = 6.5$ meV and counting for 10 min per point. (c) Bulk susceptibility measured under ZFC conditions, with a field of 5 Oe parallel to the a-b plane. Lines are guides to the eyes, except that the the solid line in (b) is fit to the data using a mean-field theory, [260] as described in the text. Error bars represent square roots of counts, and dashed lines indicate the T_c.

Anyhow, it explains the the incommensurability of the resonance peak. For other energies and temperatures above T_c, the anisotropy still persists. Similar results have been reported by a couple other groups, [363, 378–380] which suggest that the magnetic excitations are anisotropic, dispersing only along the transverse direction to (0.5,0.5). This is certainly not the the spin-wave like excitation, as in $CaFe_2As_2$, [381, 382] in which case one would expect to see cone-shaped dispersions. While the Fermi surface nesting is in principle compatible with the observation of the incommensurate resonance, the dispersion of isolated intensity peaks along a single direction is quite unusual and requires consideration of factors beyond the degree of electronic correlation. In fact, this puzzle is solved by considering coupling of spin and orbital correlations, which will produce anisotropic form factor, and a dispersion only along the transverse direction. [366]

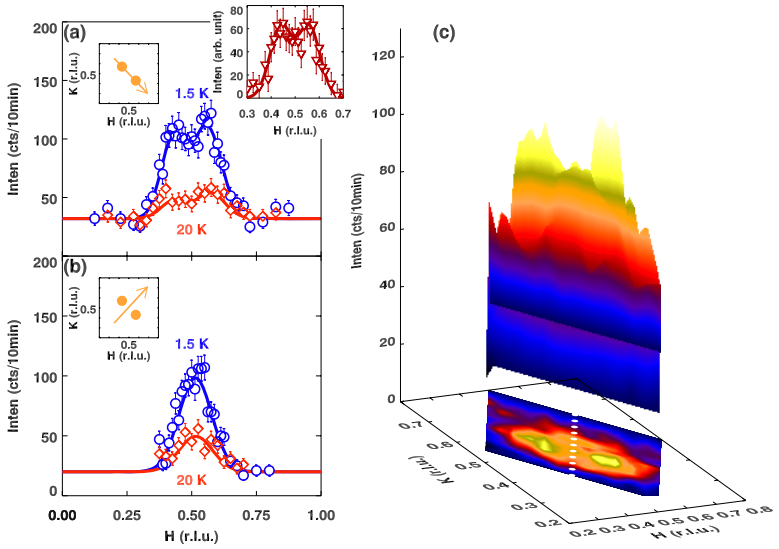

Figure 5.8: Incommensurate resonance in **Q**, peaking at $(0.5 \pm \delta, 0.5 \mp \delta)$, transversely to (0.5,0.5), at $\hbar\omega = 6.5$ meV. (a) and (b) show the **Q** scans at 1.5 and 20 K, below and above T_c, with scans directions shown in the left insets. Upper right inset is obtained by subtracting 20 K data from 1.5 K data. (c) is the plot of the **Q** dependence of the intensity at 6.5 meV.

Magnetic-field effect

Now we turn to the magnetic-field effect on the resonance. If the observed resonance is intrinsically related to the superconductivity, and since the superconductivity, and hence the pairing, is sensitive to magnetic field, one would naturally expect that an external magnetic field can also impact the resonance accordingly, as seen in $YBa_2Cu_3O_{6.6}$ [383] and in $La_{1.82}Sr_{0.18}CuO_4$ [384]. Indeed, the magnetic field effect on the resonance in Fe-based superconductors has been observed in the 1:2:2 system $BaFe_{1.9}Ni_{0.1}As_2$,[385] where the resonance energy and intensity have been partially reduced by an external field. We have carried out an inelastic neutron scattering study on $FeTe_{0.5}Se_{0.5}$ to study this problem. We find that in a 7-T magnetic field parallel to the a-b plane, the superconductivity is partially suppressed, with reduced T_c of 12 K. In the field, the resonance starts to appear at the reduced T_c, with lower intensity than that measured in zero field. This behavior demonstrates that the magnetic excitations have a close association with the superconductivity.

In Fig. 5.9, we show background (20 K data, zero field) subtracted scans performed at different temperatures. At $T = 12$ K, the difference between data taken with and without the field is very clear. With further cooling, the

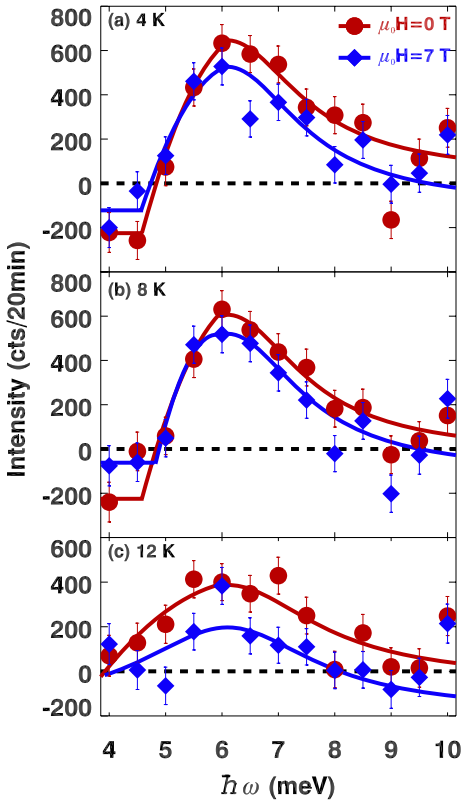

Figure 5.9: Constant-**Q** scans at (0.5,0.5,0), after subtraction of the zero-filed scan at 20 K. (a) $T = 4$ K, (b) 8 K, (c) 12 K, for $\mu_0 H = 0$ T (circles), and 7 T (diamonds). Lines through data are guides for the eye.

difference is still observable but becomes less pronounced. At $T = 4$ K, the peak intensity for the 7-T scan is about 10% to 20% smaller than that of the zero-field data, while the 7-T spectrum seems to have more intensity filled in below the gap (~ 5 meV). We have also performed **Q** scans at the resonance energy with and without field. Due to the large background, the results are inconclusive and therefore are not shown.

There is a sum rule for scattering from spin-spin correlations, and hence one might expect that the reduction of the resonance intensity by the field should result in an increase of spectral weight below the gap, as commonly seen in cuprates, [193, 208, 386, 387] as well as in $BaFe_{1.9}Ni_{0.1}As_2$ [385]. As discussed above, it is consistent with our results in principle, but the large background makes it impossible to follow the behavior to lower energies. In cuprates, Demler *et al.* analyzed a model of coexisting but competing phases of superconductivity and SDW order, [32] and successfully predicted the field-

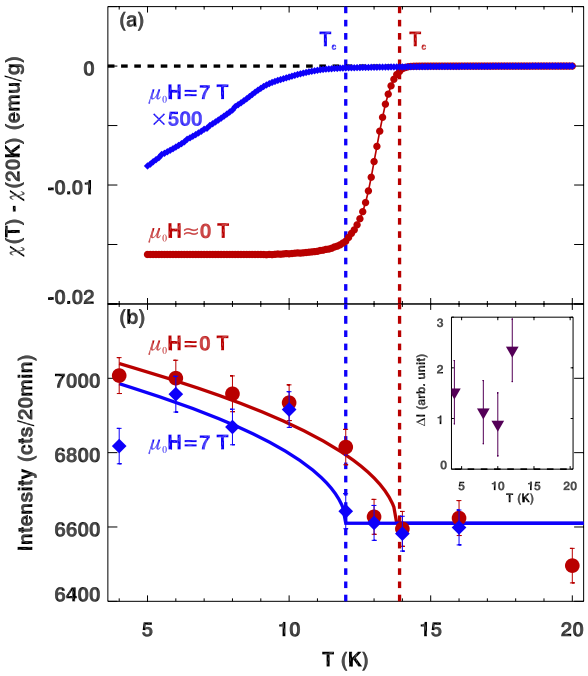

Figure 5.10: (a) Susceptibility measured with $\mu_0 H = 0.0005$ T (red circles) and 7 T (blue diamonds), with field parallel to the a-b plane. Dashed lines indicate the T_c's. (b) Resonance intensity at $(0.5, 0.5, 0)$ integrated from 6 meV to 7 meV. The solid lines are fits using mean-field theory, with T_c obtained from (a). Inset shows the difference of the resonance intensities for 0 T and 7 T, integrated from 5 meV to 8 meV.

induced static magnetic order observed experimentally. [84, 214, 376] We have searched for SDW order around (0.5,0.5), but no evidence of such field-induced order was found.

We have measured the bulk susceptibility in 0-T and 7-T field as well, and the results are shown in Fig. 5.10(a). In zero field, the system enters a superconducting state at 14 K, and becomes fully diamagnetic below 12 K. In the 7-T field, superconductivity is partially suppressed, and T_c has been reduced to 12 K. As a result of the suppressed superconductivity, the resonance intensity has also been reduced as shown in Fig. 5.9.

Fig. 5.10(b) gives another perspective of the impact of the field on the resonance. There we plot the intensity, integrated from 6 meV to 7 meV, as a function temperature obtained for the measurements with and without the field. The intensity $I(T)$ was fit with the mean-field theory [260] using T_c's determined by the onset of the diamagnetism in Fig. 5.10(a). In both 0 T

and 7 T, the resonance intensity starts to appear below respective T_c, and increases with cooling. At low temperatures, the intensity at 7 T is lower than the zero-field value. To confirm that the intensity is reduced at 7 T, we plot in the inset of Fig. 5.10(b) the difference between intensity at 0 T and 7 T, ΔI, integrated from 5 meV to 8 meV; one can see that the intensity difference is well above zero.

With Fig. 5.10, one can better understand the results in Fig. 5.9, especially the most pronounced field effect at 12 K. In zero field, the sample is in superconducting state at 12 K, where the resonance has finite intensity; in the 7-T field, the system is driven to normal state at this temperature, and the resonance intensity is approaching background level.

From the data, it is clear that the magnetic field depresses the superconductivity, and also reduces the onset temperature and intensity of the resonance. In principle, if the resonance is directly associated with the superconducting volume of the sample, the intensity ratio I_{7T}/I_{0T} should be roughly proportional to $1 - H/H_{c2}$, where H is the applied field, and H_{c2} is the upper critical field. [383] Our results showing a change $\sim 10\%$ in the resonance intensity, suggesting that H_{c2} is ~ 70 T, which is comparable to the range estimated in other studies. [343, 346] Although no significant change in the resonance with field was identified for the 40% Se sample in Ref. [362], we believe that our results are consistent with that study within the error bars. The fact that the field also suppresses the resonance intensity in $BaFe_{1.9}Ni_{0.1}As_2$ [385] suggests that this should be common in Fe-based superconductors.

In summary, we observed a resonance at $\hbar\Omega_0 \approx 6.5$ meV in $FeTe_{0.5}Se_{0.5}$ ($T_c = 14$ K). The temperature dependence of the intensity is consistent with the scaling $1 - (T/T_c)^{1/2}$. A 7-T magnetic field partially suppresses superconductivity, and lowers T_c to about 12 K, determined from the bulk susceptibility. In the field, the resonance starts to appear at the lowered T_c, 12 K, with intensity reduced. These results are consistent with the picture that the resonance is related to quasiparticle scattering in the superconducting phase, and is reduced when superconductivity becomes weaker, either by heating or applying an external magnetic field.

There are of course, still issues not fully resolved based on our results. For example, the quality of our data does not allow us to accurately determine the resonance energy. It is therefore hard to find out whether the resonance energy can be affected by the external magnetic field or not, although it has been shown that the former is the case in $BaFe_{1.9}Ni_{0.1}As_2$. [385] We have measured the susceptibility with field perpendicular to *a*-*b* plane, and it is shown that there is only weak anisotropy in the superconducting state. It will be interesting to see how the resonance responds to a *c*-axis magnetic

field. Another interesting issue is to search for the Zeeman splitting of the resonance mode under an external field, which is a good test of whether this is a singlet-triplet excitation. Zhao *et al.* [385] tried to tackle this problem using a 14.5-T field, but the results are inconclusive—the resonance in $BaFe_{1.9}Ni_{0.1}As_2$ broadens in the field, but no clear split was observed, probably due to the finite resonance width and coarse energy resolution. Qiu *et al.* [362] applied a 7-T magnetic field on $FeTe_{0.6}Se_{0.4}$, but no splitting is visible from their results; in a more recent experiment, with a larger field (14 T) and improved background, they were able to resolve the Zeeman splitting, directly establishing its triplet character [388].

5.2.4 Disappearance of static magnetic order and evolution of spin fluctuations

The parent compound for $Fe_{1+y}Te_{1-x}Se_x$ has a "bicollinear" or "E-type" antiferromagnetic order [see Fig. 4.3(a)], modulated along the $(0.5, 0)$ in-plane direction. [352, 353] Recently, there has been a report implying that superconductivity can coexist with the bicollinear structure on the atomic scale. [389] It should be quite interesting to see how the magnetic structure (static or dynamic) evolves from the E-type bicollinear configuration of the parent compound to the C-type collinear configuration in the superconducting region in the 11 system. [374, 390]

We performed neutron scattering studies to probe the magnetic order and fluctuations in a few samples from the 11 family for Se dopings ranging from 30% to 50% and with varying superconducting properties. All neutron scattering data have been normalized into absolute units ($\mu_B{}^2 \cdot \mathrm{eV}^{-1}/\mathrm{Fe}$), using incoherent elastic scattering intensities from the samples. Our results suggest that static magnetic order exists in all non-superconducting samples. (Here, by non-superconducting we mean an absence of bulk superconductivity.) This order is short-ranged and occurs at in-plane wave vectors of the type $(0.5, 0)$. For the fully superconducting samples, no static magnetic order is found. With the disappearance of static magnetic order, the associated low-energy magnetic excitations near $(0.5, 0)$ also go away, as one might expect. Magnetic excitations near $(0.5, 0.5)$ gradually become dominant as the material becomes more superconducting. While Se doping plays an essential role, it is clearly not the only determining factor regarding the superconductivity and the magnetic correlations. Samples with similar Se doping but differing in Fe content can have very different superconducting properties and corresponding magnetic structures/fluctuations. Our results clearly indicate that static bicollinear (E-type) magnetic orders in the 11 system compete with and suppress superconduc-

Table 5.1: List of the $Fe_{1+y}Te_{1-x}Se_x$ samples, superconducting and non-superconducting 30% Se doped sampleS (SC30 and NSC30), superconducting 50% Se doped (SC50) and non-superconducting 45% Se doped sample (NSC45) used in this study, with their composition y and x, T_c, room-temperature lattice parameters (from powder x-ray diffraction), a ($b = a$), and c, and sample mass m.

Sample	y	x	T_c (K)	a (Å)	c (Å)	m (g)
SC30	0.00	0.3	14	3.815	6.140	12.7
NSC30	0.05	0.3	–	3.808	6.120	7.4
SC50	0.00	0.5	14	3.811	6.129	9.0
NSC45	0.05	0.45	–	3.807	6.047	6.4

tivity. Superconductivity only appears when the system evolves towards fluctuating collinear C-type magnetic correlations, which appear to be universal across all known Fe-based superconductor families.

The single-crystal samples used in the experiment with their nominal compositions, and various characteristic properties are listed in Table 5.1. The bulk susceptibilities are shown in Fig. 5.11. From the susceptibility we can see that, although both superconducting samples show evidence of diamagnetic response at around 14 K, SC50 is clearly better in quality as far as superconducting volume fraction is concerned. With a considerable portion of its bulk volume being non-superconducting, it is possible that there is phase separation in SC30. In fact, when measuring different small pieces ($\sim$ 1 mm size) from the same SC30 sample, the superconducting volume can vary from $\lesssim 10\%$ to $\sim 80\%$, suggesting that the superconducting and non-superconducting phases could be macroscopically separated in this sample. The other samples, NSC30 and NSC45, are mostly non-superconducting, with no more than 1% of the volume giving the superconducting response.

We performed elastic magnetic scattering measurements on all samples. For the SC50 sample, there is no elastic magnetic intensity at $(0.5, 0, 0.5)$, while magnetic peaks are observed for all three other samples. In Fig. 5.12, we plot H and L scans through this antiferromagnetic wavevector for the SC30 and NSC45 samples at $T = 4$ K. The same measurements for NSC30 have been shown in § 5.2.2. The H and L scans performed at higher temperature ($T = 34$ K) show no peak structure and are therefore used as backgrounds to be subtracted from the data. All peaks are much broader than the resolution, indicating the short-ranged nature of the magnetic order. The H-scans are peaked near but not exactly at $H = 0.5$, similar as the results in § 5.2.2. The

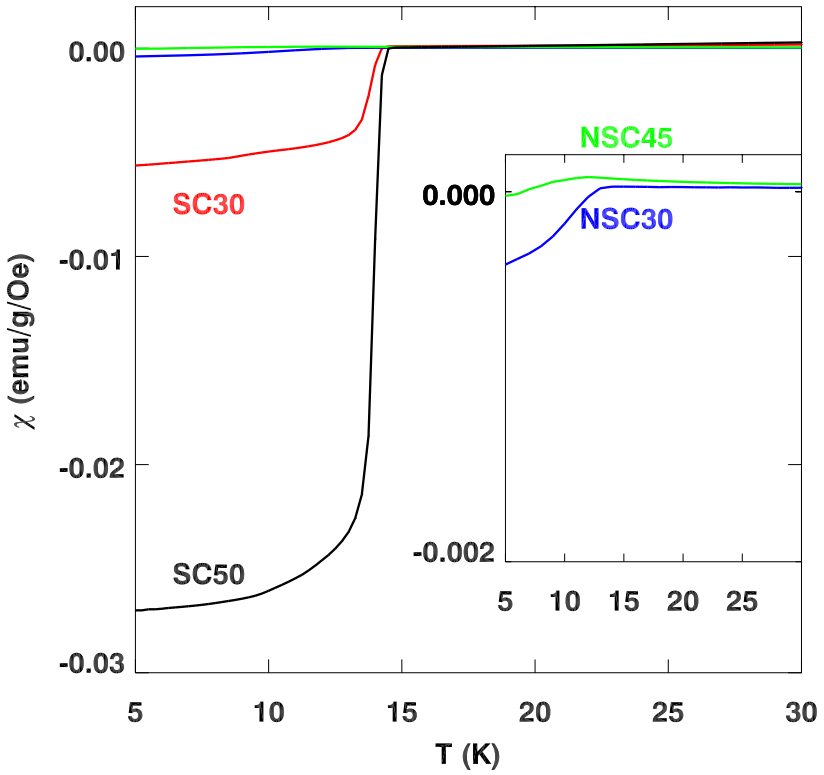

Figure 5.11: ZFC susceptibility of the four samples. The inset shows the same data from the non-superconducting samples with different scale.

L-scans, however, are qualitatively different. For lower Se doped samples, the L-scan peaks around $L = 0.5$, and intensity always goes to zero at $L = 0$. So there the magnetic order is always antiferromagnetic along the L-direction, whether short- or long-ranged. Here we see that after background subtraction, the scattering intensity at $L = 0$ is still appreciable. This suggests that although the magnetic order still has a modulation along the L-direction, which peaks around $L = 0.5$, favoring an antiferromagnetic configuration between Fe planes, the order has become much more two-dimensional. In the NSC45 sample, the 3D long-range bicollinear antiferromagnetic order of the parent compound has not been entirely destroyed, but rather greatly reduced to 2D short-range order. The ordered moment per Fe is 0.122(4) μ_B, much less than the value in the parent compound with long-range order. [352] It is nevertheless, enough to destroy superconductivity. With this static magnetic order present, even with 45% Se doping, bulk superconductivity is still not achieved. In the SC30 sample, although the sample does show a superconducting phase transition at around 14 K, the superconducting volume is smaller than for the

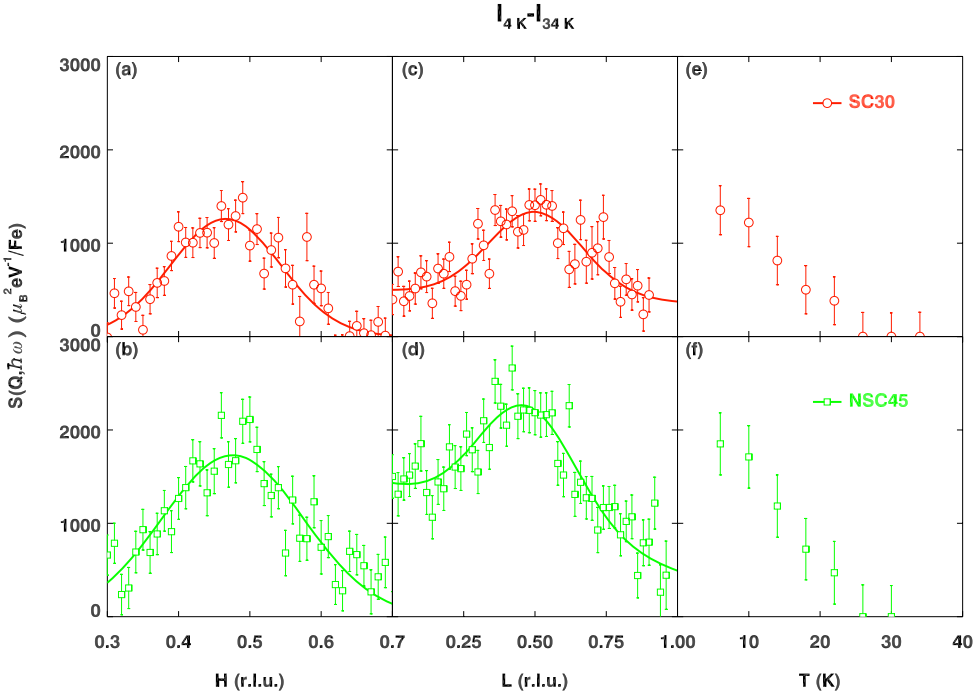

Figure 5.12: Elastic neutron scattering measurements performed on SC30 (top) and NSC45 (bottom) near $(0.5, 0, 0.5)$. (a) and (b) are intensity profiles along [100] direction (H-scans); (c) and (d) are scans along [001] direction (L-scans). (e) and (f) show the magnetic peak intensity at $(0.5, 0, 0.5)$ vs. temperature. Corresponding scans measured at $T = 34$ K are used as background, and have been subtracted from all the data shown.

SC50 sample. The ordered moment is about 0.077(4) μ_B/Fe, also much less than that in the NSC45 sample, indicating that this order may be coming from only part of the sample. Therefore there is likely a phase separation in this SC30 sample, where two phases, one superconducting and another one with a short-range magnetic order, coexist.

With the tendency of forming static bicollinear magnetic structures in the non-superconducting samples, it is natural to expect to see magnetic excitation spectra around the (0.5,0) in-plane wave-vector as well. From previous work, we know that the energy dispersion and intensity modulation along the L direction for magnetic excitations is small. We can therefore choose to perform the inelastic scattering measurements in the $(HK0)$ plane for $L = 0$. In Fig. 5.13, we plot our results taken near $(0.5, 0, 0)$. The top two panels [Fig. 5.13(a) and (b)] show energy scans at $(0.5, 0, 0)$ at $T = 4$ and 25 K. Mea-

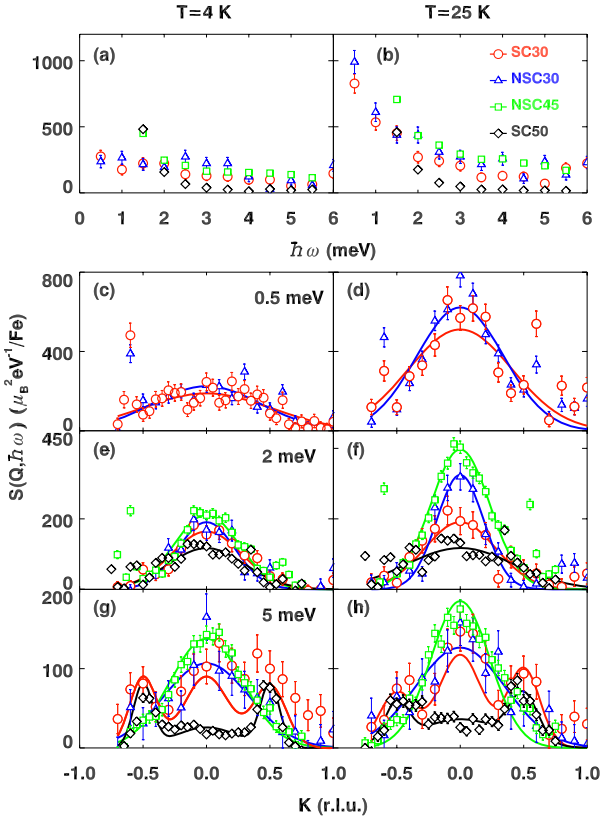

Figure 5.13: Magnetic excitations for $Fe_{1+y}Te_{1-x}Se_x$ measured around $(0.5, 0, 0)$. The left and right columns show the magnetic peak profiles for lowest temperature and 25 K respectively. (a) and (b) Constant-**Q** scans at $(0.5, 0, 0)$ taken at low T and 25 K. (c-h) Constant-energy scans at $(0.5, K, 0)$ at $\hbar\omega$ =0.5, 2 and 5 meV. A fitted K-independent background has been subtracted from all data sets.

surements for NSC45 and SC50 were taken on BT-7 with a relatively coarse energy resolution (FWHM $\sim$ 1.7meV) compared to those on SPINS (NSC30 and SC30, FWHM $\sim$ 0.3 meV), and have a large tail from scattering at $\hbar\omega = 0$. Constant-energy scans at $\hbar\omega = 0.5$, 2, and 5 meV [Fig. 5.13(c)-(h)] along the K direction across $(0.5, 0, 0)$ clearly show that for NSC30, SC30 and NSC45, there is significant spectral weight at low energies. For both 30%-Se samples, where we have measurements with higher energy resolution, one can see that the intensity at $\hbar\omega = 0.5$ meV increases on warming from 4 K to 25 K. The increase is much less pronounced at $\hbar\omega = 5$ meV. This behavior is likely due to a transfer of spectral weight from the elastic peak into low energy channels when the static order dissolves with heating. For SC50, the low-energy spin

excitations near $(0.5, 0, 0)$ are weak, and not strongly temperature dependent, which is consistent with the fact that there is no static order near (0.5,0) in this sample. The two small peaks near $K = \pm 0.5$ observed from samples SC30 and SC50 at $\hbar\omega = 5$ meV, suggest that there is additional spectral weight developing near the (0.5,0.5) wave-vector, corresponding to dynamic collinear spin correlations in the superconducting samples.

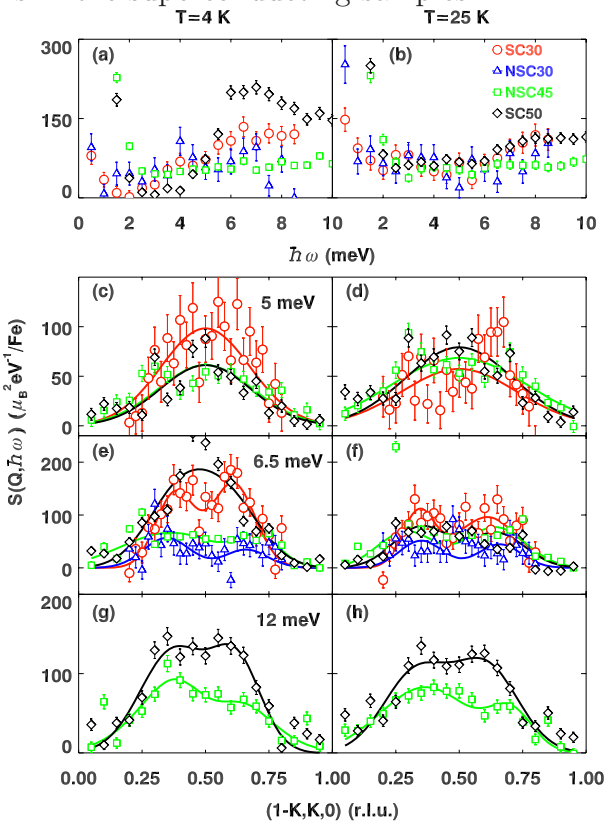

Figure 5.14: Magnetic excitations measured around $(0.5, 0.5, 0)$. The left and right columns show the magnetic peak profiles for lowest temperature and 25 K respectively. (a) and (b) Constant-$\mathbf{Q}$ scans at $(0.5, 0.5, 0)$ taken at low T and 25 K. (c-h) Constant-energy scans at $(0.5, 0.5, 0)$, taken along the transverse direction at $\hbar\omega = 5$, 6.5 and 12 meV. A fitted constant background has been subtracted from all data sets.

In Fig. 5.14, we show measurements near $(0.5, 0.5, 0)$. For SC50, a clear resonance is observed when comparing the energy scans performed at 4 K and 25 K, as discussed in previous section. In Fig. 5.14(c)-(h), constant-energy scans at $\hbar\omega = 5$, 6.5, and 12 meV performed in the direction transverse to $\mathbf{Q} = (0.5, 0.5)$ are shown. Similar to SC50, but less pronounced, we can also

see a resonating feature in SC30 in the scans of $\hbar\omega = 6.5$ and 5 meV.

For the non-superconducting samples, there is no temperature effect observed for data taken between 4 K and 25 K. For NSC30, we did a constant-energy scan near $(0.5, 0.5)$ only at $\hbar\omega = 6.5$ meV, and the intensity is very low compared to either its own magnetic scattering near $(0.5, 0)$ or those from the other samples near $(0.5, 0.5)$. It is clear that the low-energy spin excitations are mostly focused around $(0.5, 0)$ for NSC30. The NSC45 sample has Se doping very close to SC50, and also very similar magnetic excitation spectrum near $(0.5, 0.5)$ compared to that from the latter in its normal state ($T = 25$ K). However, with no superconducting transition, its spectrum at low temperature ($T = 4$ K) does not differ much from that at $T = 25$ K.

The implications of our results are very clear for NSC30 and SC50. For NSC30, a short-range static magnetic order is present at low temperature near $(0.5, 0)$, corresponding to a 3D bicollinear E-type spin structure. Its low-energy magnetic excitations are also focused near $(0.5, 0)$. With the static order, no superconductivity is achieved in this sample. For the SC50 sample, there is no static order and the low-energy magnetic excitation spectrum is mostly shifted to the $(0.5, 0.5)$ region, corresponding to collinear C-type spin correlations. Similar to the situation in the 1111 or 122 systems, [304, 311, 391] this collinear configuration without static order appears to favor superconductivity.

The results for NSC45 are more complicated. Here, with Se doping close to SC50, the magnetic excitations near the $(0.5, 0.5)$ point are rather similar to the superconducting samples, except that the resonating feature is missing. Apparently, having magnetic excitations near $(0.5, 0.5)$ associated with the collinear spin configuration is not sufficient for superconductivity to emerge. Also having a static 2D-like magnetic order with bicollinear structure is able to completely suppress superconductivity in this sample. Of course, the tetragonal crystal structure gives no energetic distinction between the ordering wave vectors $(0.5, 0)$ and $(0.5, 0.5)$, so that the magnetic configuration is relatively soft. There is likely a mixed phase where the bicollinear and collinear magnetic configurations coexist, on a microscopic level, similar to that of the mixed C-E phase in manganites, [392] as suggested in Ref. [390].

The case for SC30 is, in fact, quite intriguing. A 2D-like short-range static order exists at low temperature, while low-energy magnetic excitations are found both around $(0.5, 0)$ and $(0.5, 0.5)$ with comparable spectral weight. Therefore, the magnetic excitation spectrum actually looks very similar to that in NSC45, yet there is bulk superconductivity in SC30 when the static magnetic order is also present. Compared to NSC45, the ratio of spectral weight near (0.5,0.5) to that near (0.5,0) is higher in SC30, indicating a larger volume of the sample favoring a collinear spin configuration. The resonance oc-

curs below T_c, showing an enhancement of spectral weight only near $(0.5, 0.5)$. This indicates that superconductivity only exists in the part of the sample with dynamic collinear spin correlations. Although it is conceivable that the static order and superconductivity could coexist in the same domains as suggested by previous μSR work, [389] it is also possible to have a system with macroscopic phase separation, where the volume of local collinear or bicollinear regions are large enough to form separate domains. In this case, the features near $(0.5, 0)$ (elastic magnetic peak and low-energy magnetic excitations), and those near $(0.5, 0.5)$ come from different regions. This scenario would be consistent with the (varying) susceptibility results for different small pieces taken at different locations from this sample, and agrees with results from all other samples where static magnetic order and superconductivity do not coexist locally.

Why would samples with similar Se content *e. g.*, NSC30 vs. SC30, NSC45 vs. SC50 show dramatically different behaviors? Some believe that the Fe content also plays important roles. [352] Having higher Fe content in the parent compound could drive the order from commensurate to incommensurate, [352] while its effect is less clear for the superconducting region. It is less likely though that the excess Fe are simply isolated magnetic impurities that destroy superconductivity, since the static magnetic order and the changes in low-energy spin excitations observed in our measurements cannot be explained in such a simple manner. It has been suggested that excessive Fe atoms, or even the Te/Se disorder, may enhance the bicollinear antiferromagnetic correlation in its competition with the collinear correlation, and therefore reduce the superconducting phase coherence. [390] It has also been predicted that lowering the height of the chalcogen (Te/Se) positions can drive the 11 system from bicollinear to collinear spin configuration. [390, 393] In our samples, the excessive Fe doping appears to make the lattice parameters a and c slightly shorter, for similar Se doping levels. It is not yet clear how a smaller c could affect the magnetic structure. But a smaller a would actually favor a bicollinear structure—if we consider the Fe-Te/Se-Fe bond—to maintain the same bond length and lower the free energy, the chalcogen height would need to increase when a decreases, the system is therefore driven towards the bicollinear configuration. More theoretical work and first principle calculations are of course necessary to fully understand the details of this effect.

Despite the uncertainties in what the underlying cause for the difference in these samples is, it is evident that the magnetic structure/fluctuations are intimately coupled to superconductivity in the 11 system. If the magnetic correlations in the system favors a bicollinear (E-type) spin configuration, which sometimes can eventually lead to static order, superconductivity is then suppressed. The collinear (C-type) spin configuration, which is universal across

the superconducting regions of all Iron-based superconductor families, is what is required, but not sufficient, for the emergence of superconductivity. There are also cases where magnetic correlations favoring these two configurations coexist and compete. Overall, our results suggest that magnetic correlations are important in the Iron-based superconductor families, and the proper tuning of these correlations may be the key in enhancing superconductivity.

5.3 Summary

In this Chapter, I have shown systematic neutron scattering results on the magnetic order (static/dynamic) in $Fe_{1+y}Te_{1-x}Se_x$. It is found that the long-range antiferromagnetic order becomes short-ranged upon Se doping. In this system, both the magnetic order and superconductivity can be tuned not only by Se doping, but also by the Fe content.

The spin dynamics also show systematic changes with Se doping—when the Se doping is low, the system favors a a bicollinear (E-type) spin configuration, which is the structure for the parent compound; with increasing Se content, the spectral weight near (0.5,0.5) is increasing, which means that the spins order in a collinear (C-type) manner. For superconducting sample, a neutron-spin resonance appears when the system is cooled below T_c around (0.5,0.5) with energy ~ 6.5 meV.

We have also studied the $\mathbf{Q}$ and magnetic-field dependence of the resonance, and we found that the resonance is incommensurate in $\mathbf{Q}$, peaking at $(0.5 \pm \delta, 0.5 \mp \delta)$, in a direction transverse to (0.5,0.5). It is also found that the magnetic excitations are anisotropic, dispersing only along the transverse direction to (0.5,0.5), which can be explained by the coupling of spin and orbital freedom. The magnetic field shows its effect on the resonance by reducing both the onset temperature and the intensity, as a result of the suppressed superconductivity, demonstrating close relationship between resonance and superconductivity.

Our results for the $Fe_{1+y}Te_{1-x}Se_x$ show clearly that magnetism is playing a very big role in the superconductivity in Iron-based superconductors, and magnetic excitation is quite likely to be related to the electron pairing.

Chapter 6

Conclusions

In this final Chapter of my **Dissertation**, I am going to summarize the results on the two types of high-T_c superconductor systems, $La_{2-x}Ba_xCuO_4$, and $Fe_{1+y}Te_{1-x}Se_x$. Also, I will discuss some of the possible future works.

6.1 Summary of results

Crystal growth I have shown that by using floating-zone technique, I have successfully grown crystals for $La_{2-x}Ba_xCuO_4$ with x ranging from 0 to 15.5%. The crystals are characterized by microscope, susceptibility, and x-ray and neutron diffraction, all of which demonstrate that they are high-quality single crystals. With these high-quality large-size single crystals, neutron scattering work can be carried out.

For the Iron-based superconductor, $Fe_{1+y}Te_{1-x}Se_x$. I used the horizontal unidirectional solidification method to grow large-size high-quality single crystals. The crystals grown have nice cleavage surface, which is the a-b plane. Now, a series of $Fe_{1+y}Te_{1-x}Se_x$ single crystals are available with Se concentration ranging from 0 to 0.7. Also, we have some samples with fixed x and varying y, which show different magnetic and superconducting properties.

Neutron scattering studies With the crystals grown, neutron scattering measurements have been performed on both systems.

In $La_{2-x}Ba_xCuO_4$, I have studied the doping dependence of the stripe order and superconductivity with $x = 0.095$, 0.115, 0.125, and 0.135 by doing neutron scattering, susceptibility, and transport measurements. It is found that static spin-stripe order exists in all these four compositions, and competes with superconductivity, with one of the evidences that

when the T_c shows a maximum at $x = 0.095$, the stripe-order peak intensity is the lowest, and on the other hand, when the T_c has a minimum, the stripe order appears to be strongest (by having a highest magnetic order intensity, ordering temperature, and largest spin-spin correlation length). In an external magnetic field, the bulk superconductivity in $La_{2-x}Ba_xCuO_4$ with $x = 0.095$, and 1/8 are suppressed, while the static magnetic order is enhanced in both samples. It appears likely that the stripe order frustrates the Josephson coupling between the layers, and renders superconductivity only in the a-b planes. The impurity effect has also been studied by doping 1% Zn into $La_{2-x}Ba_xCuO_4$ ($x = 9.5\%$). By comparing the susceptibility, thermopower and thermal conductivity in the samples with and without Zn, it is clear that the superconductivity has been partially depressed, with T_c reduced from 32 K (Zn-free sample) to 17 K (1% Zn-doped sample). As a result, the magnetic order in the sample with 1% Zn doping is largely enhanced. Upon application of a magnetic field, the spin-stripe order in both samples get enhanced. All these results clearly show that the static magnetic and superconducting order are competing with each other.

In the Iron-based superconductors, $Fe_{1+y}Te_{1-x}Se_x$, the results are qualitatively similar as the cuprate for the static magnetic order. There is long-range antiferromagnetic order in the parent compound $Fe_{1+y}Te$, which is gradually suppressed by doping Se into the system. And then there is a regime where short-range SDW order coexists and competes with superconductivity. The optimal superconductivity happens at a doping with $x \approx 0.5$, and the superconductivity extends all the way to $x = 1$, in the pure $Fe_{1+y}Se$. The magnetic and superconducting properties are not only sensitive to the Se content, but also sensitive to the excess Fe concentration. For instance, the incommensurability is depending on the extra Iron. Here, the incommensurate peak is only seen on one side with lower $\mathbf{Q} = (0.5 - \delta, 0)$, which can be explained by the imbalance ferromagnetic/antiferromagnetic correlations between neighboring spins. In samples with similar Se doping but different Fe contents, both the superconducting and magnetic properties can be drastically different.

Systematic inelastic neutron scattering studies have shown that with Se doping, the system prefer a collinear type spin configuration, which seems to be required for superconductivity. If the spin configuration tends to be the bicollinear type, which is the case for samples with no or low Se doping, where long- and short-range SDW order is observed, then superconductivity is reduced. In the superconducting samples, with spin configurations favoring collinear type, a neutron-spin resonance is

observed below T_c, around the nesting wave-vector in both 30% and 50% Se doped samples. A magnetic field has been applied to see how the resonance in the $FeTe_{0.5}Se_{0.5}$ sample responds to it, and it is found that both the onset temperature and the intensity of the resonance has been reduced, as a result of the depressed superconductivity, providing strong evidence for the close relationship between resonance and superconductivity. **Q**-dependence study of the resonance reveals that the resonance is peaking at $(0.5 \pm \delta, 0.5 \mp \delta)$ in plane. Furthermore, the magnetic excitations around (0.5,0.5) are found to be anisotropic, which are dispersing only along the direction transverse to (0.5,0.5). The anisotropy is likely due to the spin and orbital coupling effects.

In both systems, it is demonstrated that magnetism is playing an important role in superconductivity. In the cuprate superconductors, superconductivity competes with the static magnetic order, and appears after the suppression of the magnetic order, in the phase where magnetic fluctuations survive. In Iron-based superconductors, we have shown that spin fluctuations are closely related to the superconductivity, especially the resonance mode observed in the magnetic excitation spectrum below T_c, which is sensitive to an external magnetic field.

Overall, our results are consistent with the idea that magnetic fluctuations are crucial for the pairing in high-T_c superconductivity. Eventually, we may see a successful high-T_c mechanism which considers spin excitations as the glue for the electrons. Then it will be promising that superconductors that are more appropriate for practical use can be designed by using a good theory.

6.2 Future works

Of course, there are still many things that can be done on both Copper- and Iron-based superconductors.

As for $La_{2-x}Ba_xCuO_4$, because of the limited sample availability, many neutron scattering works that have been performed on other cuprate systems have not been done on $La_{2-x}Ba_xCuO_4$, for instance, studying the spin dynamics for the underdoped, and optimally doped samples, which will be important to understand how magnetic excitations are playing roles in the superconductivity. It will be also interesting to search for the 2D superconductivity, as in $La_{2-x}Ba_xCuO_4$ $x = 1/8$, and 0.095. There are static stripe orders in all the samples we have studied, and if stripe order is to frustrate the 3D superconductivity and constrain the superconducting correlations within the plane, we may be able to see it in other samples. In $La_{1.905}Ba_{0.095}CuO_4$, we know that

the stripe order is enhanced in the magnetic field, and we observed the 2D superconducting state. We know that doping 1% Zn into the sample enhances the stripe order, and reduces the superconductivity, which looks similar as the magnetic-field effect, then we expect that the 2D superconductivity should also appear in this sample. Even from the crystal-growth aspect, there are still work to be done. Right now, the highest doping level we can reach is 15.5%. To go beyond this, we may need to employ high-pressure furnace. We have successfully doped 1% Zn into $La_{1.905}Ba_{0.095}CuO_4$, and it should be also worthwhile to dope Zn in samples with other Ba concentrations. Doping more Zn into the $La_{2-x}Ba_xCuO_4$ samples could also be interesting to see the competition between static stripe order and superconductivity more clearly.

The $Fe_{1+y}Te_{1-x}Se_x$ system is relatively new (about two years since its discovery). Although research progress on the Iron-based superconductors has been made every day, there are still many questions remain to be answered. For example, we now know that magnetism is important to the superconductivity, but the origin of the magnetism in Iron-based superconductors is still controversial. [394, 395] Some argued that the magnetism is itinerant in nature, which can be described by the Fermi surface nesting, [313, 317, 360, 372, 381, 396–400] while some believed that it is arising from localized d electrons, [401–403] and third proposal which is the "hybrid of the these two—some d electrons are effectively localized while others are metallic [404]. There is even one more suggesting that none of these is the case, but instead, the magnetism derives simply from the energy gain associated with transfer to lower energy of one-electron DOS spectral weight. [307] Certainly, these discrepancies have to be solved before one can fully understand how the magnetism is playing roles in the superconductivity. The magnetic-field effect will be another potential interesting point. Since the field is known to suppress the superconductivity, the magnetic correlations should respond to the field accordingly. We have shown evidence for the spin and orbital coupling in the 11 system, and it will be good to have more evidences supporting this argument. Turning to the sample-growth side, we now only have samples with Se doping to 0.7. We are trying to see whether we can push it forward and get large-size single crystals.

Bibliography

[1] H. K. Onnes, Commun. Phys. Lab. **12**, 120 (1911).

[2] H. K. Onnes, Comm. Leiden. **120b** (1911).

[3] W. Meissner and R. Ochsenfeld, Naturwissenschaften **21**, 787 (1933).

[4] J. Bardeen, L. N. Cooper, and J. R. Schrieffer, Phys. Rev. **108**, 1175 (1957).

[5] J. G. Bednorz and K. A. Müller, Z. Phys. B **64**, 189 (1986).

[6] P. Dai, B. C. Chakoumakos, G. F. Sun, K. W. Wong, Y. Xin, and D. F. Lu, Physica C **243**, 201 (1995).

[7] Y. Kamihara, H. Hiramatsu, M. Hirano, R. Kawamura, H. Yanagi, T. Kamiya, and H. Hosono, J. Am. Chem. Soc. p. 10012 (2006).

[8] Y. Kamihara, T. Watanabe, M. Hirano, and H. Hosono, J. Am. Chem. Soc. **130**, 3296 (2008).

[9] X. H. Chen, T. Wu, G. Wu, R. H. Liu, H. Chen, and D. F. Fang, Nature **453**, 761 (2008).

[10] Z.-A. Ren, W. Lu, J. Yang, W. Yi, X.-L. Shen, Z.-C. Li, G.-C. Che, X.-L. Dong, L.-L. Sun, F. Zhou, et al., Chin. Phys. Lett. **25**, 2215 (2008).

[11] M. K. Wu, J. R. Ashburn, C. J. Torng, P. H. Hor, R. L. Meng, L. Gao, Z. J. Huang, Y. Q. Wang, and C. W. Chu, Phys. Rev. Lett. **58**, 908 (1987).

[12] Z. X. Zhao, L. Q. Chen, Q. S. Yang, Y. Z. Huaug, G. H. Chen, R. M. Tang, G. R. Liu, C. G. Cui, L. Chen, L. H. Wang, et al., Kexue Tongbao **6**, 412 (1987).

[13] N. F. Mott and R. Peierls, Proc. Phys. Soc. London **49**, 72 (1937).

[14] N. F. Mott, Proc. Phys. Soc. A **62**, 416 (1949).

[15] P. W. Anderson, Science **235**, 1196 (1987).

[16] I. Affleck and J. B. Marston, Phys. Rev. B **37**, 3774 (1988).

[17] J. B. Marston and I. Affleck, Phys. Rev. B **39**, 11538 (1989).

[18] T. C. Hsu, J. B. Marston, and I. Affleck, Phys. Rev. B **43**, 2866 (1991).

[19] X.-G. Wen and P. A. Lee, Phys. Rev. Lett. **76**, 503 (1996).

[20] J.-i. Kishine, P. A. Lee, and X.-G. Wen, Phys. Rev. Lett. **86**, 5365 (2001).

[21] J. Zaanen and O. Gunnarsson, Phys. Rev. B **40**, 7391 (1989).

[22] S. A. Kivelson, E. Fradkin, and V. J. Emery, Nature **393**, 550 (1998).

[23] E. Berg, E. Fradkin, and S. A. Kivelson, Phys. Rev. B **79**, 064515 (2009).

[24] E. Berg, D. Orgad, and S. A. Kivelson, Phys. Rev. B **78**, 094509 (2008).

[25] S. A. Kivelson and E. Fradkin, *Handbook of High-Temperature Superconductivity* (Springer, New York, 2007), chap. How Optimal Inhomogeneity Produces High Temperature Superconductivity.

[26] E. Berg, E. Fradkin, S. A. Kivelson, and J. M. Tranquada, New J. Phys. **11**, 115004 (2009).

[27] O. Zachar, S. A. Kivelson, and V. J. Emery, Phys. Rev. B **57**, 1422 (1998).

[28] S. R. White and D. J. Scalapino, Phys. Rev. Lett. **80**, 1272 (1998).

[29] U. Löw, V. J. Emery, K. Fabricius, and S. A. Kivelson, Phys. Rev. Lett. **72**, 1918 (1994).

[30] S.-C. Zhang, Science **275**, 1089 (1997).

[31] M. Vojta and S. Sachdev, Phys. Rev. Lett. **83**, 3916 (1999).

[32] E. Demler, S. Sachdev, and Y. Zhang, Phys. Rev. Lett. **87**, 067202 (2001).

[33] C. M. Varma, Phys. Rev. B **61**, 3804(R) (2000).

[34] M. Franz, D. E. Sheehy, and Z. Tešanović, Phys. Rev. Lett. **88**, 257005 (2002).

[35] T. Senthil and M. P. A. Fisher, Phys. Rev. B **62**, 7850 (2000).

[36] S. Chakravarty, R. B. Laughlin, D. K. Morr, and C. Nayak, Phys. Rev. B **63**, 094503 (2001).

[37] A. Mourachkine, *High-Temperature Superconductivity in Cuprates:The Nonlinear Mechanism and Tunneling Measurements* (Kluwer Academic Publisher, 2002), chap. Bisoliton Model Of Superconductivity.

[38] T. P. Sheahen, *Introduction to High-Temperature Superconductivity* (Kluwer Academic Publisher, 2002), chap. Theory of HTSCs.

[39] S. Fujita and S. Godoy, *Theory of High Temperature Superconductivity* (Kluwer Academic Publisher, 2001).

[40] A. Damascelli, Z. Hussain, and Z.-X. Shen, Rev. Mod. Phys. **75**, 473 (2003).

[41] N. C. Yeh, Bull. Asso. Asia Paciffic Phys. Soc. **12**, 2 (2002).

[42] J. Orenstein and A. J. Millis, Science **288**, 468 (2000).

[43] P. A. Lee, N. Nagaosa, and X.-G. Wen, Rev. Mod. Phys. **78**, 17 (2006).

[44] E. W. Carlson, V. J. Emery, S. A. Kivelson, and D. Orgad, *The Physics of Conventional and Unconventional Superconductors* (Springer-Verlag, 2002), chap. Concepts in High Temperature Superconductivity.

[45] R. J. Birgeneau, C. Stock, J. M. Tranquada, and K. Yamada, J. Phys. Soc. Jpn. **75**, 111003 (2006).

[46] J. M. Tranquada, *Handbook of High Temperature Superconductors: Theory and Experiment* (Springer, 2007), chap. Neutron Scattering Studies of Antiferromagnetic Correlations in Cuprates.

[47] J. M. Tranquada, *Neutron scattering in Layered Copper-Oxide Superconductors* (Kluwer, Dordrecht, The Netherlands, 1998).

[48] A. R. Moodenbaugh, Y. Xu, M. Suenaga, T. J. Folkerts, and R. N. Shelton, Phys. Rev. B **38**, 4596 (1988).

[49] D. Vaknin, S. K. Sinha, D. E. Moncton, D. C. Johnston, J. M. Newsam, C. R. Safinya, and H. E. King, Phys. Rev. Lett. **58**, 2802 (1987).

[50] T. Freltoft, J. P. Remeika, D. E. Moncton, A. S. Cooper, J. E. Fischer, D. Harshman, G. Shirane, S. K. Sinha, and D. Vaknin, Phys. Rev. B **36**, 826 (1987).

[51] R. Coldea, S. M. Hayden, G. Aeppli, T. G. Perring, C. D. Frost, T. E. Mason, S.-W. Cheong, and Z. Fisk, Phys. Rev. Lett. **86**, 5377 (2001).

[52] Y. S. Lee, R. J. Birgeneau, M. A. Kastner, Y. Endoh, S. Wakimoto, K. Yamada, R. W. Erwin, S.-H. Lee, and G. Shirane, Phys. Rev. B **60**, 3643 (1999).

[53] M. Matsuda, M. Fujita, K. Yamada, R. J. Birgeneau, Y. Endoh, and G. Shirane, Phys. Rev. B **65**, 134515 (2002).

[54] S. Wakimoto, R. J. Birgeneau, M. A. Kastner, Y. S. Lee, R. Erwin, P. M. Gehring, S. H. Lee, M. Fujita, K. Yamada, Y. Endoh, et al., Phys. Rev. B **61**, 3699 (2000).

[55] M. Matsuda, M. Fujita, K. Yamada, R. J. Birgeneau, M. A. Kastner, H. Hiraka, Y. Endoh, S. Wakimoto, and G. Shirane, Phys. Rev. B **62**, 9148 (2000).

[56] S. Wakimoto, R. J. Birgeneau, Y. S. Lee, and G. Shirane, Phys. Rev. B **63**, 172501 (2001).

[57] M. Fujita, K. Yamada, H. Hiraka, P. M. Gehring, S. H. Lee, S. Wakimoto, and G. Shirane, Phys. Rev. B **65**, 064505 (2002).

[58] K. Yamada, C. H. Lee, K. Kurahashi, J. Wada, S. Wakimoto, S. Ueki, H. Kimura, Y. Endoh, S. Hosoya, G. Shirane, et al., Phys. Rev. B **57**, 6165 (1998).

[59] M. Matsuda, Y. S. Lee, M. Greven, M. A. Kastner, R. J. Birgeneau, K. Yamada, Y. Endoh, P. Böni, S.-H. Lee, S. Wakimoto, et al., Phys. Rev. B **61**, 4326 (2000).

[60] T. Suzuki, T. Goto, K. Chiba, T. Shinoda, T. Fukase, H. Kimura, K. Yamada, M. Ohashi, and Y. Yamaguchi, Phys. Rev. B **57**, R3229 (1998).

[61] H. Kimura, K. Hirota, H. Matsushita, K. Yamada, Y. Endoh, S. H. Lee, C. F. Majkrzak, R. Erwin, G. Shirane, M. Greven, et al., Phys. Rev. B **59**, 6517 (1999).

[62] J. M. Tranquada, B. J. Sternlieb, J. D. Axe, Y. Nakamura, and S. Uchida, Nature **375**, 561 (1995).

[63] J. M. Tranquada, J. D. Axe, N. Ichikawa, A. R. Moodenbaugh, Y. Nakamura, and S. Uchida, Phys. Rev. Lett. **78**, 338 (1997).

[64] M. Fujita, H. Goka, K. Yamada, and M. Matsuda, Phys. Rev. Lett. **88**, 167008 (2002).

[65] E. G. Moon and S. Sachdev, Phys. Rev. B **80**, 035117 (2009).

[66] V. J. Emery, S. A. Kivelson, and O. Zachar, Phys. Rev. B **56**, 6120 (1997).

[67] H. A. Mook, P. Dai, S. M. Hayden, G. Aeppli, T. G. Perring, and F. Doğan, Nature **395**, 580 (1998).

[68] A. V. Balatsky and P. Bourges, Phys. Rev. Lett. **82**, 5337 (1999).

[69] S. A. Kivelson, E. Fradkin, V. Oganesyan, I. P. Bindloss, J. M. Tranquada, A. Kapitulnik, and C. Howald, Rev. Mod. Phys. **75**, 1201 (2003).

[70] H. J. Schulz, Phys. Rev. Lett. **64**, 1445 (1990).

[71] M. Inui and P. B. Littlewood, Phys. Rev. B **44**, 4415 (1991).

[72] D. Poiblanc and T. M. Rice, Phys. Rev. B **39**, 9749 (1989).

[73] V. J. Emery and S. A. Kivelson, Nature **347**, 434 (1995).

[74] V. J. Emery and S. A. Kivelson, Phys. Rev. Lett. **74**, 3253 (1995).

[75] U. Löw, V. J. Emery, K. Fabricius, and S. A. Kivelson, Phys. Rev. Lett. **72**, 1918 (1994).

[76] J. M. Tranquada, J. D. Axe, N. Ichikawa, Y. Nakamura, S. Uchida, and B. Nachumi, Phys. Rev. B **54**, 7489 (1996).

[77] N. Ichikawa, S. Uchida, J. M. Tranquada, T. Niemöller, P. M. Gehring, S.-H. Lee, and J. R. Schneider, Phys. Rev. Lett. **85**, 1738 (2000).

[78] J. M. Tranquada, P. Wochner, and D. J. Buttrey, Phys. Rev. Lett. **79**, 2133 (1997).

[79] T. Niemöeller, N. Ichikawa, T. Frello, H. Huennefeld, N. H. Andersen, S. Uchida, J. R. Schneider, and J. M. Tranquada, Euro. Phys. J. B **12**, 509 (1999).

[80] P. Dai, H. A. Mook, and F. Doğan, Phys. Rev. Lett. **80**, 1738 (1998).

[81] C. Stock, W. J. L. Buyers, R. Liang, D. Peets, Z. Tun, D. Bonn, W. N. Hardy, and R. J. Birgeneau, Phys. Rev. B **69**, 014502 (2004).

[82] H. A. Mook, P. Dai, and F. Doğan, Phys. Rev. Lett. **88**, 097004 (2002).

[83] P. Dai, H. A. Mook, R. D. Hunt, and F. Doğan, Phys. Rev. B **63**, 054525 (2001).

[84] D. Haug, V. Hinkov, A. Suchaneck, D. S. Inosov, N. B. Christensen, C. Niedermayer, P. Bourges, Y. Sidis, J. T. Park, A. Ivanov, et al., Phys. Rev. Lett. **103**, 017001 (2009).

[85] C. Stock, W. J. L. Buyers, Z. Tun, R. Liang, D. Peets, D. Bonn, W. N. Hardy, and L. Taillefer, Phys. Rev. B **66**, 024505 (2002).

[86] K. Kakurai, S. Shamoto, T. Kiyokura, M. Sato, J. M. Tranquada, and G. Shirane, Phys. Rev. B **48**, 3485 (1993).

[87] R. P. Sharma, T. Venkatesan, Z. H. Zhang, J. R. Liu, R. Chu, and W. K. Chu, Phys. Rev. Lett. **77**, 4624 (1996).

[88] C. Howald, H. Eisaki, N. Kaneko, M. Greven, and A. Kapitulnik, Phys. Rev. B **67**, 014533 (2003).

[89] J. E. Hoffman, E. W. Hudson, K. M. Lang, V. Madhavan, H. Eisaki, S. Uchida, and J. C. Davis, Science **295**, 466 (2002).

[90] S. Mori, C. H. Chen, and S.-W. Cheong, Phys. Rev. Lett. **81**, 3972 (1998).

[91] J. M. Tranquada, D. J. Buttrey, V. Sachan, and J. E. Lorenzo, Phys. Rev. Lett. **73**, 1003 (1994).

[92] S.-H. Lee and S.-W. Cheong, Phys. Rev. Lett. **79**, 2514 (1997).

[93] H. Yoshizawa, T. Kakeshita, R. Kajimoto, T. Tanabe, T. Katsufuji, and Y. Tokura, Phys. Rev. B **61**, 854(R) (2000).

[94] C.-H. Du, M. E. Ghazi, Y. Su, I. Pape, P. D. Hatton, S. D. Brown, W. G. Stirling, M. J. Cooper, and S.-W. Cheong, Phys. Rev. Lett. **84**, 3911 (2000).

[95] J. M. Tranquada, K. Nakajima, M. Braden, L. Pintschovius, and R. J. McQueeney, Phys. Rev. Lett. **88**, 075505 (2002).

[96] J. M. Tranquada, D. J. Buttrey, and V. Sachan, Phys. Rev. B **54**, 12318 (1996).

[97] S. Wakimoto, H. Kimura, K. Ishii, K. Ikeuchi, T. Adachi, M. Fujita, K. Kakurai, Y. Koike, J. Mizuki, Y. Noda, et al., Phys. Rev. Lett. **102**, 157001 (2009).

[98] J. M. Tranquada, J. Phys. Chem. Solids **59**, 2150 (1998).

[99] V. J. Emery, S. A. Kivelson, and J. M. Tranquada, Proc. Natl. Acad. Sci. USA **96**, 8814 (1999).

[100] D. J. Scalapino, E. Loh, and J. E. Hirsch, Phys. Rev. B **34**, 8190 (1986).

[101] P. Monthoux, A. V. Balatsky, and D. Pines, Phys. Rev. Lett. **67**, 3448 (1991).

[102] E. Demler, W. Hanke, and S.-C. Zhang, Rev. Mod. Phys. **76**, 909 (2004).

[103] C. Niedermayer, C. Bernhard, T. Blasius, A. Golnik, A. Moodenbaugh, and J. I. Budnick, Phys. Rev. Lett. **80**, 3843 (1998).

[104] N. B. Christensen, H. M. Rønnow, J. Mesot, R. A. Ewings, N. Momono, M. Oda, M. Ido, M. Enderle, D. F. McMorrow, and A. T. Boothroyd, Phys. Rev. Lett. **98**, 197003 (2007).

[105] A. H. C. Neto and C. M. Smith, *Charge Inhomogeneities in Strongly Correlated Systems* (Kluwer, 2004).

[106] M. K. Crawford, R. L. Harlow, E. M. McCarron, W. E. Farneth, J. D. Axe, H. Chou, and Q. Huang, Phys. Rev. B **44**, 7749 (1991).

[107] Y. Koike, A. Kobayashi, T. Kawaguchi, M. Kato, T. Noji, Y. Ono, T. Hikita, and Y. Saito, Solid State Commun. **82**, 889 (1992).

[108] M. Akoshima and Y. Koike, J. Phys. Soc. Jpn. **67**, 3653 (1998).

[109] Y. Koike, S. Takeuchi, H. Sato, Y. Hama, M. Kato, Y. Ono, and S. Katano, J. Low. Temp. Phys. **105**, 317 (1996).

[110] Y. Koike, N. Kakinuma, M. Aoyama, T. Adachi, H. Sato, and T. Noji, J. Low. Temp. Phys. **117**, 1163 (1999).

[111] T. Adachi, T. Noji, H. Sato, Y. Koike, T. Nishizaki, and N. Kobayashi, J. Low. Temp. Phys. **117**, 1151 (1999).

[112] M. Akoshima, T. Noji, Y. Ono, and Y. Koike, Phys. Rev. B **57**, 7491 (1998).

[113] N. Kakinuma, Y. Ono, and Y. Koike, Phys. Rev. B **59**, 1491 (1999).

[114] C. C. Homes, S. V. Dordevic, G. D. Gu, Q. Li, T. Valla, and J. M. Tranquada, Phys. Rev. Lett. **96**, 257002 (2006).

[115] T. Valla, A. V. Fedorov, J. Lee, J. C. Davis, and G. D. Gu, Science **314**, 1914 (2006).

[116] Q. Li, M. Hücker, G. D. Gu, A. M. Tsvelik, and J. M. Tranquada, Phys. Rev. Lett. **99**, 067001 (2007).

[117] M. v. Zimmermann, A. Vigliante, T. Niemller, N. Ichikawa, T. Frello, J. Madsen, P. Wochner, S. Uchida, N. H. Andersen, J. M. Tranquada, et al., Euro. Phys. Lett. **41**, 629 (1998).

[118] A. Himeda, T. Kato, and M. Ogata, Phys. Rev. Lett. **88**, 117001 (2002).

[119] E. Berg, E. Fradkin, E.-A. Kim, S. A. Kivelson, V. Oganesyan, J. M. Tranquada, and S. C. Zhang, Phys. Rev. Lett. **99**, 127003 (2007).

[120] M. Raczkowski, M. Capello, D. Poilblanc, R. Frésard, and A. M. Oleś, Phys. Rev. B **76**, 140505 (2007).

[121] M. Capello, M. Raczkowski, and D. Poilblanc, Phys. Rev. B **77**, 224502 (2008).

[122] K. Yang, W. Q. Chen, T. M. Rice, M. Sigrist, and F. Zhang, New J. Phys. **11**, 055053 (2009).

[123] C.-P. Chou, N. Fukushima, and T. K. Lee, Phys. Rev. B **78**, 134530 (2008).

[124] Y.-J. Kim, J. P. Hill, S. Komiya, Y. Ando, D. Casa, T. Gog, and C. T. Venkataraman, Phys. Rev. B **70**, 094524 (2004).

[125] B. Khaykovich, S. Wakimoto, R. J. Birgeneau, M. A. Kastner, Y. S. Lee, P. Smeibidl, P. Vorderwisch, and K. Yamada, Phys. Rev. B **71**, 220508 (2005).

[126] S. Wakimoto, H. Zhang, K. Yamada, I. Swainson, H. Kim, and R. J. Birgeneau, Phys. Rev. Lett. **92**, 217004 (2004).

[127] S. Wakimoto, K. Yamada, J. M. Tranquada, C. D. Frost, R. J. Birgeneau, and H. Zhang, Phys. Rev. Lett. **98**, 247003 (2007).

[128] M. Kofu, H. Kimura, and K. Hirota, Phys. Rev B **72**, 064502 (2005).

[129] M. Kofu, H. Kimura, H. Ishida, T. Matsumura, and K. Hirota, Phys. Rev. B **79**, 184508 (2009).

[130] S. Wakimoto, R. J. Birgeneau, A. Kagedan, H. Kim, I. Swainson, K. Yamada, and H. Zhang, Phys. Rev. B **72**, 064521 (2005).

[131] S. Wakimoto, S. Lee, P. M. Gehring, R. J. Birgeneau, and G. Shirane, J. Phy. Soc. Jpn. **73**, 3413 (2004).

[132] H. Kimura, M. Kofu, Y. Matsumoto, and K. Hirota, Phys. Rev. Lett. **91**, 067002 (2003).

[133] A. A. Schafgans, A. D. LaForge, S. V. Dordevic, M. M. Qazilbash, W. J. Padilla, K. S. Burch, Z. Q. Li, S. Komiya, Y. Ando, and D. N. Basov, Phys. Rev. Lett. **104**, 157002 (2010).

[134] M. Hücker, Y.-J. Kim, G. D. Gu, J. M. Tranquada, B. D. Gaulin, and J. W. Lynn, Phys. Rev. B **71**, 094510 (2005).

[135] T. E. Mason, A. Schröder, G. Aeppli, H. A. Mook, and S. M. Hayden, Phys. Rev. Lett. **77**, 1604 (1996).

[136] B. Lake, G. Aeppli, T. E. Mason, A. Schröer, D. F. McMorrow, K. Lefmann, M. Isshiki, M. Nohara, H. Takagi, and S. M. Hayden, Nature **400**, 43 (1999).

[137] J. M. Tranquada, C. H. Lee, K. Yamada, Y. S. Lee, L. P. Regnault, and H. M. Rønnow, Phys. Rev. B **69**, 174507 (2004).

[138] R. Gilardi, A. Hiess, N. Momono, M. Oda, M. Ido, and J. Mesot, Euro. Phys. Lett. **66**, 840 (2004).

[139] N. B. Christensen, D. F. McMorrow, H. M. Rønnow, B. Lake, S. M. Hayden, G. Aeppli, T. G. Perring, M. Mangkorntong, M. Nohara, and H. Tagaki, Phys. Rev. Lett. **93**, 147002 (2004).

[140] S. M. Hayden, H. A. Mook, P. Dai, T. G. Perring, and Doğan, Nature **429**, 531 (2004).

[141] D. Reznik, P. Bourges, L. Pintschovius, Y. Endoh, Y. Sidis, T. Matsui, and S. Tajima, Phys. Rev. Lett. **93**, 207003 (2004).

[142] C. Stock, W. J. L. Buyers, R. A. Cowley, P. S. Clegg, R. Coldea, C. D. Frost, R. Liang, D. Peets, D. Bonn, W. N. Hardy, et al., Phys. Rev. B **71**, 024522 (2005).

[143] S. Pailhès, Y. Sidis, P. Bourges, V. Hinkov, A. Ivanov, C. Ulrich, L. P. Regnault, and B. Keimer, Phys. Rev. Lett. **93**, 167001 (2004).

[144] P. Bourges, in *The Gap Symmetry and Fluctuations in High Temperature Superconductors*, edited by J. Bok, G. Deutscher, D. Pavuna, and S. A. Wolf (Plenum, New York, 1998), p. 349.

[145] E. J. H. P. M., L. S. K. J., D. J. H. J., and B. V. A. M., J. Crystal Growth **118**, 477 (1992).

[146] T. Li, P. Kes, N. Hien, J. Franse, and A. Menovsky, J. Crystal Growth **135**, 481 (1994).

[147] M. Vershinin, S. Misra, S. Ono, Y. Abe, Y. Ando, and A. Yazdani, Jpn. J. App. Phys **303**, 1995 (2004).

[148] H. F. Fong, P. Bourges, Y. Sidis, L. P. Regnault, A. Ivanov, G. D. Gu, N. Koshizuka, and B. Keimer, Nature **398**, 588 (1999).

[149] J. Lee, K. Fujita, A. R. Schmidt, C. K. Kim, H. Eisaki, S. Uchida, and J. C. Davis, Science **325**, 1099 (2009).

[150] G. Xu, G. D. Gu, M. Hücker, B. Fauque, T. G. Perring, L. P. Regnault, and J. M. Tranquada, Nature Phys. **5**, 642 (2009).

[151] J. S. Wen, Z. J. Xu, G. Y. Xu, M. Hücker, J. M. Tranquada, and G. D. Gu, J. Crystal Growth **310**, 1401 (2008).

[152] K. K. Gomes, A. N. Pasupathy, A. Pushp, S. Ono, Y. Ando, and A. Yazdani1, Nature **407**, 569 (2007).

[153] Y.-J. Kim, G. D. Gu, T. Gog, and D. Casa, Phys. Rev. B **77**, 064520 (2008).

[154] J. M. Tranquada, H. Woo, T. G. Perring, H. Goka, G. D. Gu, G. Xu, M. Fujita, and K. Yamada, Nature **429**, 534 (2004).

[155] G. Xu, J. M. Tranquada, T. G. Perring, G. D. Gu, M. Fujita, and K. Yamada, Phys. Rev. B **76**, 014508 (2007).

[156] M. Fujita, H. Goka, K. Yamada, J. M. Tranquada, and L. P. Regnault, Phys. Rev. B **70**, 104517 (2004).

[157] M. Fujita, H. Goka, K. Yamada, and M. Matsuda, Phys. Rev. B **66**, 184503 (2002).

[158] M. Hücker, G. D. Gu, and J. M. Tranquada, Phys. Rev. B **78**, 214507 (2008).

[159] M. Hücker, M. v. Zimmermann, M. Debessai, J. S. Schilling, J. M. Tranquada, and G. D. Gu, Phys. Rev. Lett. **104**, 057004 (2010).

[160] S. R. Dunsiger, Y. Zhao, B. D. Gaulin, Y. Qiu, P. Bourges, Y. Sidis, J. R. D. Copley, A. Kallin, E. M. Mazurek, and H. A. Dabkowska, Phys. Rev. B **78**, 092507 (2008).

[161] Y. Zhao, B. D. Gaulin, J. P. Castellan, J. P. C. Ruff, S. R. Dunsiger, G. D. Gu, and H. A. Dabkowska, Phys. Rev. B **76**, 184121 (2007).

[162] S. R. Dunsiger, Y. Zhao, Z. Yamani, W. J. L. Buyers, H. A. Dabkowska, and B. D. Gaulin, Phys. Rev. B **77**, 224410 (2008).

[163] J. Kim, A. Kagedan, G. D. Gu, C. S. Nelson, T. Gog, D. Casa, and Y.-J. Kim, Phys. Rev. B **77**, 180513(R) (2008).

[164] M. Fujita, H. Goka, M. Enoki, and K. Yamada, Physica B **403**, 1044 (2008).

[165] M. Fujita, H. Goka, T. Adachi, Y. Koike, and K. Yamada, Physica C **426**, 257 (2005).

[166] J. Yu, Y. Yanagida, H. Takashima, Y. Inaguma, M. Itoh, and T. Nakamura, Physica C **209**, 442 (1993).

[167] T. Ito and K. Oka, Physica C **231**, 305 (1994).

[168] M. K. R. Khan, H. Tanabe, I. Tanaka, and H. Kojima, Physica C **258**, 315 (1996).

[169] T. Adachi, T. Noji, and Y. Koike, Phys. Rev. B **64**, 144524 (2001).

[170] X. Yan, J. Zhou, X. Niu, X. Chen, Q. Tu, and X. Wu, J. Crystal Growth **242**, 161 (2001).

[171] J. Meng, G. Liu, W. Zhang, L. Zhao, H. Liu, W. Lu, X. Dong, and X. J. Zhou, Supercond. Sci. Technol. **22**, 045010 (2009).

[172] H. Luo, P. Cheng, L. Fang, and H. Wen, Supercond. Sci. Technol. **21**, 125024 (2007).

[173] H. Luo, L. Fang, G. Mu, and H. Wen, J. Crystal Growth **305**, 222 (2007).

[174] B. I. Belevtsev, D. G. Naugle, K. D. D. Rathnayaka, A. Parasiris, and J. Fink-Finowicki, Physica B **355**, 341 (2005).

[175] A. M. Balbashov and S. K. Egorov, J. Crystal Growth **52**, 498 (1981).

[176] F. C. Chou, E. T. Abel, J. H. Cho, and Y. S. Lee, J. Phys. Chem. Solids **66**, 155 (2005).

[177] S. Takekawa and H. Nozaki, J. Crystal Growth **92**, 681 (1988).

[178] I. Shigaki, K. Kitahama, and K. Shibutani, Jpn. J. App. Phys. **29**, L2013 (1990).

[179] M. Menken, A. Winkelman, and A. Menovsky, J. Crystal Growth **113**, 9 (1991).

[180] J. Emmen, S. Lenczowski, J. Dalderop, and V. Brabers, J. Crystal Growth **118**, 477 (1992).

[181] G. Gu, K. Takamuku, N. Koshizuka, and S. Tanaka, J. Crystal Growth **130**, 325 (1993).

[182] G. Gu, T. Egi, N. Koshizuka, P. Miles, G. Russell, and S. Kennedy, Physica C **263**, 180 (1996).

[183] G. Shirane, S. M. Shapiro, and J. M. Tranquada, *Neutron Scattering with a Triple-Axis Spectrometer: Basic Techniques* (Cambridge University Press, Cambridge, 2002).

[184] G. L. Squires, *Introduction to the Theory of Thermal Neutron Scattering* (Dover, Mineola, NY, 1996).

[185] R. Pynn, *Neutron Scattering: A Primer* (Los Alamos Science, 1990).

[186] I. A. Zaliznyak and S.-H. Lee, *Modern Techniques for Characterizing Magnetic Materials* (Springer, Heidelberg, 2005), chap. Magnetic Neutron Scattering.

[187] R. Scherm and B. Fåk, *Neutron and X-Ray Spectroscopy* (Springer, 2006), chap. Inelastic Neutron Scattering: Introduction.

[188] S. W. Lovesey, *Theory of neutron scattering from condensed matter* (Clarendon Press, Oxford, 1984).

[189] R. Scherm, Ann. Physique **7**, 349 (1972).

[190] D. Price and K. Sköld, *Methods of Experimental Physics* (Academic Press, New York, 1986), vol. 23A, chap. Neutron Scattering.

[191] R. Currat, *Neutron and X-Ray Spectroscopy* (Springer, 2006), chap. Three-Axis Inelastic Neutron Scattering.

[192] J. M. Tranquada, G. D. Gu, M. Hücker, Q. Jie, H.-J. Kang, R. Klingeler, Q. Li, N. Tristan, J. S. Wen, G. Y. Xu, et al., Phys. Rev. B **78**, 174529 (2008).

[193] Jinsheng Wen, Zhijun Xu, Guangyong Xu, J. M. Tranquada, Genda Gu, S. Chang, and H. J. Kang, Phys. Rev. B **78**, 212506 (2008).

[194] M. Hücker and M. v. Zimmermann and G. D. Gu and Z. J. Xu and J. S. Wen and Guangyong Xu and H. J. Kang and A. Zheludev and J. M. Tranquada, *Stripe order in superconducting* $La_{2-x}Ba_xCuO_4$ *for* $0.095 \leq x \leq 0.155$ (2010), `arXiv:1005.5191`.

[195] Jinsheng Wen, Q. Jie, Q. Li, M. Hücker, M. v. Zimmermann, Z. Xu, D. K. Singh, L. Zhang, G. Gu, and J. M. Tranquada, *Magnetic-field-induced decoupling of superconducting layers in a copperoxide compound* (2010), submitted to Nature.

[196] M. Hücker and M. v. Zimmermann and Z. J. Xu and J. S. Wen and G. D. Gu, *Zn doping dependence of stripes in* $La_{1.905}Ba_{0.095}CuO_4$ (2010), submitted to J. Supercond. Nov. Magn.

[197] Jinsheng Wen, Z. Xu, Q. Jie, A. Zheludev, B. Winn, W. Tian, Q. Li, G. Gu, and J. M. Tranquada, *Neutron scattering and transport investigation on striped superconductors* $La_{1.905}Ba_{0.095}CuO_4$ *with and without Zn*, unpublished.

[198] M. Hücker and M. v. Zimmermann and Z. J. Xu and J. S. Wen and G. D. Gu and J. M. Tranquada, *Magnetic field dependence of charge stripes in underdoped* $La_{2-x}Ba_xCuO_4$, unpublished.

[199] J. Fink, E. Schierle, E. Weschke, J. Geck, D. Hawthorn, V. Soltwisch, H. Wadati, H.-H. Wu, H. A. Dürr, N. Wizent, et al., Phys. Rev. B **79**, 100502 (2009).

[200] J. M. Tranquada, N. Ichikawa, and S. Uchida, Phys. Rev. B **59**, 14712 (1999).

[201] P. Wochner, J. M. Tranquada, D. J. Buttrey, and V. Sachan, Phys. Rev. B **57**, 1066 (1998).

[202] P. A. Lee, Rep. Prog. Phys. **71**, 012501 (2008).

[203] C.-H. Lee, K. Yamada, Y. Endoh, G. Shirane, R. J. Birgeneau, M. A. Kastner, M. Greven, , and Y.-J. Kim, J. Phys. Soc. Jpn **69**, 1170 (2000).

[204] P. Bourges, Y. Sidis, H. F. Fong, L. P. Regnault, J. Bossy, A. Ivanov, and B. Keimer, Science **288**, 1234 (2000).

[205] P. Bourges, H. F. Fong, L. P. Regnault, J. Bossy, C. Vettier, D. L. Milius, I. A. Aksay, and B. Keimer, Phys. Rev. B **56**, 11439(R) (1997).

[206] J. M. Tranquada, Proc. SPIE **5932**, 59320C (2005).

[207] E. Arrigoni, E. Fradkin, and S. A. Kivelson, Phys. Rev. B **69**, 214519 (2004).

[208] B. Lake, G. Aeppli, K. N. Clausen, D. F. McMorrow, K. Lefmann, N. E. Hussey, N. Mangkorntong, M. Nohara, H. Takagi, T. E. Mason, et al., Science **291**, 1759 (2001).

[209] J. M. Tranquada, G. D. Gu, M. Hücker, Q. Jie, H.-J. Kang, R. Klingeler, Q. Li, N. Tristan, J. S. Wen, G. Y. Xu, et al., Phys. Rev. B **78**, 174529 (2008).

[210] P. Dai, H. A. Mook, G. Aeppli, S. M. Hayden, F. Doğan, J. Yu, Y. Yanagida, H. Takashima, Y. Inaguma, M. Itoh, et al., Nature **406**, 965 (2000).

[211] P. Bourges, H. Casalta, L. P. Regnault, J. Bossy, P. Burlet, C. Vettier, E. Beaugnon, P. Gautier-Picard, and R. Tournier, Physica B **234**, 830 (1997).

[212] Y. Ando and K. Segawa, Phys. Rev. Lett. **88**, 167005 (2002).

[213] S. Katano, M. Sato, K. Yamada, T. Suzuki, and T. Fukase, Phys. Rev. B **62**, 14677 (R) (2000).

[214] B. Lake, H. M. Rønnow, N. B. Christensen, G. Aeppli, K. Lefmann, D. F. McMorrow, P. Vorderwisch, P. Smeibidl, N. Mangkorntong, T. Sasagawa, et al., Nature **415**, 299 (2002).

[215] J. Chang, C. Niedermayer, R. Gilardi, N. B. Christensen, H. M. R. nnow, D. F. McMorrow, M. Ay, J. Stahn, O. Sobolev, A. Hiess, et al., Phys. Rev. B **78**, 104525 (2008).

[216] B. Khaykovich, Y. S. Lee, R. W. Erwin, S.-H. Lee, S. Wakimoto, K. J. Thomas, M. A. Kastner, and R. J. Birgeneau, Phys. Rev. B **66**, 014528 (2002).

[217] B. Khaykovich, R. J. Birgeneau, F. C. Chou, R. W. Erwin, M. A. Kastner, S.-H. Lee, Y. S. Lee, P. Smeibidl, P. Vorderwisch, and S. Wakimoto, Phys. Rev. B **67**, 054501 (2003).

[218] S. Wakimoto, R. J. Birgeneau, Y. Fujimaki, N. Ichikawa, T. Kasuga, Y. J. Kim, K. M. Kojima, S.-H. Lee, H. Niko, J. M. Tranquada, et al., Phys. Rev. B **67**, 184419 (2003).

[219] A. T. Savici, A. Fukaya, I. M. Gat-Malureanu, T. Ito, P. L. Russo, Y. J. Uemura, C. R. Wiebe, P. P. Kyriakou, G. J. MacDougall, M. T. Rovers, et al., Phys. Rev. Lett. **95**, 157001 (2005).

[220] C. J. Peters, R. J. Birgeneau, M. A. Kastner, H. Yoshizawa, Y. Endoh, J. Tranquada, G. Shirane, Y. Hidaka, M. Oda, M. Suzuki, et al., Phys. Rev. B **37**, 9761 (1988).

[221] R. Kleiner, F. Steinmeyer, G. Kunkel, and P. Müller, Phys. Rev. Lett. **68**, 2394 (1992).

[222] K. B. Efetov, Sov. Phys. JETP **49**, 905 (1979).

[223] S. E. Korshunov and A. I. Larkin, Phys. Rev. B **46**, 6395 (1992).

[224] L. Li, Y. Wang, S. Komiya, S. Ono, Y. Ando, G. D. Gu, and N. P. Ong, Phys. Rev. B **81**, 054510 (2010).

[225] S. Tajima, T. Noda, H. Eisaki, and S. Uchida, Phys. Rev. Lett. **86**, 500 (2001).

[226] B. D. Josephson, Rev. Mod. Phys. **36**, 216 (1964).

[227] M. E. Fisher and J. S. Langer, Phys. Rev. Lett. **20**, 665 (1968).

[228] K. S. Raman, V. Oganesyan, and S. L. Sondhi, Phys. Rev. B **79**, 174528 (2009).

[229] A. E. Koshelev, L. I. Glazman, and A. I. Larkin, Phys. Rev. B **53**, 2786 (1996).

[230] A. A. Schafgans et al., *Breakdown of the universal josephson relation in spin ordered cuprate superconductors*, unpublished.

[231] C. S. O'Hern, T. C. Lubensky, and J. Toner, Phys. Rev. Lett. **83**, 2745 (1999).

[232] Y. Ando, G. S. Boebinger, A. Passner, T. Kimura, and K. Kishio, Phys. Rev. Lett. **75**, 4662 (1995).

[233] T. Adachi, N. Kitajima, T. Manabe, Y. Koike, K. Kudo, T. Sasaki, and N. Kobayashi, Phys. Rev. B **71**, 104516 (2005).

[234] S. Komiya, Y. Ando, X. F. Sun, and A. N. Lavrov, Phys. Rev. B **65**, 214535 (2002).

[235] A. D. LaForge, A. A. Schafgans, S. V. Dordevic, W. J. Padilla, K. S. Burch, Z. Q. Li, K. Segawa, S. Komiya, Y. Ando, J. M. Tranquada, et al., Phys. Rev. B **81**, 064510 (2010).

[236] L. Li, J. G. Checkelsky, S. Komiya, Y. Ando, and N. P. Ong, Nature Phys. **3**, 311 (2007).

[237] B. L. Winn, H. Kimura, D. N. Argyriou, N. Aso, K. Hirota, M. Kofu, and M. Matsuura, Physica B **385**, 153 (2006).

[238] A. V. Mahajan, H. Alloul, G. Collin, and J. F. Marucco, Phys. Rev. Lett. **72**, 3100 (1994).

[239] H. Mikuni, T. Adachi, S. Yairi, M. Kato, Y. Koike, I. Watanabe, and K. Nagamine, Phys. Rev. B **68**, 024524 (2003).

[240] T. Nakano, N. Momono, T. Nagata, M. Oda, and M. Ido, Phys. Rev. B **58**, 5831 (1998).

[241] H. Alloul, P. Mendels, H. Casalta, J. F. Marucco, and J. Arabski, Phys. Rev. Lett. **67**, 3140 (1991).

[242] K. Terashima, T. Sato, K. Nakayama, T. Arakane, T. Takahashi, M. Kofu, and K. Hirota, Phys. Rev. B **77**, 092501 (2008).

[243] T. Adachi, N. Oki, Risdiana, S. Yairi, Y. Koike, and I. Watanabe, Phys. Rev. B **78**, 134515 (2008).

[244] M. Matsuda, R. J. Birgeneau, H. Chou, Y. Endoh, M. A. Kastner, H. Kojima, K. Kuroda, G. Shirane, I. Tanaka, and K. Yamada, J. Phys. Soc. Jpn. **62**, 443 (1993).

[245] G. Xiao, M. Z. Cieplak, J. Q. Xiao, and C. L. Chien, Phys. Rev. B **42**, 8752 (1990).

[246] B. Nachumi, A. Keren, K. Kojima, M. Larkin, G. M. Luke, J. Merrin, O. Tchernyshöv, Y. J. Uemura, N. Ichikawa, M. Goto, et al., Phys. Rev. Lett. **77**, 5421 (1996).

[247] P. Mendels, H. Alloul, J. H. Brewer, G. D. Morris, T. L. Duty, S. Johnston, E. J. Ansaldo, G. Collin, J. F. Marucco, C. Niedermayer, et al., Phys. Rev. B **49**, 10035 (1994).

[248] K. Hirota, Physica C **357-360**, 61 (2001).

[249] K. Hirota, K. Yamada, I. Tanaka, and H. Kojima, Physica B **241-243**, 817 (1998).

[250] C. Bernhard, J. L. Tallon, C. Bucci, R. De Renzi, G. Guidi, G. V. M. Williams, and C. Niedermayer, Phys. Rev. Lett. **77**, 2304 (1996).

[251] X. F. Sun, J. Takeya, S. Komiya, and Y. Ando, Phys. Rev. B **67**, 104503 (2003).

[252] Y. Fukuzumi, K. Mizuhashi, K. Takenaka, and S. Uchida, Phys. Rev. Lett. **76**, 684 (1996).

[253] J. M. Tranquada, N. Ichikawa, K. Kakurai, and S. Uchida, J. Phys. Chem. Solids **60**, 1019 (1999).

[254] Y. Sidis, P. Bourges, B. Hennion, L. P. Regnault, R. Villeneuve, G. Collin, and J. F. Marucco, Phys. Rev. B **53**, 6811 (1996).

[255] Y. Sidis, P. Bourges, H. F. Fong, B. Keimer, L. P. Regnault, J. Bossy, A. Ivanov, B. Hennion, P. Gautier-Picard, G. Collin, et al., Phys. Rev. Lett. **84**, 5900 (2000).

[256] O. Anegawa, Y. Okajima, S. Tanda, and K. Yamaya, Phys. Rev. B **63**, 140506 (2001).

[257] P. H. Egli, *Thermoelectricity* (Wiley, Michigan, 1961).

[258] G. S. Nolas, J. Shar, and H. J. Goldsmid, *Thermoelectrics: basic principles and new materials developments* (Springer, 1962).

[259] S. Boutiche, *Unified thermopower in the variable range hopping regime* (2009), `arXiv:0902.0200`.

[260] N. W. Ashcroft and N. D. Mermin, *Solid State Physics* (Brooks Cole, 1976).

[261] C. Kittel, *Introduction to Solid State Physics* (Wiley, 2004), 8th ed.

[262] M. Sutherland, D. G. Hawthorn, R. W. Hill, F. Ronning, S. Wakimoto, H. Zhang, C. Proust, E. Boaknin, C. Lupien, L. Taillefer, et al., Phys. Rev. B **67**, 174520 (2003).

[263] H. Takahashi, K. Igawa, K. Arii, Y. Kamihara, M. Hirano, and H. Hosono, Nature **453**, 376 (2008).

[264] K. Ishida, Y. Nakai, and H. Hosono, J. Phys. Soc. Jpn. **78**, 062001 (2009).

[265] H. Hosono, J. Phys. Soc. Jpn. Supplement C **77**, 1 (2008).

[266] J. W. Lynn and P. Dai, Physcia C **469**, 469 (2009).

[267] M. D. Lumsden and A. D. Christianson, J. Phys.: Condens. Matter **22**, 203203 (2010).

[268] C. W. Chu and B. Lorenz, Physica C **469**, 385 (2009).

[269] Y. Mizuguchi and Y. Takano, *A review of Fe-chalcogenide superconductors: the simplest Fe-based superconductor* (2010), `arXiv:1003.2696`.

[270] A. S. Sefat, R. Jin, M. A. McGuire, B. C. Sales, D. J. Singh, and D. Mandrus, Phys. Rev. Lett. **101**, 117004 (2008).

[271] M. Rotter, M. Tegel, and D. Johrendt, Phys. Rev. Lett. **101**, 107006 (2008).

[272] G. F. Chen, Z. Li, G. Li, W. Z. Hu, J. Dong, X. D. Zhang, P. Zheng, N. L. Wang, and J. L. Luo, Chin. Phys. Lett. **25**, 3403 (2008).

[273] D. S. Inosov, A. Leineweber, X. Yang, J. T. Park, N. B. Christensen, R. Dinnebier, G. L. Sun, C. Niedermayer, D. Haug, P. W. Stephens, et al., Phys. Rev. B **79**, 224503 (2009).

[274] Z. Deng, X. C. Wang, Q. Liu, S. J. Zhang, Y. X. Lv, J. L. Zhu, R. Yu, and C. Jin, Europhys. Lett. **87**, 3704 (2009).

[275] X. C. Wang, Q. Q. Liu, Y. X. Lv, W. B. Gao, L. X. Yang, R. C. Yu, F. Y. Li, and C. Q. Jin, Solid State Commun. **148**, 538 (2008).

[276] M. J. Pitcher, D. R. Parker, P. Adamson, S. J. C. Herkelrath, A. T. Boothroyd, and S. J. Clarke, Chem. Commun. **45**, 5918 (2008).

[277] C. W. Chu, F. Chen, M. Gooch, A. M. Guloy, B. Lorenz, B. Lv, K. Sasmal, Z. J. Tang, J. H. Tapp, and Y. Y. Xue, Physica C **469**, 326 (2009).

[278] J. H. Tapp, Z. Tang, B. Lv, K. Sasmal, B. Lorenz, P. C. W. Chu, and A. M. Guloy, Phys. Rev. B **78**, 060505 (2008).

[279] Z. Deng, X. C. Wang, Q. Q. Liu, S. J. Zhang, Y. X. Lv, J. L. Zhu, R. C. Yu, and C. Q. Jin, Europhys. Lett. **87**, 37004 (2009).

[280] S. J. Zhang, X. C. Wang, Q. Q. Liu, Y. X. Lv, X. H. Yu, Z. J. Lin, Y. S. Zhao, L. Wang, Y. Ding, H. K. Mao, et al., Euro. Phys. Lett. **88**, 47008 (2009).

[281] F.-C. Hsu, J.-Y. Luo, K.-W. Yeh, T.-K. Chen, T.-W. Huang, P. M. Wu, Y.-C. Lee, Y.-L. Huang, Y.-Y. Chu, D.-C. Yan, et al., Proc. Natl. Acad. Sci. USA **105**, 14262 (2008).

[282] K.-W. Yeh, T.-W. Huang, Y.-L. Huang, T.-K. Chen, F.-C. Hsu, P. M. Wu, Y.-C. Lee, Y.-Y. Chu, C.-L. Chen, J.-Y. Luo, et al., Europhys. Lett. **84**, 37002 (2008).

[283] B. C. Sales, A. S. Sefat, M. A. McGuire, R. Y. Jin, D. Mandrus, and Y. Mozharivskyj, Phys. Rev. B **79**, 094521 (2009).

[284] S. Medvedev, T. M. McQueen, I. Trojan, T. Palasyuk, M. I. Eremets, R. J. Cava, S. Naghavi, F. Casper, V. Ksenofontov, G. Wortmann, et al., Nature Mater. **8**, 630 (2009).

[285] T. M. McQueen, Q. Huang, V. Ksenofontov, C. Felser, Q. Xu, H. Zandbergen, Y. S. Hor, J. Allred, A. J. Williams, D. Qu, et al., Phys. Rev. B **79**, 014522 (2009).

[286] A. J. Williams, T. M. McQueen, and R. J. Cava, Solid State Commun. **149**, 1507 (2009).

[287] B. I. Zimmer, W. Jeitschko, J. H. Albering, R. Glaum, and M. Reehuis, J. Alloys and Compounds **229**, 238 (1995).

[288] R. Pottgen and D. Johrendt, Z. Naturforsch **63**, 1135 (2008).

[289] M. Pfisterer and G. Nagorsen, Z. Naturforsch. B **35**, 703 (1980).

[290] J. Zhao, Q. Huang, C. de la Cruz, J. W. Lynn, M. D. Lumsden, Z. A. Ren, J. Yang, X. Shen, X. Dong, Z. Zhao, et al., Phys. Rev. B **78**, 132504 (2008).

[291] C. Lester, J.-H. Chu, J. G. Analytis, S. C. Capelli, A. S. Erickson, C. L. Condron, M. F. Toney, I. R. Fisher, and S. M. Hayden, Phys. Rev. B **79**, 144523 (2009).

[292] P. Quebe, L. Terbüchte, and W. Jeitschko, J. Alloys Compd. **302**, 70 (2000).

[293] D. Fruchart, P. Convert, P. Wolfers, R. Madar, J. P. Senateur, and R. Fruchart, Mater. Res. Bull. **10**, 169 (1975).

[294] Y. Qiu, W. Bao, Q. Huang, T. Yildirim, J. M. Simmons, M. A. Green, J. W. Lynn, Y. C. Gasparovic, J. Li, T. Wu, et al., Phys. Rev. Lett. **101**, 257002 (2008).

[295] N. Kumar, S. Chi, Y. Chen, K. G. Rana, A. K. Nigam, A. Thamizhavel, W. Ratcliff, II, S. K. Dhar, and J. W. Lynn, Phys. Rev. B **80**, 144524 (2009).

[296] T. M. McQueen, M. Regulacio, A. J. Williams, Q. Huang, J. W. Lynn, Y. S. Hor, D. V. West, M. A. Green, and R. J. Cava, Phys. Rev. B **78**, 024521 (2008).

[297] D. J. Singh, Physica C **469**, 418 (2009).

[298] J. Zhao, Q. Huang, C. de la Cruz, S. Li, J. W. Lynn, Y. Chen, M. A. Green, G. F. Chen, G. Li, Z. Li, et al., Nature Mater. **7**, 953 (2008).

[299] A. J. Drew, C. Niedermayer, P. J. Baker, F. L. Pratt, S. J. Blundell, T. Lancaster, R. H. Liu, G. Wu, X. H. Chen, I. Watanabe, et al., Nature Mater. **8**, 310 (2009).

[300] M. Rotter, M. Pangerl, M. Tegel, and D. Johrendt, Angew. Chem. Int.. Ed. **47**, 7949 (2008).

[301] H. Chen, Y. Ren, Y. Qiu, W. bao, R. H. Liu, G. Wu, T. Wu, Y. L. Xie, X. F. Wang, Q. Huang, et al., Europhys. Lett. **85**, 17006 (2009).

[302] L. Fang, H. Luo, P. Cheng, Z. Wang, Y. Jia, G. Mu, B. Shen, I. I. Mazin, L. Shan, C. Ren, et al., Phys. Rev. B **80**, 140508(R) (2009).

[303] J.-H. Chu, J. G. Analytis, C. Kucharczyk, and I. R. Fisher, Phys. Rev. B **79**, 014506 (2009).

[304] C. de la Cruz, Q. Huang, J. W. Lynn, J. Li, W. Ratcliff, J. L. Zarestzky, H. A. Mook, G. F. Chen, J. L. Luo, N. L. Wang, et al., Nature **453**, 899 (2008).

[305] Q. Huang, Y. Qiu, W. Bao, M. A. Green, J. W. Lynn, Y. C. Gasparovic, T. Wu, G. Wu, and X. H. Chen, Phys. Rev. Lett. **101**, 257003 (2008).

[306] Y. Chen, J. W. Lynn, J. Li, G. Li, G. F. Chen, J. L. Luo, N. L. Wang, P. Dai, C. de la Cruz, and H. A. Mook, Phys. Rev. B **78**, 064515 (2008).

[307] M. D. Johannes and I. I. Mazin, Phys. Rev. B **79**, 220510 (R) (2009).

[308] S. D. Wilson, Z. Yamani, C. R. Rotundu, B. Freelon, E. Bourret-Courchesne, and R. J. Birgeneau, Phys. Rev. B **79**, 184519 (2009).

[309] M. Kofu, Y. Qiu, W. bao, S. H. Lee, S. Chang, T. Wu, G. Wu, and X. H. Chen, New J. Phys. **11**, 055001 (2009).

[310] H. Luetkens, H. H. Klauss, M. Kraken, F. J. Litterst, T. Dellmann, R. Klingeler, C. Hess, R. Khasanov, A. Amato, C. Baines, et al., Nature Mater. **8**, 305 (2009).

[311] Q. Huang, J. Zhao, J. W. Lynn, G. F. Chen, J. L. Luo, N. L. Wang, and P. Dai, Phys. Rev. B **78**, 054529 (2008).

[312] M. A. McGuire, A. D. Christianson, A. S. Sefat, B. C. Sales, M. D. Lumsden, R. Jin, E. A. Payzant, D. Mandrus, Y. Luan, V. Keppens, et al., Phys. Rev. B **78**, 094517 (2008).

[313] I. I. Mazin, D. J. Singh, M. D. Johannes, and M. H. Du, Phys. Rev. Lett. **101**, 057003 (2008).

[314] K. Kuroki, S. Onari, R. Arita, H. Usui, Y. Tanaka, H. Kontani, and H. Aoki, Phys. Rev. Lett. **101**, 087004 (2008).

[315] F. Ma and Z.-Y. Lu, Phys. Rev. B **78**, 033111 (2008).

[316] J. Dong, H. J. Zhang, G. Xu, Z. Li, G. Li, W. Z. Hu, D. Wu, G. F. Chen, X. Dai, J. L. Luo, et al., Europhys. Lett. **83**, 27006 (2008).

[317] V. Cvetkovic and Z. Tesanovic, Europhys. Lett. **85**, 37002 (2009).

[318] S. Graser, T. A. Maier, P. J. Hirschfeld, and D. J. Scalapino, New J. Phys. **11**, 025016 (2009).

[319] A. D. Christianson, E. A. Goremychkin, R. Osborn, S. Rosenkranz, M. D. Lumsden, C. D. Malliakas, l S. Todorov, H. Claus, D. Y. Chung, M. G. Kanatzidis, et al., Nature **456**, 930 (2008).

[320] M. D. Lumsden, A. D. Christianson, D. Parshall, M. B. Stone, S. E. Nagler, G. J. MacDougall, H. A. Mook, K. Lokshin, T. Egami, D. L. Abernathy, et al., Phys. Rev. Lett. **102**, 107005 (2009).

[321] S. Chi, A. Schneidewind, J. Zhao, L. W. Harriger, L. Li, Y. Luo, G. Cao, Z. Xu, M. Loewenhaupt, J. Hu, et al., Phys. Rev. Lett. **102**, 107006 (2009).

[322] S. Li, Y. Chen, S. Chang, J. W. Lynn, L. Li, Y. Luo, G. Cao, Z. Xu, and P. Dai, Phys. Rev. B **79**, 174527 (2009).

[323] D. S. Inosov, J. T. Park, P. Bourges, D. L. Sun, Y. Sidis, A. Schneidewind, K. Hradil, D. Haug, C. T. Lin, B. Keimer, et al., Nature Phys. **6**, 178 (2010).

[324] S. Shamoto, M. Ishikado, A. D. Christianson, M. D. Lumsden, S. Wakimoto, K. Kodama, A. Iyo, and M. Arai, *Inelastic neutron scattering study on the resonance mode in an optimally doped superconductor* $LaFeAsO_{0.92}F_{0.08}$ (2010), `arXiv:1006.4640`.

[325] P. Dai, H. A. Mook, S. M. Hayden, G. Aeppli, T. G. Perring, R. D. Hunt, and F. Doğan, Science **284**, 1344 (1999).

[326] D. K. Morr and D. Pines, Phys. Rev. Lett. **81**, 1086 (1998).

[327] H. F. Fong, P. Bourges, Y. Sidis, L. P. Regnault, A. Ivanov, G. D. Gu, N. Koshizuka, and B. Keimer, Nature **398**, 588 (1999).

[328] S. D. Wilson, P. Dai, S. Li, S. Chi, H. J. Kang, and J. W. Lynn, Nature **442**, 59 (2006).

[329] Z. Hao and A. V. Chubukov, Phys. Rev. B **79**, 224513 (2009).

[330] I. Eremin, D. K. Morr, A. V. Chubukov, K. H. Bennemann, and M. R. Norman, Phys. Rev. Lett. **94**, 147001 (2005).

[331] J. Zhao, P. Dai, S. Li, P. G. Freeman, Y. Onose, and Y. Tokura, Phys. Rev. Lett. **99**, 017001 (2007).

[332] H. He, P. Bourges, Y. Sidis, C. Ulrich, L. P. Regnault, S. Pailhés, N. S. Berzigiarova, N. N. Kolesnikov, and B. Keimer, Science **295**, 1045 (2002).

[333] C. D. Batista, G. Ortiz, and A. V. Balatsky, Phys. Rev. B **64**, 172508 (2001).

[334] C. Liu, G. D. Samolyuk, Y. Lee, N. Ni, T. Kondo, A. F. Santander-Syro, S. L. Bud'ko, J. L. McChesney, E. Rotenberg, T. Valla, et al., Phys. Rev. Lett. **101**, 177005 (2008).

[335] V. B. Zabolotnyy, D. S. Inosov, D. V. Evtushinsky, A. Koitzsch, A. A. Kordyuk, G. L. Sun, J. T. Park, D. Haug, V. Hinkov, A. V. Boris, et al., Nature **457**, 569 (2009).

[336] K. Terashima, Y. Sekiba, J. H. Bowen, K. Nakayama, T. Kawahara, T. Sato, P. Richard, Y.-M. Xu, L. J. Li, G. H. Cao, et al., Proc. Natl. Acad. Sci. USA **106**, 7330 (2009).

[337] K. Seo, B. A. Bernevig, and J. Hu, Phys. Rev. Lett. **101**, 206404 (2008).

[338] I. I. Mazin and J. Schmalian, Physica C **469**, 614 (2009).

[339] T. A. Maier and D. J. Scalapino, Phys. Rev. B **78**, 020514(R) (2008).

[340] T. A. Maier, S. Graser, D. J. Scalapino, and P. Hirschfeld, Phys. Rev. B **79**, 134520 (2009).

[341] M. H. Fang, H. M. Pham, B. Qian, T. J. Liu, E. K. Vehstedt, Y. Liu, L. Spinu, and Z. Q. Mao, Phys. Rev. B **78**, 224503 (2008).

[342] G. F. Chen, Z. G. Chen, J. Dong, W. Z. Hu, G. Li, X. D. Zhang, P. Zheng, J. L. Luo, and N. L. Wang, Phys. Rev. B **79**, 140509(R) (2009).

[343] W. Si, Z.-W. Lin, Q. Jie, W.-G. Yin, J. Zhou, G. Gu, P. D. Johnson, and Q. Li, Appl. Phys. Lett. **95**, 052504 (2009).

[344] Y. Mizuguchi, F. Tomioka, S. Tsuda, T. Yamaguchi, and Y. Takano, J. Phys. Soc. Jpn. **78**, 074712 (2009).

[345] Y. F. Nie, E. Brahimi, J. I. Budnick, W. A. Hines, M. Jain, and B. O. Wells, Appl. Phys. Lett. **94**, 242505 (2009).

[346] T. Kida, T. Matsunaga, M. Hagiwara, Y. Mizuguchi, Y. Takano, and K. Kindo, J. Phys. Soc. Jpn **78**, 113701 (2009).

[347] U. Patel, J. Hua, S. H. Yu, S. Avci, Z. L. Xiao, H. Claus, J. Schlueter, V. V. Vlasko-Vlasov, U. Welp, and W. K. Kwok, Appl. Phys. Lett. **94**, 082508 (2009).

[348] T. Taen, Y. Tsuchiya, Y. Nakajima, and T. Tamegai, Phys. Rev. B **80**, 092502 (2009).

[349] K. W. Yeh, C. T. Ke, T. W. Huang, T. K. Chen, Y. L. Huang, P. M. Wu, and M. K. Wu, Cryst. Growth Des. **9**, 4847 (2009).

[350] T. Imai, K. Ahilan, F. L. Ning, T. M. McQueen, and R. J. Cava, Phys. Rev. Lett. **102**, 177005 (2009).

[351] T. M. McQueen, A. J. Williams, P. W. Stephens, J. Tao, Y. Zhu, V. Ksenofontov, F. Casper, C. Felser, and R. J. Cava, Phys. Rev. Lett. **103**, 057002 (2009).

[352] W. Bao, Y. Qiu, Q. Huang, M. A. Green, P. Zajdel, M. R. Fitzsimmons, M. Zhernenkov, M. Fang, B. Qian, E. K. Vehstedt, et al., Phys. Rev. Lett. **102**, 247001 (2009).

[353] S. Li, C. de la Cruz, Q. Huang, Y. Chen, J. W. Lynn, J. Hu, Y.-L. Huang, F.-C. Hsu, K.-W. Yeh, M. kuen Wu, et al., Phys. Rev. B **79**, 054503 (2009).

[354] Y. Mizuguchi, F. Tomioka, S. Tsuda, T. Yamaguchi, and Y. Takano, Appl. Phys. Lett. **94**, 012503 (2009).

[355] Y. Mizuguchi, F. Tomioka, S. Tsuda, T. Yamaguchi, and Y. Takano, Physica C **469**, 1027 (2009).

[356] J. Zhao, W. R. II, J. W. Lynn, G. F. Chen, J. L. Luo, N. L. Wang, J. Hu, and P. Dai, Phys. Rev. B **78**, 140504(R) (2008).

[357] M. de Souza, A. Haghighirad, U. Tutsch, W. Assmus, and M. Lang, *Synthesis, structural and physical properties of δ-FeSe*$_{1-x}$ (2010), `arXiv:1006.0073`.

[358] K. Haule, J. H. Shim, and G. Kotliar, Phys. Rev. Lett. **100**, 226402 (2008).

[359] T. Yildirim, Phys. Rev. Lett. **101**, 057010 (2008).

[360] A. Subedi, L. Zhang, D. J. Singh, and M.-H. Du, Phys. Rev. B **78**, 134514 (2008).

[361] F. Ma, W. Ji, J. Hu, Z.-Y. Lu, and T. Xiang, Phys. Rev. Lett. **102**, 177003 (2009).

[362] Y. Qiu, W. Bao, Y. Zhao, C. Broholm, V. Stanev, Z. Tesanovic, Y. C. Gasparovic, S. Chang, J. Hu, B. Qian, et al., Phys. Rev. Lett. **103**, 067008 (2009).

[363] H. A. Mook, M. D. Lumsden, A. D. Christianson, S. E. Nagler, B. C. Sales, R. Jin, M. A. McGuire, A. S. Sefat, D. Mandrus, T. Egami, et al., Phys. Rev. Lett. **104**, 187002 (2010).

[364] Jinsheng Wen, Guangyong Xu, Zhijun Xu, Zhi Wei Lin, Qiang Li, W. Ratcliff, G. Gu, and J. M. Tranquada, Phys. Rev. B **80**, 104506 (2009).

[365] Jinsheng Wen, G. Xu, Z. Xu, Z. W. Lin, Q. Li, Y. Chen, S. Chi, G. Gu, and J. M. Tranquada, Phys. Rev. B **81**, 100513(R) (2010).

[366] S.-H. Lee, G. Xu, W. Ku, J. S. Wen, C. C. Lee, N. Katayama, Z. J. Xu, S. Ji, Z. W. Lin, G. D. Gu, et al., Phys. Rev. B **81**, 220502(R) (2010).

[367] C. C. Homes, A. Akrap, J. S. Wen, Z. J. Xu, Z. W. Lin, Q. Li, and G. D. Gu, Phys. Rev. B **81**, 180508(R) (2010).

[368] Z. Xu, Jinsheng Wen, G. Xu, Q. Jie, Z. Lin, Q. Li, S. Chi, D. K. Singh, G. Gu, and J. M. Tranquada, *Disappearance of static magnetic order and evolution of spin fluctuations in* $Fe_{1+\delta}Se_xTe_{1-x}$ (2010), `arXiv:1005.4856`.

[369] N. Katayama, S. Ji, D. Louca, S.-H. Lee, M. Fujita, T. J. Sato, J. S. Wen, Z. J. Xu, G. D. Gu, G. Xu, et al., *Investigation of the spin-glass regime between the antiferromagnetic and superconducting phases in* $Fe_{1+y}Se_xTe_{1-x}$ (2010), `arXiv:1003.4525`.

[370] C. C. Homes, A. Akrap, J. Wen, Z. Xu, Z. W. Lin, Q. Li, and G. Gu, *Optical properties of the iron-chalcogenide superconductor* $FeTe_{0.55}Se_{0.45}$ (2010), (submitted to J. Phys. Chem. Solids), `arXiv:1007.1447`.

[371] W. K. Park, C. R. Hunt, H. Z. Arham, Z. J. Xu, J. S. Wen, Z. W. Lin, Q. Li, G. D. Gu, and L. H. Greene, *Strong Coupling Superconductivity in Iron-Chalcogenide* $FeTe_{0.55}Se_{0.45}$ (2010), `arXiv:1005.0190`.

[372] L. Zhang, D. J. Singh, and M. H. Du, Phys. Rev. B **79**, 012506 (2009).

[373] T. J. Liu, X. Ke, B. Qian, J. Hu, D. Fobes, E. K. Vehstedt, H. Pham, J. H. Yang, M. H. Fang, L. Spinu, et al., Phys. Rev. B **80**, 174509 (2009).

[374] C. Fang, B. A. Bernevig, and J. Hu, Europhys. Lett. **86**, 67005 (2009).

[375] A. Guinier, *X-Ray Diffraction in Crystals, Imperfect Crystals, and Amorphous Bodies* (Dover, New York, 1994), chap. 9.

[376] B. Lake, K. Lefmann, N. B. Christensen, G. Aeppli, D. F. Mcmorrow, H. M. Ronnow, P. Vorderwisch, P. Smeibidl, N. Mangkorntong, T. Sasagawa, et al., Nature Mater. **4**, 658 (2005).

[377] R. M. Fernandes and J. Schmalian, *Competing order and nature of the pairing state in the iron pnictides* (2010), `arXiv:1005.2437`.

[378] M. D. Lumsden, A. D. Christianson, E. A. Goremychkin, S. E. Nagler, H. A. Mook, M. B. Stone, D. L. Abernathy, T. Guidi, G. J. MacDougall, C. De La Cruz, et al., Nature Phys. **6**, 182 (2010).

[379] D. N. Argyriou, A. Hiess, A. Akbari, I. Eremin, M. M. Korshunov, J. Hu, B. Qian, Z. Mao, Y. Qiu, C. Broholm, et al., Phys. Rev. B **81**, 220503 (2010).

[380] S. Li, C. Zhang, M. Wang, H. Luo, E. Faulhaber, A. Schneidewind, J. Hu, T. Xiang, and P. Dai, *Hour-glass dispersion in spin excitations of superconducting* $FeSe_{0.4}Te_{0.6}$ (2010), `arXiv:1001.1505`.

[381] S. O. Diallo, V. P. Antropov, T. G. Perring, C. Broholm, J. J. Pulikkotil, N. Ni, S. L. Bud'ko, P. C. Canfield, A. Kreyssig, A. I. Goldman, et al., Phys. Rev. Lett. **102**, 187206 (2009).

[382] J. Zhao, D. T. Adroja, D.-X. Yao, R. Bewley, S. Li, X. F. Wang, G. Wu, X. H. Chen, J. Hu, and P. Dai, Nature Phys. **5**, 555 (2009).

[383] P. Dai, H. A. Mook, G. Aeppli, S. M. Hayden, F. Doğan, J. Yu, Y. Yanagida, H. Takashima, Y. Inaguma, M. Itoh, et al., Nature **406**, 965 (2000).

[384] J. M. Tranquada, C. H. Lee, K. Yamada, Y. S. Lee, L. P. Regnault, and H. M. Rønnow, Phys. Rev. B **69**, 174507 (2004).

[385] J. Zhao, L.-P. Regnault, C. Zhang, M. Wang, Z. Li, F. Zhou, Z. Zhao, C. Fang, J. Hu, and P. Dai, Phys. Rev. B **81**, 180505 (2010).

[386] M. Kofu, S. H. Lee, M. Fujita, H. J. Kang, H. Eisaki, and K. Yamada, Phys. Rev. Lett. **102**, 047001 (2009).

[387] S. D. Wilson, S. Li, J. Zhao, G. Mu, H.-H. Wen, J. W. Lynn, P. G. Freeman, L.-P. Regnault, K. Habicht, and P. Dai, Proc. Natl. Acad. Sci. USA **104**, 15259 (2007).

[388] W. Bao, A. T. Savici, G. E. Granroth, C. Broholm, K. Habicht, Y. Qiu, J. Hu, T. Liu, and Z. Q. Mao, *A Triplet Resonance in Superconducting* $FeSe_{0.4}Te_{0.6}$ (2010), `arXiv:1002.1617`.

[389] R. Khasanov, M. Bendele, A. Amato, P. Babkevich, A. T. Boothroyd, A. Cervellino, K. Conder, S. N. Gvasaliya, H. Keller, H.-H. Klauss, et al., Phys. Rev. B **80**, 140511 (2009).

[390] W. Yin, C. Lee, and W. Ku, *A unified picture for magnetic correlations in iron-based high-temperature superconductors* (2010), `arXiv:1003.0512`.

[391] Y. Qiu, M. Kofu, W. Bao, S.-H. Lee, Q. Huang, T. Yildirim, J. R. D. Copley, J. W. Lynn, T. Wu, G. Wu, et al., Phys. Rev. B **78**, 052508 (2008).

[392] T. Hotta, M. Moraghebi, A. Feiguin, A. Moreo, S. Yunoki, and E. Dagotto, Phys. Rev. Lett. **90**, 247203 (2003).

[393] C.-Y. Moon and H. J. Choi, Phys. Rev. Lett. **104**, 057003 (2010).

[394] Z. Tesanovic, Physics **2**, 60 (2009).

[395] D. P. Alexander V. Balatsky, Physics **2**, 59 (2009).

[396] D. J. Singh and M.-H. Du, Phys. Rev. Lett. **100**, 237003 (2008).

[397] Z. P. Yin, S. Lebègue, M. J. Han, B. P. Neal, S. Y. Savrasov, and W. E. Pickett, Phys. Rev. Lett. **101**, 047001 (2008).

[398] M. J. Han and S. Y. Savrasov, Phys. Rev. Lett. **103**, 067001 (2009).

[399] K. Matan, R. Morinaga, K. Iida, and T. J. Sato, Phys. Rev. B **79**, 054526 (2009).

[400] L. Ke, M. van Schilfgaarde, J. J. Pulikkotil, T. Kotani, and V. P. Antropov, *Low Energy, Coherent, Stoner-like Excitations in* $CaFe_2As_2$ (2010), `arXiv:1004.2934`.

[401] A. M. Turner, F. Wang, and A. Vishwanath, Phys. Rev. B **80**, 224504 (2009).

[402] R. Klingeler, N. Leps, I. Hellmann, A. Popa, U. Stockert, C. Hess, V. Kataev, H.-J. Grafe, F. Hammerath, G. Lang, et al., Phys. Rev. B **81**, 024506 (2010).

[403] S. Chadov, D. Schärf, G. H. Fecher, C. Felser, L. Zhang, and D. J. Singh, Phys. Rev. B **81**, 104523 (2010).

[404] J. Wu, P. Phillips, and A. H. Castro Neto, Phys. Rev. Lett. **101**, 126401 (2008).